2022

Evaluating the stability of terps in the Netherlands

MSC THESIS

MATTEO ALBERTO ROSSETTI (4160940)

Contents

Preface

This thesis was written by Matteo Alberto Rossetti, MSc student at TU Delft and now junior geotechnical advisor at Fugro.

All the work presented was made possible thanks to the assistance, guidance, and patience provided by supervisors Dominique Ngan-Tillard and Ronald Brinkgreve, to whom great deal of gratitude and appreciation is owed.

Significant contributions were also made by Giovanni Piunno, particularly in assisting with the model making procedures involved in this thesis.

An additional personal thank you is owed to the TU Delft technical support staff, specifically Wim Verwaal and Roland Klasen, who were of great help with all laboratory testing procedures performed for this thesis.

Last but certainly not least, thank you to Alberto Rossetti; a friend, a mentor and, most importantly, a wonderful father, without which I would not be where I am today.

1 Introduction

1.1 Project scope

Terps are artificial dwelling mounds mostly found in the northern regions of the Netherlands and Germany, built to provide safe ground against water in such areas affected by flooding, storm surges, and high tides. In the Netherlands, these occur in the provinces of Friesland and Groningen, with their origins dating back to as far as 500 BC, and up the 1200s, after which the dike became the preferred flood protection structure.

Over time, the soil contained within these terps became highly fertilized due to the deposition and decay of organic waste deposited by their inhabitants. For this reason, a large number of terps were entirely or partially excavated throughout the 18th and 19th centuries, with the extracted fertile terp material being reused to fertilize farm fields across the Netherlands. As a result, only a fraction of the originally constructed terps remain to this day, many of which are now protected as archaeological monuments (van den Doel, 2016).

From a geo-engineering perspective, of the terps that remain today, those that have been partially excavated are of particular interest due to the slopes created by the excavations. These slopes, often featuring a sharp boundary between excavated and intact sections of the terp, vary considerably in shape and composition, and their response to external disturbances has yet to be studied in detail.

A better understanding of the state of these slopes would not just be of importance due to their historical and cultural relevance, but also for general safety. Modern day activities performed in direct proximity of the terp slopes include, among other things, large-scale agriculture, and archaeological field studies, sometimes carried out simultaneously. Failure of these slopes could therefore pose a danger to human life, and not just the loss of a valued archaeological monument.

To further aggravate stability concerns, a large number of terps in the Dutch province of Groningen are located in areas recently affected by earthquakes, resulting directly from gas extraction activities. These earthquakes subject the region to unprecedented dynamic loads, which could very well affect the integrity of the terps found within it.

In order to address the unknowns tied to the behaviour of the terp slopes, the Dutch Cultural Heritage Agency (RCE) commissioned TU Delft to produce a study involving both static and dynamic slope stability analyses. The static slope stability analyses are the focus of this thesis, which will present, discuss, and expand on what was done in the RCE project.

1.2 Connection with the RCE project

This thesis report is heavily based on the work that was done in the aforementioned project on behalf of the Dutch Cultural Heritage Agency (RCE). In this project, multiple reference terp slopes were represented in the form of finite element models, created in Plaxis. These models were made based on the most unfavourable terp slope geometries found in Groningen and Friesland, and were tested for stability under both static and dynamic loading conditions.

The dynamic slope stability analyses involved simulating the relatively recent phenomenon of induced seismic activity in the province of Groningen, resulting directly from gas extraction activities in the region. Since 1986, approximately 1000 of these induced earthquakes have occurred in the northeast of the Netherlands, with the heaviest having registered a magnitude of 3.6 on the Richter scale. The dynamic slope stability analyses were performed by Dr. Giovanni Piunno, and are outside the scope of this thesis. Consequently, while the dynamic analyses are presented in the report delivered to RCE, these are not included in this thesis report.

The static loading conditions were made to simulate the presence of a large combine harvester nearby the top edge of the slopes. During the preparatory literature study, it was in fact found that heavy agricultural machinery was commonly operated in direct proximity of the terp slopes. Acquiring an understanding on how such activities could affect slope stability is thus of considerable value.

This thesis will present the component of the project dedicated to the static slope stability analysis, including all the preparatory phases involved. Furthermore, the work done on behalf of RCE will be expanded on by providing further insight on the parameter determination process, as well as a post-analysis considerations section. In this added section, the results of supplementary oedometer tests performed to validate the soil parameters used in the finite element models involved in the project will be presented, as well as well as discussions regarding the application of drained vs. undrained, and 2D vs. 3D safety analyses.

1.3 Problem statement

As was discussed in section 1.1, the current state of terps in Groningen and Friesland, in combination with the modern-day activities conducted in their direct proximity, have led to growing concerns regarding the stability of the terp slopes. This thesis aims at addressing these concerns by answering the following main research question:

- To what extent are the slopes of terps in Groningen and Friesland at risk of being unstable?

In order to tackle this problem, multiple aspects need to be considered. As these are best addressed individually, the main research question can be broken down into the following secondary research questions:

1. Could terp slopes present a danger of collapse in their current state, without any external loading applied?
2. What types of external loads can one expect to the terp slopes to be subjected to, and how could these contribute to their instability?
3. At what distance from the slope edge would external loads lead to potential slope collapse?
4. What dangers can be associated to the land use in proximity of the terp slopes, in relation to their potential instability?

1.4 Report outline

In this first chapter of the report, the thesis topic was introduced, and research questions were defined. The second chapter will feature the preliminary study performed for this project, specifically regarding terp locations, geometries, land use, and available geotechnical data at the locations of interest.

Based on the information obtained in the preliminary research phase, specific existing terps were selected as reference for the making of the models, and this process will be discussed in chapter 3. Reference values for input parameters required for these models were obtained in the data analysis and elaboration phase, which is detailed in chapter 4, and followed by chapter 5, in which the models themselves are presented and discussed, together with the various scenarios considered for analysis.

The results obtained from the static slope stability analyses will be presented in chapter 6, and discussed in chapter 7.

Chapter 8 will feature post-analysis considerations related to the models themselves, also featuring topics of interest encountered during the modelling process.

The conclusions drawn from this project, directly answering the research questions outlined in section 1.3, will be presented in chapter 9, followed by the final recommendations in chapter 10.

2 Preliminary Research

The assessment of the stability of the Dutch terp slopes was to be carried out via a series of finite element analyses on Plaxis. As the finite element models involved in these analyses were to be based on existing terp slopes, the first major stage of this project consisted of a selection process aimed at identifying suitable reference terps.

2.1 Terp locations

The preliminary research began with an inventory of all terps in the provinces of Friesland and Groningen, made possible thanks to a database dating November 2019, provided to TU Delft by the Dutch Cultural Heritage Agency (RCE). From this database, one could then apply a further selection process based on desired criteria.

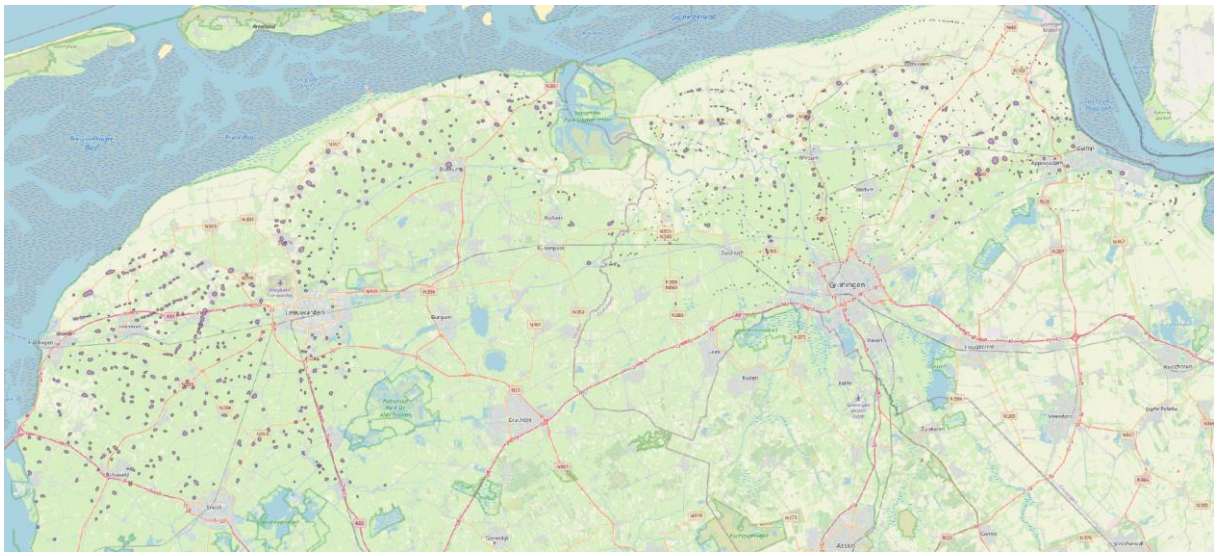

Figure 1: Overview of all terps within Groningen and Friesland (QGIS)

The first selection criterium involved considering terps for which existing data, useful for the development of a reference terp model, was readily available. A report on nationally protected terps, labelled as Dutch archaeological monuments, was recently produced by RAAP Archaeological Consultancy. This report (RAAPrap_4644) included a study of the slopes belonging to these terps (van der Kroft & Varwijk, 2020), providing an inventory of slope heights, (maximum) inclinations, lengths, as well as other general information. This study served as the starting point for the selection of suitable reference terps.

From the domain of monument terps obtained in the aforementioned report, the selection was once again restricted based on the presence of slopes resulting from excavation, forming “steep sides”. The 79 terps featuring such steep sides can be seen in Figure 2, marked in yellow.

The choice of terps to consider as basis for the reference models were those featuring at least one slope with height larger than 3 m and inclination greater than 30 °, also shown in Figure 2, and marked in red.

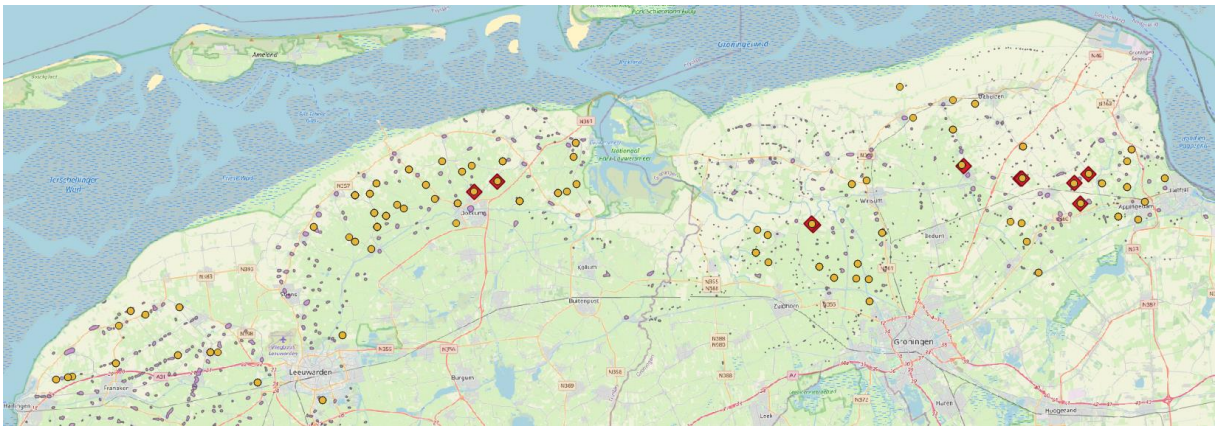

Figure 2: Selection of terps based on slope height and inclination

2.2 Terp slope geometries

As mentioned in the previous subchapter, the data gathering phase of this project included the collection of geometric information related to a large sample of terp slopes in both Friesland and Groningen, obtained from the RAAP report. The slope geometries presented in the report are summarized in Figure 3, in which slope heights and inclinations are plotted on the x-axis and y-axis, respectively.

All terp slopes with both height larger than 3 m and inclination larger than 30° were classified as stability risks and served as initial candidates for the reference models to be made in PLAXIS. These amounted to a total of 18 slopes, shown in the white quadrant in Figure 3. Note that due to two slopes having identical heights and inclinations, only 17 points are visible in the quadrant.

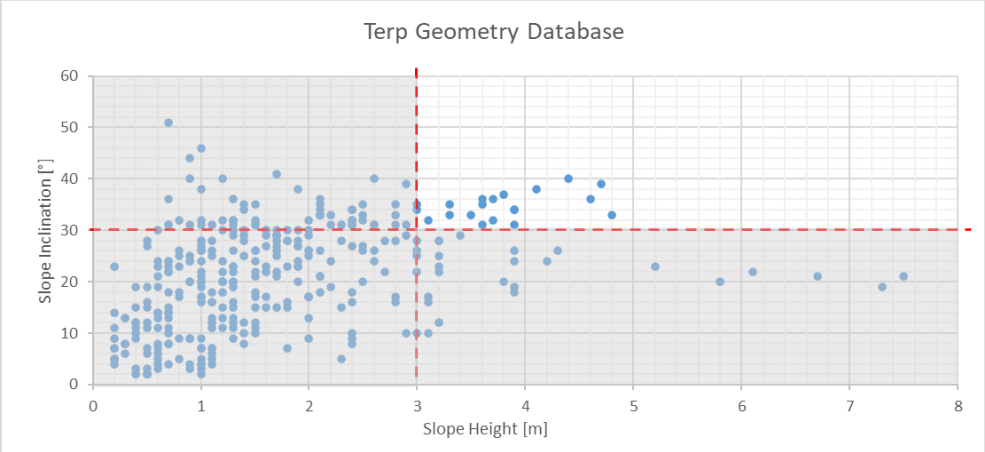

Figure 3: Selection of slopes of interest based on minimum inclination and height

The 18 slopes considered are part of 8 individual terps, listed in Table 1. It should be noted that each of these terps is registered as a national monument (Rijksmonument) by the Dutch Cultural Heritage Agency (RCE). Furthermore, certain stretches of land in the Netherlands are classified as archaeological monuments by the same organization.

In this case, one can see that different archaeological monument areas can be found within the same terp, and multiple potentially unstable slopes may be situated within the same archaeological monument area. For example, the Ezinge terp (Rijksmonument 522164) features two separate archaeological monuments (5312 & 11643), each of which contain two potentially unstable slopes.

Table 1: Terp slopes classified as stability risks

Terp	Province	Archaeological Monument	Rijksmonument	Slopes of interest
Aaslum	Friesland	400	45892	2
Wetsens	Friesland	403	45895	1
Toornwerd	Groningen	884	45763	3
Westeremden	Groningen	900	45975	1
Leermens	Groningen	908	46193	3
Eenum	Groningen	910	46195	2
Ezinge	Groningen	5312	522164	2
Ezinge	Groningen	11643	522164	2
Wirdum	Groningen	11710	45746	1
Westeremden	Groningen	11713	45975	1

The mean, median and mode slope heights and inclination resulting from a statistical analysis performed on the slopes classified as stability risks are provided in Table 2, below.

Table 2: Mean, Median, and Mode of slope height and inclination (minimum 3 m height, 30 ° inclination)

Statistical parameter	Slope Height [m]	Slope Inclination [°]
Mean	3.86	34.72
Median	3.75	34.5
Mode	3.6	36

2.3 Terp land use

Another important aspect to be considered in the preliminary studies was the manner in which the land on top of the terps was being utilized, as this would have direct consequences on the type of external loads that would need to be represented in the finite element models.

From the preliminary studies, it emerged that agricultural activities are often being performed on top of the terps. Specifically, reports on the subject detail the year-long operation of heavy agricultural machinery for the harvesting of grain (Postma, 2010).

The report specifically indicates the use of John Deere combine harvesters, machines typically weighing between 25 – 35 tons, depending on the model, shown in operation in Figure 4. From this photograph, one can see how these machines are operated on top of the terps, even in direct proximity of the slope edge.

Among the many other agricultural activities reported to be occurring on terps in Groningen and Friesland (fertilizing, harrowing, etc.), the operation of combine harvesters was selected as the reference loading case for the models in this project, due to their considerable weight and repeated use throughout the year.

These machines consist mainly of a large tractor with elevated driving cab, with a cutting platform mounted in the front and used to cut and collect crops. The grains are mechanically separated from the crops and (momentarily) stored inside an internal grain tank. These components, together with a large fuel tank, account for the majority of the weight of the machine, and must thus be included in the determination of the loads involved. The characterization of these loads is described in detail in Appendix A of this report.

Figure 4: Photo of combine harvester in operation next to terp slope (Postma, 2010)

2.4 Geotechnical data gathering

Having assessed which terp slopes could serve as suitable references in terms of geometry, the next step in the preliminary research phase involved further restricting the domain of terps listed in Table 1 based on the available geotechnical data required for modelling. Specifically, this involved identifying for which of the listed terps sufficient soil investigations were available to study, from which one could obtain insight on the stratigraphy and material properties of the soil in and beneath the slopes.

In the Netherlands, a vast database of geotechnical data is publicly available via the online platform DINOloket. This includes cone penetration tests (CPTs), borehole data, and lithostratigraphic interpretations.

Furthermore, via the BRO Digital Geological Model (DGM) and BRO GeoTop, DINOloket also provides digital models of the geological layers in the subsurface (see Appendix B.1). BRO DGM is a regional-scale model, illustrating geological layers up to a depth of 500 m below the surface. BRO GeoTop is a smaller-scale model but based on a higher density of boreholes, thus providing a more detailed geological stratigraphy up to a depth of 50 m below the surface.

CPTs were considered of particular value due to the possibility of extracting several geotechnical parameters directly from data via a multitude of empirical formulae. Using QGIS, the locations of all CPTs available on DINOloket were mapped together with those of the selected potential reference terps. It emerged that the Wirdum, Toornwerd, and Wetsens terps featured CPTs currently available on this database.

The borehole data available on DINOloket, while not as useful as the CPTs in terms of parameter determination, can be used to gain insight on the different soil layers inside and beneath the terps. This data comes in the form of a lithostratigraphic interpretation for each borehole, and varies in quality levels. The assigned quality levels range from level 1, being the most reliable due to individual

validations performed in the context of the Digital Geological Model (DGM), to level 3, for which the lithostratigraphic interpretations are automated and only subject to random checks (see Appendix B.2).

As was done for the CPTs, DINOloket was searched in an effort to find borehole data recorded on top of or immediately next to the terps listed in Table 1. Such data was found for all terps except for Leermens and Ezinge, although only Aaslum, Toornwerd, and Eenum featured level 1 lithostratigraphic interpretations.

In an effort to obtain a larger selection of geotechnical data, the list of terps presented in Table 1 was forwarded to several municipalities and geo-engineering companies. A request was made for any possible ground investigation results in their possession, which were not present on DINOloket. This resulted to be particularly fruitful, as both companies Fugro and Wiertsma & Partners shared a total of eight CPTs, all performed on top or in direct proximity of the Westeremden terp. Of these, six were provided by Fugro, all performed in 2018 for a project concerning the construction of a temporary school building in Westeremden. The remaining two provided by Wiertsma & Partners were part of the ground investigation phase for the construction of a new village house, dating early 2020.

In addition, it came to be known that an archaeological investigation was recently carried out on the Westeremden terp by the archaeology department of MUG Ingernieursbureau, on behalf of the Cultural Heritage Agency of the Netherlands (RCE) and the Ons Dorpshuis Westeremden Foundation. As part of this investigation, several core samples have been extracted from the ground directly on top of the terp, and one of these core samples was made available for study in this project.

The geotechnical data obtained during the preliminary research phase is summarized in Table 3, below. One can see that no CPTs were obtained for the Aaslum, Leermens, Eenum, and Ezinge terps. Given the importance of CPTs for the determination of several geotechnical parameters, these were immediately recognized as unlikely candidates for model reference terps.

Table 3: Overview of gathered geotechnical data for each terp

Terp	**Total CPTs**	**DINOloket borehole data**	**Verified (level 1) lithostratigraphic interpretation**	**Borehole samples**
Aalsum	0	2	1	0
Wetsens	1	1	0	0
Toornwerd	1	1	1	0
Westeremden	8	2	0	1
Leermens	0	0	0	0
Eenum	0	2	1	0
Ezinge	0	0	0	0
Wirdum	3	3	0	0

It is worthy to note that many CPTs have been performed on terps in Groningen in relation to a recent induced seismicity investigation. Unfortunately, these had not yet been supplied to DINOloket and were not available during the preliminary research stage of this project.

3 Selection of reference terps

Due to the abundance of geotechnical data, Westeremden was selected as the reference terp for the main model in this project. It was also decided to produce a secondary model based on a different terp, through which one could gain further insight on the effects of different slope geometries and subsoil compositions via comparison with the main model. Toornwerd was selected as reference for the secondary model.

3.1 Westeremden terp

3.1.1 Altimetric and geometric data

The Westeremden is a terp in Groningen, with its highest point reaching approximately + 5 m NAP. The terp's 7 steep sides are found on its Southern face, with the adjacent ground varying between approximately +0 m and +0.5 m NAP. The heights of these vary between 1.6 m and 4.5 m, and slope inclinations range from 23 ° and 34 °. The terp itself is registered as a Rijksmonument, and features two zones labelled as archaeological monuments. These are illustrated in Figure 5, labelled according to their archaeological monument numbers 900 and 11713. The 7 steep sides can also be seen in the same figure, labelled 900 #1 – 900 #6 and 11713.

Figure 5: Westeremden terp. Aerial photography of the site and numbering of the archaeological monuments and steep sides (left). Elevation map (right). (van der Kroft & Varwijk, 2020).

The geometry of each steep side slope is shown in Figure 6, below. Of these, slopes M900#1 and M11713#1 are the two considered as potential stability risks, given the slope heights and inclinations being larger than 3 m and 30 °, respectively. Note the presence of a small ditch at the toes of multiple slopes.

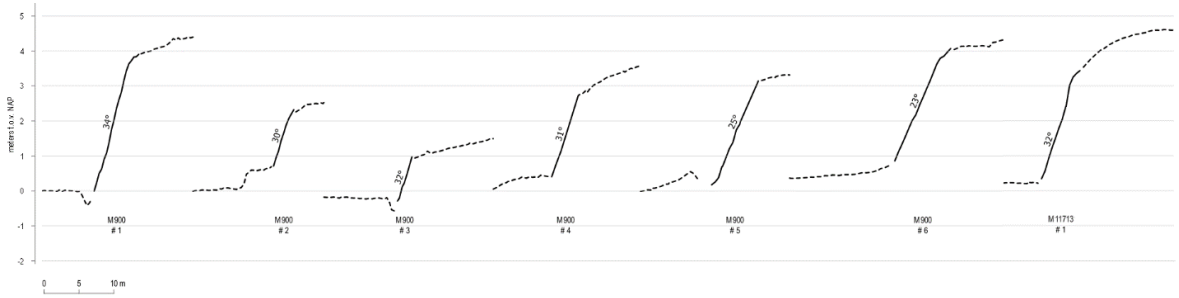

Figure 6: Geometry of the slopes from monuments 900 and 11713. (van der Kroft & Varwijk, 2020).

3.1.2 Borehole data (DINOloket)

Using BRO GeoTop (version 1.4) available on DINOloket, two geological cross sections were obtained, both running through the Westeremden terp and perpendicular to each other. These illustrate the geological units up to 50 m below surface, and can be seen in Figure 7. One can see that the Naaldwijk (NA, NAWO) and Peelo (PE) formations are the two predominant geological units present. The Boxtel (BX) formation is also clearly visible throughout the cross section, at depths of -12 up to -14 m NAP. A Nieuwkoop (NI, NIBA) peat formation is limited to sporadic, very thin strips above the BX layer.

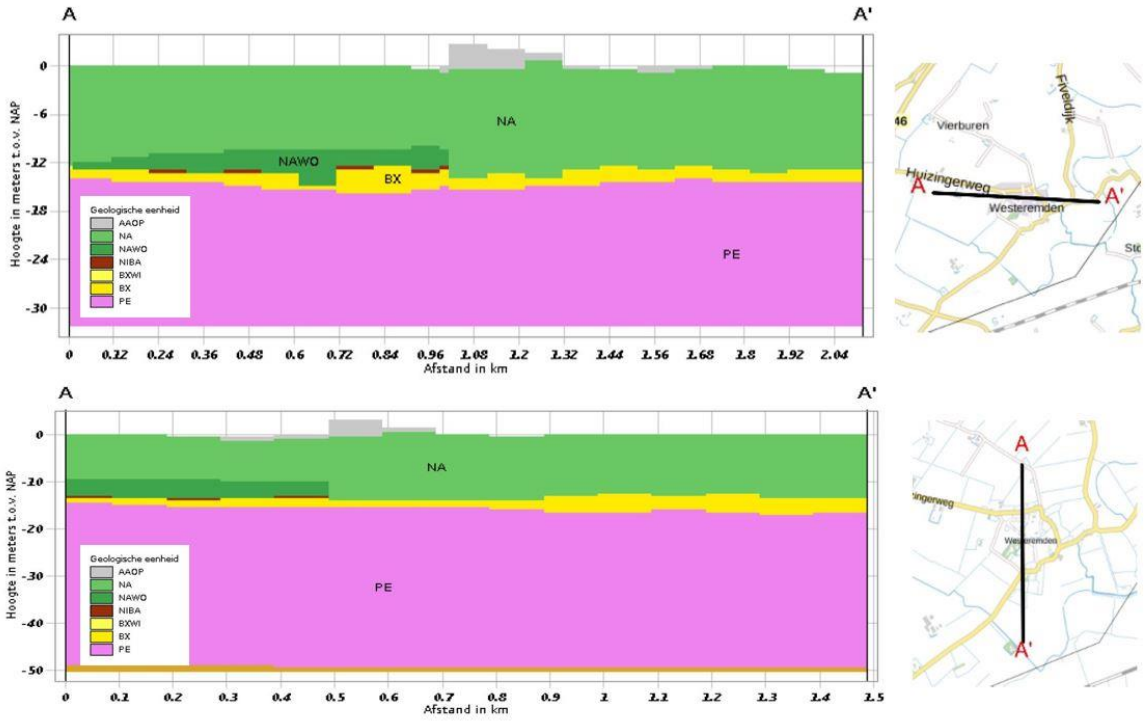

Figure 7: DINOloket BRO GeoTop v1.4 geological models, illustrating the geological units beneath Westeremden.

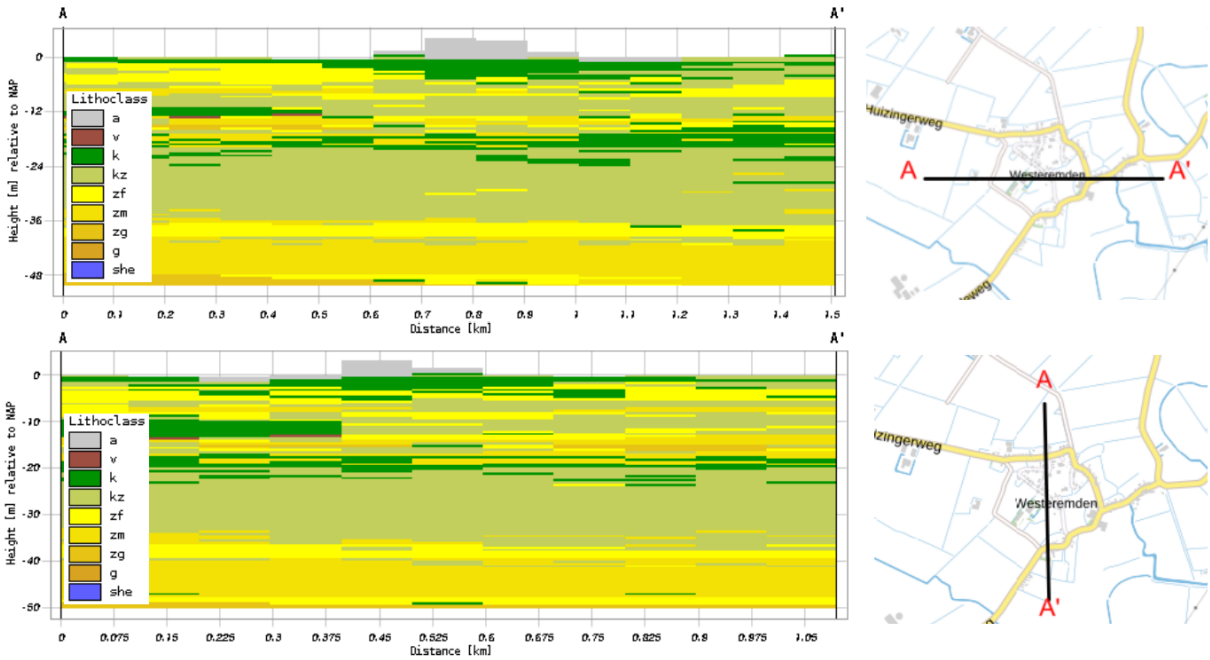

Figure 8: DINOloket BRO GeoTop v1.4 estimated lithological classes beneath Westeremden.

BRO GeoTop (version 1.4) also provides an estimate of the lithological classes in the subsurface. Once again, two cross sections were made through the Westeremden terp, as illustrated in Figure 8. One can see that the soil layers up to approximately 5 m below the surface mostly consist of clay, followed by alternating layers of clay, clayey sand, and sand. Sporadic thin layers of peat can also be seen.

Figure 9: DINOloket borehole locations in Westeremden.

3.1.3 Cone Penetration Tests

A total of 8 CPTs for the Westeremden terp were shared by Fugro and Wiertsma & Partners, all summarized in Table 4.

Table 4: Overview of CPTs obtained from Fugro and Wiertsma & Partners.

CPT ID	Source	X – coord.	Y – coord.	Ground level (NAP)
DKM001	Wiertsma & Partners	243145.6	596087.7	5.13 m
DKM002	Wiertsma & Partners	243132.3	596099	5.15 m
DKMP1	Fugro	243125.7	596315.2	0.12 m
DKMP2	Fugro	243122.6	596328.3	0.48 m
DKMP3	Fugro	243136.5	596324.7	0.24 m
DKMP4	Fugro	243150.8	596321	0.11 m
DKMP5	Fugro	243147.8	596334.1	0.26 m
DKMP4D/DKMS4	Fugro	243075	596152.7	3.22 m

Fugro provided 6 CPTs, 5 of which were performed in direct proximity of the northern edge of the terp (DKMP1, DKMP2, DKMP3, and DKMP5) and reached a depth of approximately -30 m NAP. The remaining 1 was performed on the terp itself (DKMP4D), and reached a depth of -27 m NAP. All Fugro CPTs included groundwater pressure measurements (u_2), and the DKMP4D CPT also included a dissipation test.

The Wiertsma & Partners CPTs were both performed on top of the Westeremden terp. While these CPTs offer the advantage of being located on the highest area of the terp, no water pressures were recorded. The two CPTs, labelled DKM001 and DKM002, reached depths approximately -12.5 m NAP and -25 m NAP, respectively.

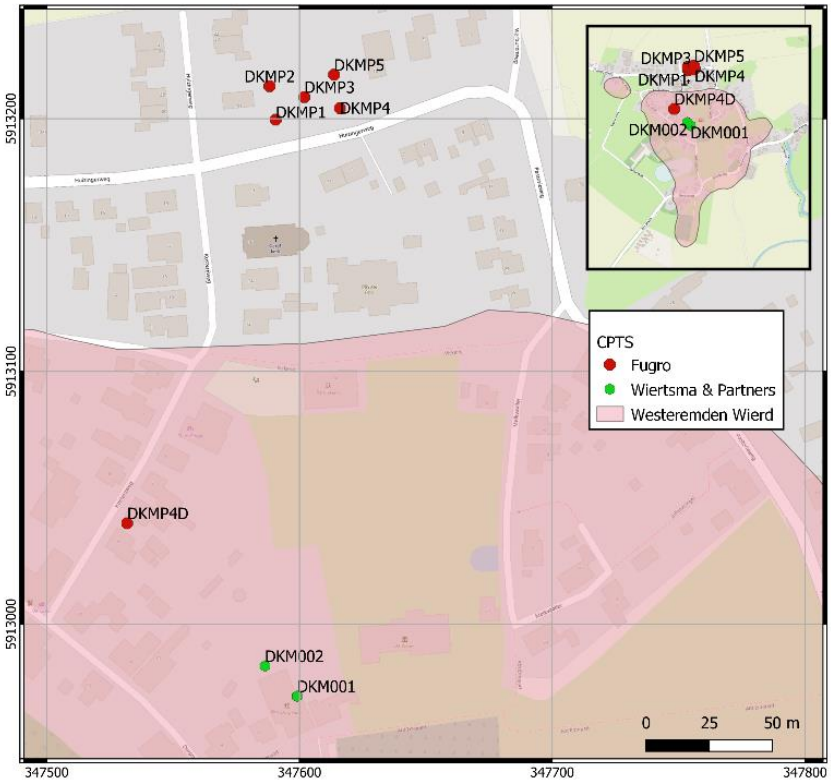

Figure 10: Fugro and Wiertsma & Partners CPTs locations in Westeremden.

An overview of the specific locations of all 8 CPTs is presented in Figure 10, above. The readings of these CPTs can be found in Appendix C. The data obtained from the Fugro CPTs in particular was central to the characterization of the subsoil and determination of many geotechnical parameters required for the modelling phase, as will be discussed in section 4 of this report.

3.1.4 Borehole core sample

As mentioned in section 2.4, a borehole core sample stemming from an archaeological investigation carried out on the Westeremden terp, on behalf of RCE and the Ons Dorpshuis Westeremden Foundation, was made available for study in this project.

The provided core sample has a total length of 8 m, delivered in 8 segments of 1 m length each, as shown in Figure 11. The soil layer classification resulting from inspection of the core segments is summarized in Table 5. As can be seen the sampled soil is quite heterogeneous, with alternating silty clay and clayey peat layers. A closer examination of the sampled soil revealed the presence of pieces of textiles, wood, ceramic, and small masonry debris throughout the entire core.

During the modelling phase, this borehole sample was used as a primary resource for the definition of the soil layers within the terp itself, in combination with the CPT data discussed in the previous subchapter.

Soil samples contained in the core segments were also subject to a series of index and laboratory tests, for the determination of geotechnical parameters. The tests performed and obtained results are presented in subsection 4.2 of this report.

Table 5: Soil classification of the Westeremden borehole sample.

Depth below ground surface	Depth from NAP	Soil description
0 to 0.2 m	+5.2 to +5.0 m	unclassified segment
0.2 to 1.82 m	+5.0 to +3.38 m	clay, extremely silty
1.82 to 2.42 m	+3.38 to +2.78 m	clay, strongly silty, slightly to moderately organic
2.42 to 3 m	+2.78 to +2.2 m	peat*, slightly to strongly clayey
3 to 3.75 m	+2.2 to +1.45 m	mixture of extremely silty clay with blocks of peat
3.75 to 3.96 m	+1.45 to +1.24 m	peat*, strongly clayey, presence pieces of wood
3.96 to 4.69 m	+1.24 to +0.51 m	clay, strongly silty, slightly to strongly organic
4.69 to 5.95 m	+0.51 to -0.75 m	peat*, slightly clayey
5.95 to 7.45 m	-0.75 to -2.25 m	clay, strongly silty with many thin silty or detritus layers
7.45 to 8 m	-2.25 to 2.8 m	clay, strongly sandy with many thin sand layers

(*) Soil layers with a high content of organic matter are all classified as peat in this borehole log, irrespective of whether these are of natural or artificial origin.

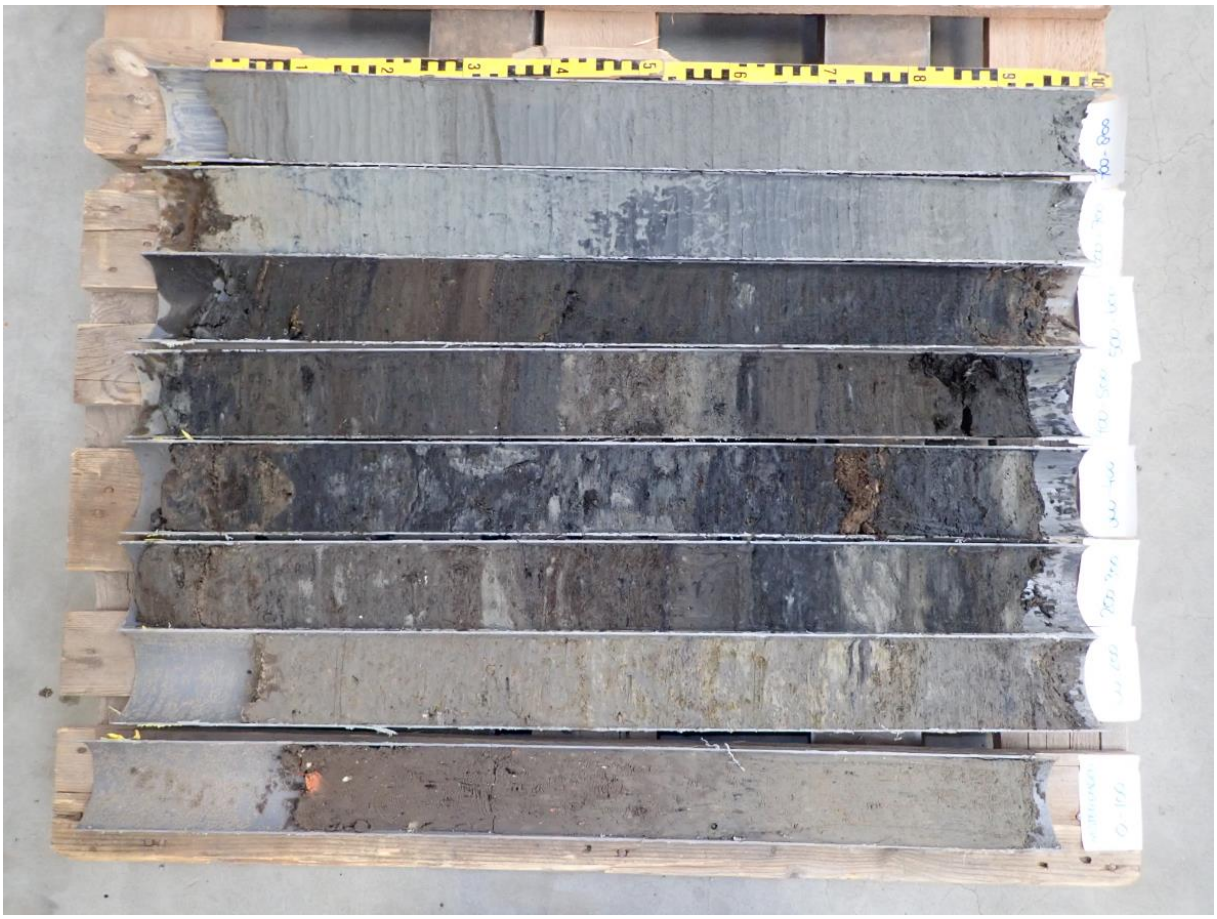

Figure 11: Photo of the Westeremden borehole sample (Van Huisman and de Kort, pers.comm. 2021).

3.2 Toornwerd terp

3.2.1 Altimetric and geometric data

The Toornwerd terp is also situated in Groningen, and its highest ground level is at roughly +4 m NAP. In total, 27 steep sides are present on this terp, spread across 7 archaeological monuments with corresponding IDs 884, and 11659 – 11664. The surrounding ground level varies between

approximately +0 m and -0.5 m NAP. Out of the 27 steep side slopes, 3 were classified as potential stability risks, all of which lie within the archaeological monument 884, situated in the middle of terp as illustrated in Figure 12. For clarity, only the steep sides classified as stability risks were labelled on monument 884. These can be see labelled as slopes 884 #4, 884 #5, and 884 #6.

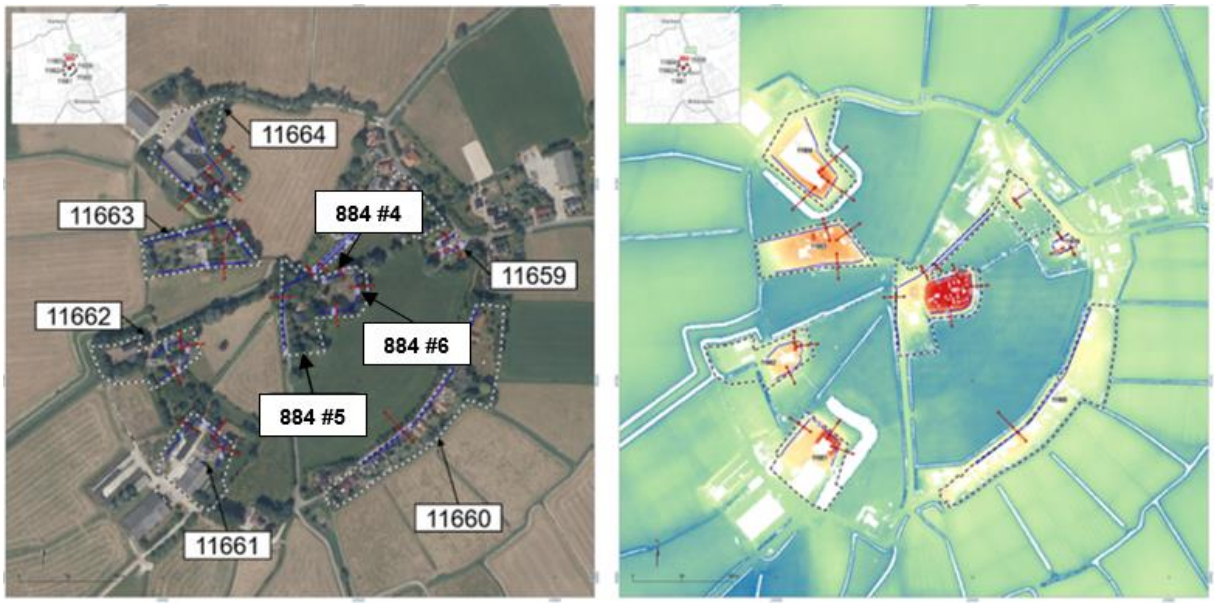

Figure 12: Toornwerd terp. Aerial photography of the site and numbering of the archaeological monuments and steep sides (left). Elevation map (right). (van der Kroft & Varwijk, 2020).

The geometry of each slope present on the archaeological monument number 884 is shown in Figure 13, below. Slopes 884 #4 – 884 #6 are shown to fall into the stability risk category due to heights and inclinations greater than 3 m and 30 °, respectively. As was the case for the Westeremden terp, a ditch is present at the toe of multiple slopes.

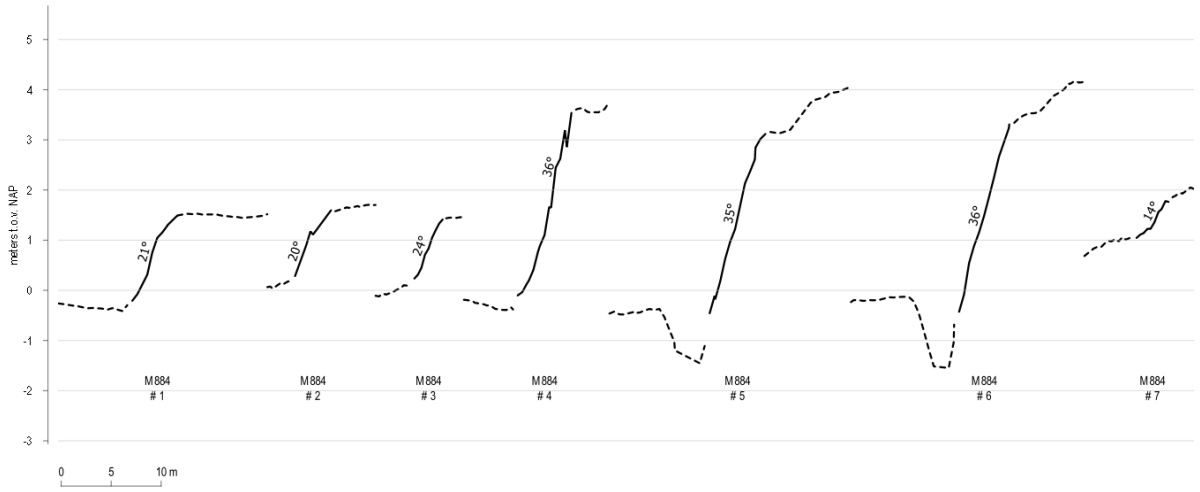

Figure 13: Geometry of the slopes of monument 884. (van der Kroft & Varwijk, 2020).

3.2.2 Borehole data (DINOloket)

BRO GeoTop (version 1.4) was once again used to produce two geological cross sections running through Toornwerd, illustrating the geological units up to 50 m below the surface. Both cross sections can be seen in Figure 14. Once again, the Naaldwijk (NA, NAWO) and Peelo (PE) formations are the predominant geological units. A thin layer of Boxtel (BX, BXWI) formation is present throughout the

cross section, at a depth of approximately -12 m NAP. A Nieuwkoop (NI, NIBA) peat is also clearly visible at depths between -10 m NAP and -12 m NAP.

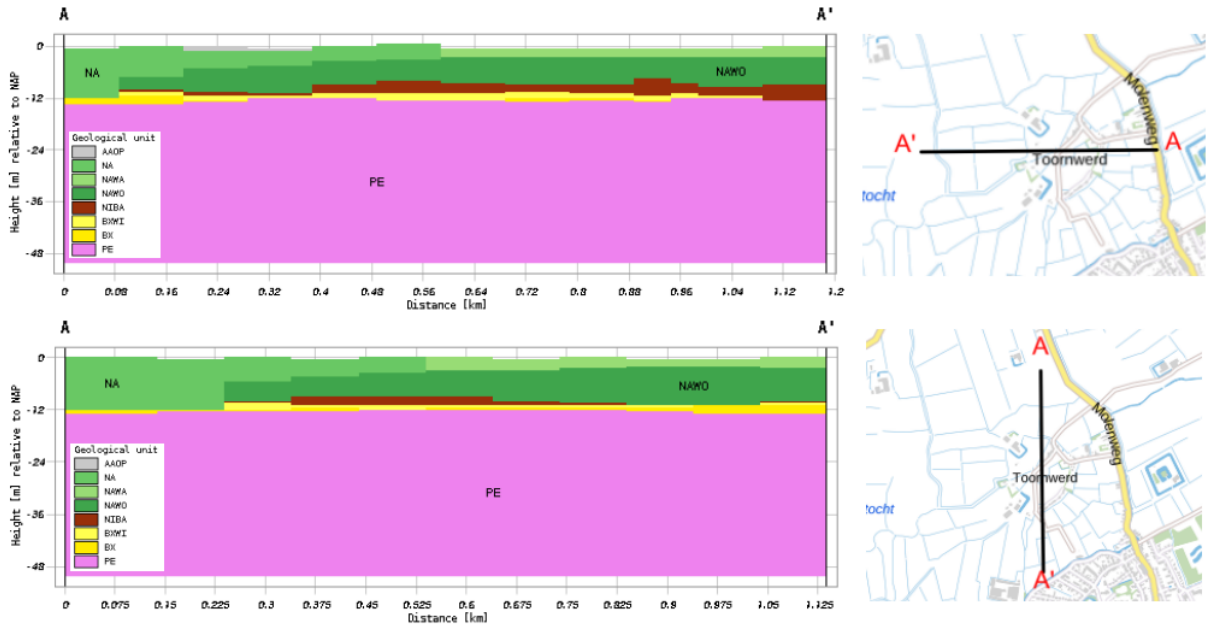

Figure 14: DINOloket BRO GeoTop v1.4 geological models, illustrating the geological units beneath Toornwerd.

The estimated lithological classes for the same cross sections, also produced with BRO GeoTop (version 1.4), are shown in Figure 15. One can see that the soil up to approximately 10 m below ground consists predominantly of clay and clayey sand layers. A peat layer is clearly visible, with varying thickness, at a depth of approximately -10 m NAP to -13 m NAP. Below this depth, the soil seems to mainly consist of clay layers with sporadic intermissions of sand.

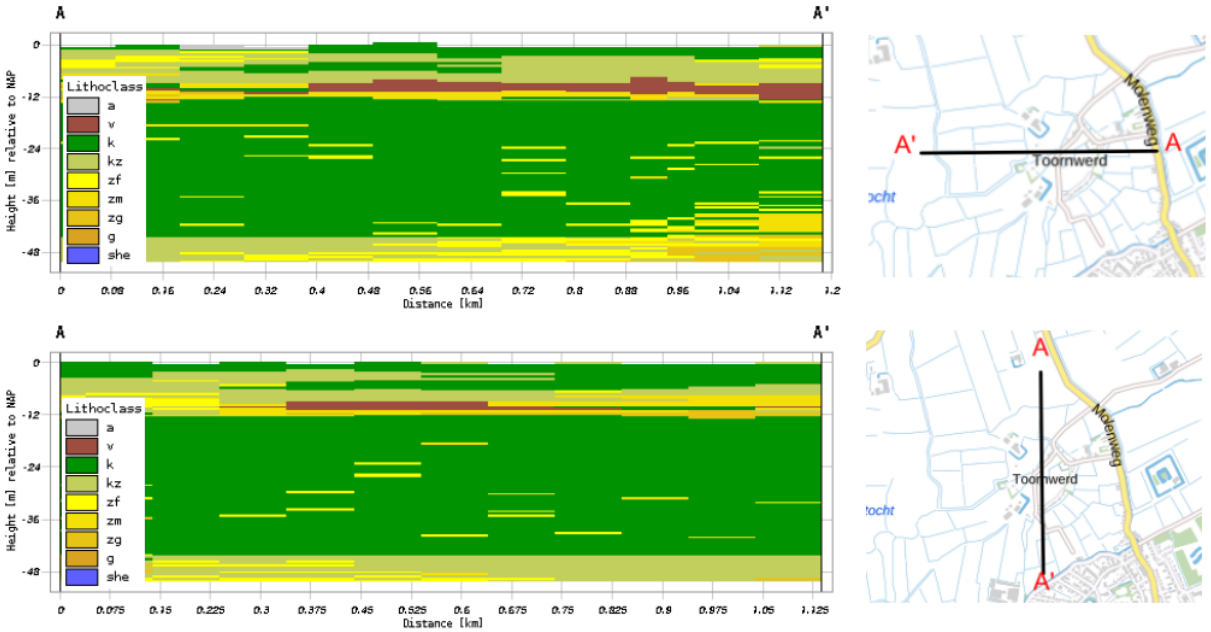

Figure 15: DINOloket BRO GeoTop v1.4 estimated lithological classes beneath Toornwerd.

As stated in section 2.4, DINOloket featured data from a borehole performed in direct proximity of the Toornwerd terp. This borehole, reaching a depth of approximately -12 m NAP, is shown in Figure 16. The provided lithology and lithostratigraphic interpretations indicate the presence of NA Clay from the

ground surface until an approximate depth of -8.7 m NAP, followed by layer of NA Sand reaching roughly -9.3 m NAP, and then another layer of NA Clay with a thickness of around 0.5 m. Between -9.8 m NAP and -10.2 m NAP, a layer of NI Peat can be seen. This is then followed by roughly 1.2 m of BX Sand, and finally a layer PE Clay.

It should be noted that the lithological interpretation provided by this borehole was labelled as quality level 1 on DINOloket, having been verified for modelling for the DGM. The provided lithostratigraphic interpretation can therefore be considered as a reliable representation of the subsurface at that location.

Figure 16: DINOloket borehole data for Toornwerd.

3.2.3 Cone Penetration Test data (DINOloket)

CPT data for the Toornwerd terp was obtained on DINOloket. The single CPT available (S07B00261), performed on the western edge of the terp, provided cone resistance and shaft friction readings from the ground surface (+1.64 m NAP) up to a depth of approximately -19.5 m NAP. The location of this CPT is shown in Figure 17. The CPTs readings can be found in Appendix D.1.

Figure 17: Location of the S07B00261 CPT in Toornwerd.

3.2.4 Archaeological investigations

As no borehole or CPT was found which could provide data describing the composition of the Toornwerd terp layers, attempts were made to obtain information from archaeological investigations performed on the terp monuments.

Information obtained from Fijma (2009), Hielkema & Jans (2009), and Meijles et al. (2016) suggest the prevalence of alternating clay and sandy clay layers within the terp. Although more detailed accounts of the terp soils would be preferred, the Toornwerd model was meant to serve as a comparative tool and thus this was deemed sufficient to produce an approximate characterization.

4 Data analysis and elaboration methods

This section of the report will outline the analysis and elaboration methods applied to the data presented in section 3. Through these methods, raw geotechnical data was converted into meaningful information directly applicable for the modelling phase, in the form of:

- Soil profiling: the identification of the different materials composing the subsoil.
- Material properties: the estimation of the mechanical strength and stiffness parameters of these materials.

4.1 Westeremden soil profiling

This section will predominantly involve the data related to Westeremden, being the main reference terp for this project and that for which the vast majority of the analysed data was concerned. The soil profiling for the secondary model (Toornwerd) is provided in Appendix D.

Data from the CPTs tied to the Westeremden terp is shown in Figure 18. The left plot illustrates the cone resistance readings for all 8 CPTs, with depth relative to the NAP on the vertical axis. The same was done for the sleeve friction readings, shown on the right plot of the figure.

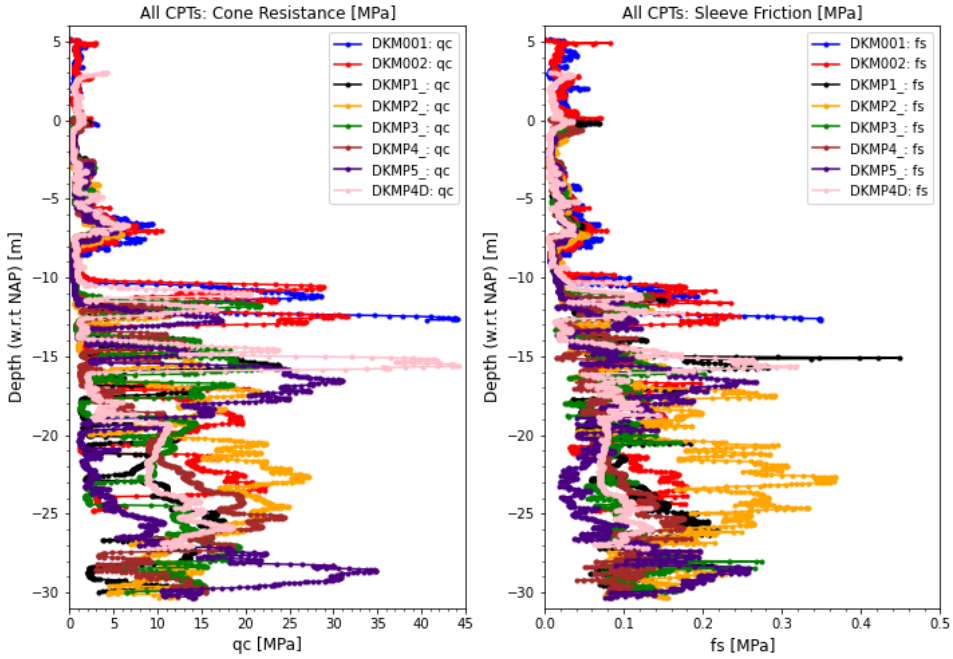

Figure 18: Westeremden CPTs. Cone resistance (left) and sleeve friction (right).

By analysing Figure 18, one can see that all 8 CPTs recorded very similar readings up to a depth of -10 m NAP. At this depth, both cone resistance and sleeve friction readings begin to vary substantially between the different CPTs. Consequently, one should also expect a significant variation in the parameters or properties extrapolated from the CPT readings taken below -10 m NAP, depending on the specific CPT considered, and thus an increase in the uncertainty of the model at such depths.

Fortunately, the uncertainty tied to the deeper layers should be of little relevance to the results of static slope stability analyses. As mentioned in section 1, however, the models to be presented in this report were also used in dynamic analyses, for which the characterization of the deeper layers indeed does have an effect on results.

Therefore, one can say that despite the terp models presented in this report also required the characterization of the deeper layers (for which the uncertainty is highest), the static stability analyses

involved in this thesis are mainly dependent on that of the shallower layers, for which the provided CPT data suggests much less uncertainty.

4.1.1 Modified SBT classification

In order to produce a stratigraphic model of the soil based on the CPT data, the Soil Behaviour Type (SBT) methods suggested by Robertson et al. (1986), Robertson (1990), and Robertson (2010) were studied. The theory behind the different SBT approaches is outlined in detail in Appendix E.1.

Out of the three versions of the SBT methods considered, it was decided to interpret the CPT data via the modified (non-normalized) SBT chart (Robertson, 2010), shown in Figure 19. Although the normalized SBTn method is generally considered the most reliable as it normalizes the CPT readings for effective overburden stress, the modified SBT chart was selected for a number of reasons.

Firstly, the SBTn method requires pore pressure readings which were not present in the CPTs obtained from Wiertsma & Partners. The modified SBT chart, considered the second most favourable method after the SBTn chart, does not require pore pressure measurements.

Additionally, the net area ratio (a) parameter required for the application of the normalized SBTn method was absent for both Fugro and Wiertsma & Partners CPTs. Although typical values range between 0.70 and 0.85, tests performed before selecting the definite SBT method indicated that results were highly sensitive to the chosen value. Consequently, any added accuracy obtained from applying the SBTn method, compared to the modified SBT charts, would be lost by using a possibly incorrect value of the net area ratio parameter.

Lastly, one should also note that when the in-situ vertical effective stress is between 50 kPa to 150 kPa there is often little difference between normalized and non-normalized SBT interpretations (Robertson, 2010). Consequently, this should be valid for at least a significant portion of the soil layers which are most relevant for a static slope stability analysis (i.e., the top 10 m of soil below the terp ground surface), with the exception of the top 3 - 4 m of soil, which are subjected to vertical effective stresses below 50 kPa.

Using the same method for all CPTs also allowed for a simpler comparison of results, as these could be represented on the same type of SBT charts, and any differences in results would not be attributed to any difference in methods. The modified SBT charts for all Westeremden CPTs are shown in Figure 20.

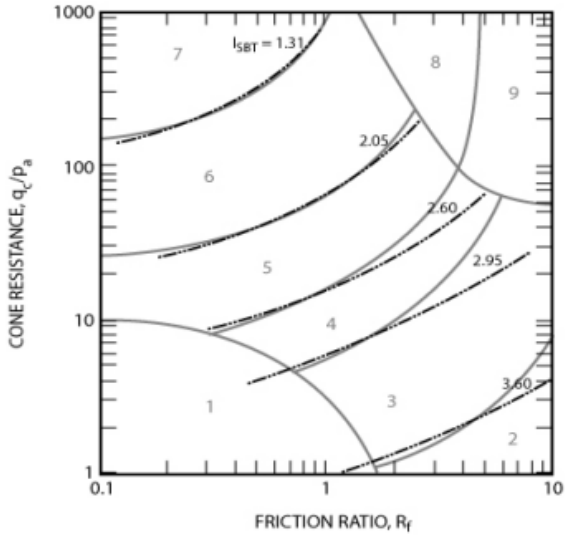

Zone	Soil Behaviour Type (SBT)
1	*Sensitive fine-grained*
2	*Clay - organic soil*
3	*Clays: clay to silty clay*
4	*Silt mixtures: clayey silt & silty clay*
5	*Sand mixtures: silty sand to sandy silt*
6	*Sands: clean sands to silty sands*
7	*Dense sand to gravelly sand*
8	*Stiff sand to clayey sand**
9	*Stiff fine-grained**

** Overconsolidated or cemented*

Figure 19: Modified (non-normalized) SBT chart (Robertson, 2010)

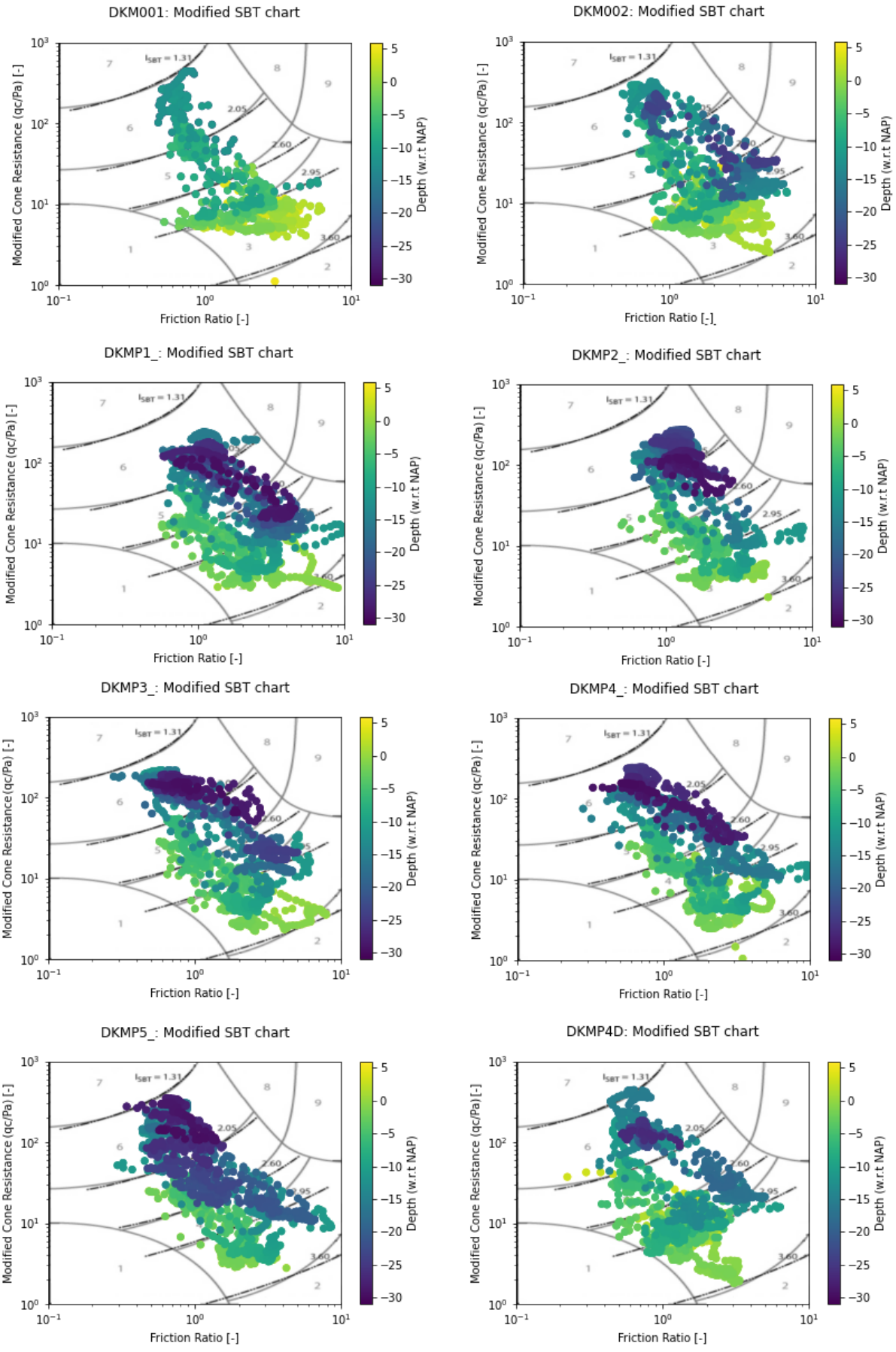

Figure 20: Modified SBT charts (Robertson, 2010) for all Westeremden CPTs.

Using the soil behaviour index (I_{SBT}) of the modified SBT method (see Appendix E.1), a stratigraphic model was also produced for each CPT. When creating these subsoil models, a further condition was applied in the form of classifying soils with a q_c < 1.5 MPa and R_f > 5% as peat. This condition follows guidelines proposed by Fugro for the application of SBT methods on Dutch soils, which otherwise often fail to identify peat directly from CPT readings.

The stratigraphic models for the 2 Wiertsma & Partners (DKM001, DKM002) and the 6 Fugro CPTs (DKMP1, DKMP2, DKMP3, DKMP4, DKMP5, DKMP4D) are shown in Figure 21.

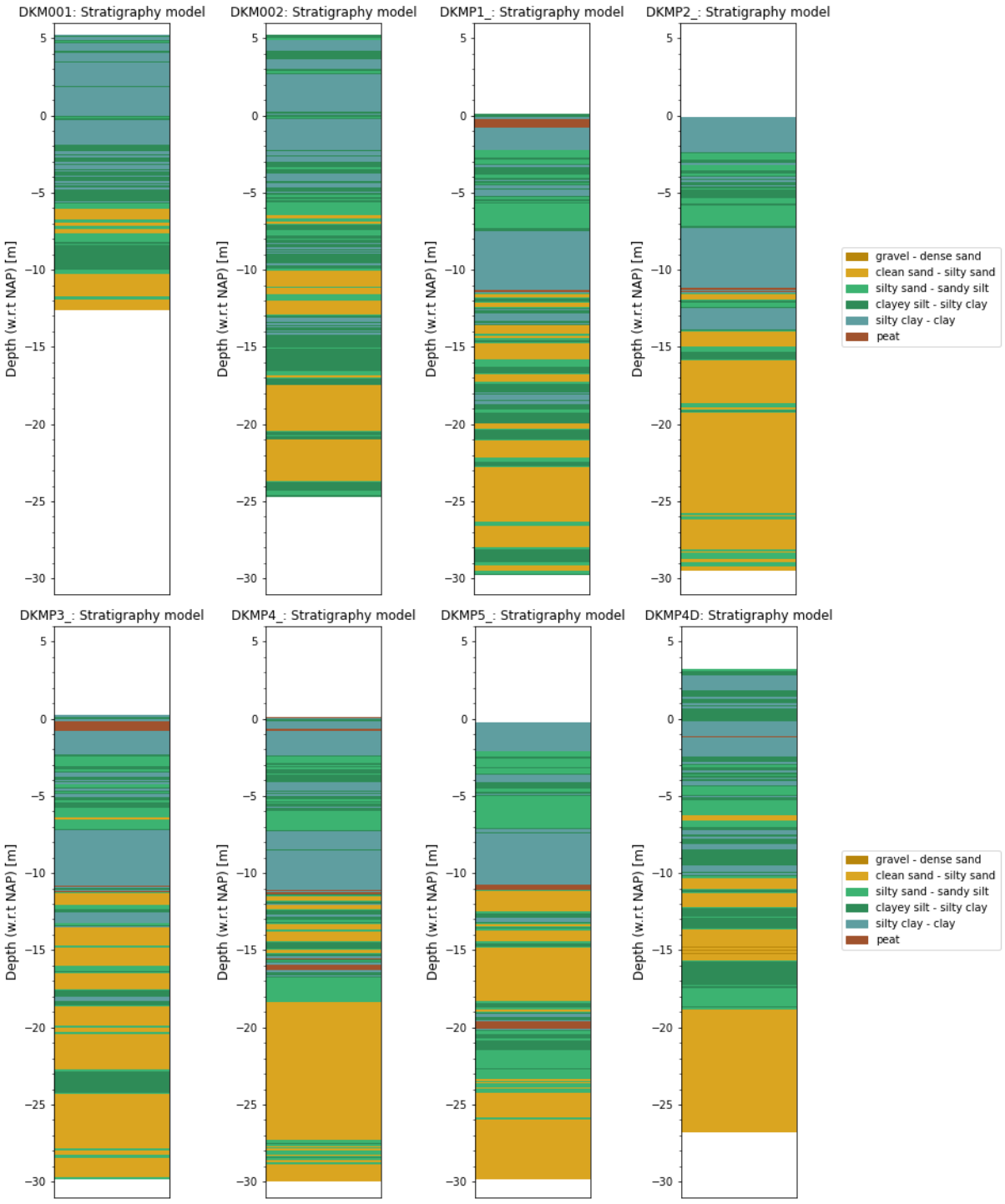

Figure 21: CPT-based subsoil models for the Westeremden CPTs.

By analysing the modified SBT charts in Figure 20 and the subsoil models in Figure 21, one notices the following general features with regard to the soil composition below Westeremden:

- The shallowest layers (above -5 m NAP) are classified predominantly as clay and silty clay for all CPTs, with the exception of a layer of sandy silt/silty sand identified between -2.5 m NAP and -3.5 m NAP and with a thickness varying between 0.5 m and 1 m, depending on the CPT.
- The deeper layers (below -11 m NAP) are mainly classified as sand and silty sand for all CPTs, with occasional clayey silt/silty clay layers appearing at different depths, depending on the CPT considered. These layers of clayey silt/silty clay vary in thickness, up to a maximum of approximately 1.5 m – 2 m.
- The soil layers in between (from -5 m NAP to -11 m NAP) are classified slightly differently depending on whether the Fugro CPTs or the Wiertsma & Partners CPTs are considered.
    - All soil classifications based on the Fugro CPTs suggest that the subsoil between -5 m NAP and -7 m NAP consists mainly of sandy silt/silty sand, with some thin layers of clayey silt/silty clay. The soil layers between -7 m NAP and -11 m NAP are almost exclusively classified as clay/silty clay.
    - Soil classifications based on the Wiertsma & Partners CPTs indicate that the region between -5 m NAP and -8 m NAP is mainly characterized by sand and silty sand/sandy silt, with some thin layers of clayey silt/silty clay. The soil layers between -8 m NAP and -10 m NAP are classified as silty clay/clayey silt.
- Peat layers with varying thicknesses were identified at depths between -0.2 m NAP and -1.1 m NAP in DKMP1, DKMP3, DKMP4 and DKMP4D. The most significant of these were peat layers with thicknesses of roughly 0.5 m identified at -0.2 m NAP in Fugro CPTs DKMP1 and DKMP3. Thin layers of peat were also detected at approximately -11 m NAP in DKMP1, DKMP2, DKMP3, DKMP4, and DKMP5.

The difference in CPT-based soil classifications below -10 m NAP is in line with what was observed in Figure 18, in which the CPT readings were shown to vary considerably below this depth. Above this depth, the subsoil characterization is reasonably similar for all CPTs.

4.1.2 Fugro soil profiling

Fugro also provided its own CPT-based stratigraphic model, for each of the CPTs performed in Westeremden. These subsoil models were formed via the normalized SBTn charts, with two modifications made to improve their applicability in Dutch soils (see Appendix E.2), and are shown in Figure 22.

The stratigraphic models provided by Fugro confirm many of the subsoil characteristics identified in the previous subsection, mainly:

- The prevalence of clay/silty clay above a depth of -5 m NAP, with a layer of silty sand found between -2.5 m NAP and -3.5 m NAP, with thickness varying between 0.5 m and 1 m.
- The deeper layers (below -11 m NAP / -12 m NAP) being mainly characterized by sand/silty sand, with silty clay layers present at different depths depending on the CPT and with a maximum thickness of 2.5 m.
- The region in between being characterized by silty sand up to a depth of approximately -7 m NAP, followed by silty clay up to -11 m NAP /-12 m NAP.
- The presence of peat layers with a thickness of 0.5 m – 0.7 m between -0.2 m NAP and -1.1 m NAP.

Figure 22: CPT-based subsoil models proposed by Fugro.

The many commonalities found between the Fugro subsoil models and those outlined in the previous subsection indicate that the modified (non-normalized) SBT method and the normalized SBTn method indeed yield similar results, thus validating the use of the former.

One should note that, despite the many similarities, some subtle differences were also observed. Perhaps the most significant of these is the shallow peat layer identified in the SBT interpretation of CPT DKMP4D, which is absent in Fugro's SBTn model. Other subtle differences were the absence of the thin layers of clean sand/gravelly sand identified in Fugro's interpretation of CPTs DKMP3 (at -11.7 m NAP) and DKMP4D (at -15.5 m NAP). These were classified as clean sands/silty sands in the SBT interpretations.

4.1.3 Definite model soil profile

Following the data analysis and elaborations made in the previous subsections, a definite soil profile to be applied for the modelling of the Westeremden subsoil was constructed, shown in Figure 23. This model was predominantly based on the soil profile obtained from the Fugro CPT DKMP1, as it was deemed to be the most representative in terms of common characteristics with all the other CPT profiles.

The proposed model distinguishes between the different geological formations outlined in subsection 3.1.2. Key characteristics include the superficial peat layer, the prevalence of clayey layers at shallow depths, and that of sandy layers in deeper soil.

For modelling convenience, an initial minimum layer thickness of 0.5 m was set when defining the individual soil layers. Where necessary, this was then reduced for specific layers based on the CPT-based shear stiffness (G_0) profile fitting process outlined in Appendix J. Once the thickness of an individual layer was established, its properties were defined based on an average of the smaller units it contained. For example, a soil layer containing alternating thin units of PE sand and PE clay was defined as PE sandy clay or PE clayey sand, depending on which unit was most prevalent.

The colours assigned to each layer represents the geological formation to which it belongs, such that Naaldwijk (NA) formations are represented in different shades of green, Nieuwkoop formations (NI) in brown, Boxtel (BX) in different shades of yellow, and Peelo (PE) in different shades of purple.

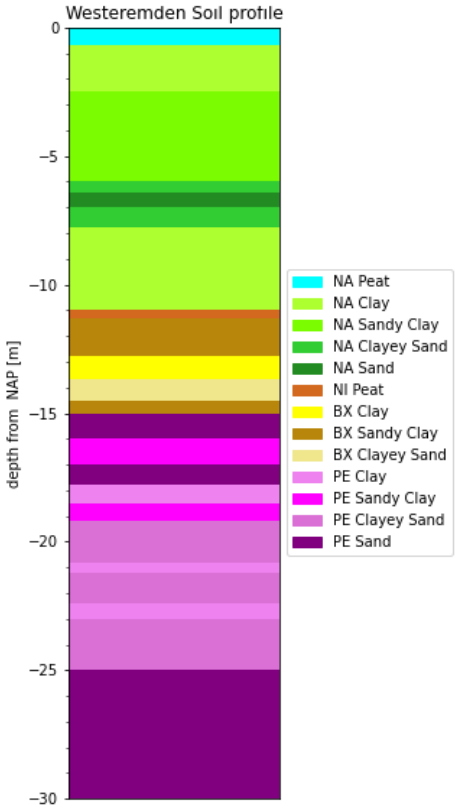

Figure 23: Definite Westeremden model subsoil profile (Piunno & Rossetti, 2021).

4.2 Laboratory tests

The soil samples obtained from the Westeremden borehole cores were made available for a series of laboratory tests, which were performed to obtain geotechnical properties which could later be used for the determination of model parameters. Tests were performed to obtain indicative values for the following geotechnical parameters of the terp soil layers:

- Undrained shear strength
- Bulk Density & water content
- Atterberg Limits, Plasticity Index & Consistency Index

4.2.1 Undrained shear strength

Indicative values for the undrained shear strength were obtained via index tests applied directly along the length of each of the eight core linings. Three different index tests were performed, being fall cone, pocket penetrometer and vane tests.

The fall cone tests were performed in intervals of approximately 10 cm, with some variation due to the necessity of avoiding foreign objects or areas considered unsuitable for testing. These tests involve the placement of a metal cone at a height just above the soil. The cone, which is supported from above, is then released and allowed to penetrate the soil freely for approximately 5 seconds. The penetration depth is measured, and then related to the undrained shear strength at the location of testing via the following formula:

$$s_u = \frac{K(m)g}{d^2}$$

In the formula above, K is the cone-factor, m is the total mass of the cone, g is the acceleration due to gravity, and d is the penetration depth. The specific apparatus used was the 22-T0029/D Cone Penetrometer, by Controls Group taken directly from the Controls Group equipment catalogue.

Pocket penetrometer tests were performed using an Eijkelkamp pocket penetrometer, which provides direct readings for the UCS (unconfined compressive strength) when pushed into the soil sample. An indicative value for the undrained shear strength can then be obtained by dividing the UCS by two. This index test was applied in proximity of the locations in which the fall cone tests were performed, with enough distance as to prevent the two tests from affecting one-another.

Vane tests were also performed at approximately the same locations, with the same criteria. The apparatus used was a handheld Shear Vane device by Gilson, from which the undrained shear strength can be directly measured. This is done by pressing the blades of the vane into the soil, applying a manual torque until failure, and then obtaining a direct reading of undrained shear strength based on the magnitude of the torque required for failure.

The obtained indicative values for undrained shear strength resulting from the three index tests described are summarized in Figure 24.

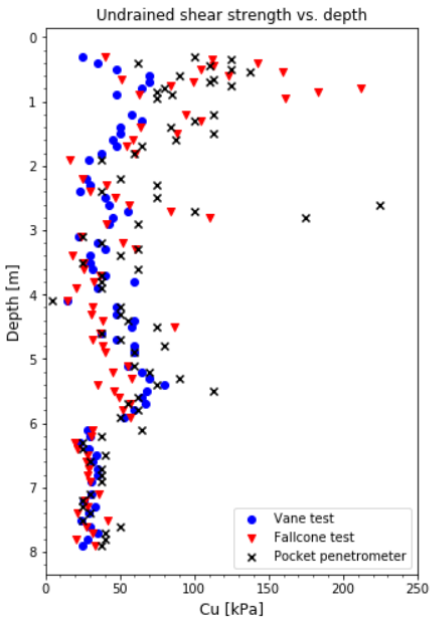

Figure 24: Undrained shear strength vs depth

4.2.2 Bulk density & water content

The bulk density and water content were both obtained by extracting samples of soil with known volumes. Two samples were taken for each 1 m lining, with volumes of 32.9 cm^3, taken at local depths of 30 cm and 80 cm, as measured from the top of each lining.

By measuring the mass of each sample and dividing by the known volume, values for bulk density were obtained at regular intervals of depth. The samples were then placed in an oven until dry, after which their mass was remeasured. The drying process involved an oven temperature of 100 °C and duration of 24 hours, with the exception of samples containing a considerable amount of organic material, which were instead dried for 48 hours at 60 °C.

The water content for each sample was then obtained by comparing the “wet” and dry masses. The obtained bulk densities and water contents can be seen in Figure 25, below.

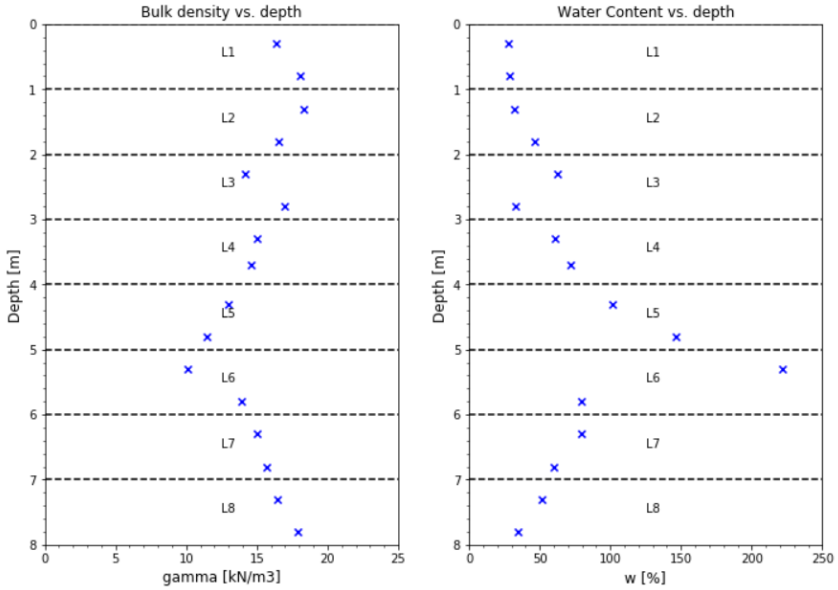

Figure 25: Bulk density and water content vs depth.

4.2.3 Atterberg Limits, Plasticity Index & Consistency Index

The Atterberg limits were obtained at approximately the same locations as for the bulk densities and water contents, with the exclusion of areas featuring non-clayey soil.

Procedures for the determination of the liquid limit once again involved the use of the 22-T0029/D Cone Penetrometer by Controls Group. In this application, samples of soil were prepared with varying degrees of water content, and each were subjected to the fall cone test. The measured penetration for each sample was then recorded, and the liquid limit was determined graphically as the water content corresponding to a fall cone penetration of 20 mm. An example is shown in Figure 26, for the lower sample in the first lining of the cores, indicating a liquid limit of 40%. The same graphs produced for the rest of the samples are available in Appendix F.

Tests for plastic limits involved small samples of soil being rolled into thin strings. The plastic limit was then obtained by measuring the water content at which significant cracking became visible, for a string diameter of 3 mm.

Based on the obtained Atterberg limits, the Plasticity Index (PI) was determined. This is the magnitude of the range of water contents at which a soil samples exhibits plastic properties (i.e., plasticity).

The left graph shown in Figure 27 summarizes the LL (red), PL (blue), and PI (black dotted line) emerging from the aforementioned laboratory tests. Note that linings 4, 5 and 6 did not feature enough clayey material to justify Atterberg limit testing.

The Consistency Index (CI) was also determined directly from the measured Atterberg Limits and water content. This is a measure of the firmness of a soil sample, and is defined by the following equation:

$$\mathrm{CI} = (\mathrm{LL} - \mathrm{W})/(\mathrm{LL} - \mathrm{PL})$$

Soils at the liquid limit or below (i.e., liquid state) are characterized by a CI ≤ 0, while a CI ≥ 1 indicates a semi-solid state. The calculated CI for each lining of pertinence can be seen in the right graph, in Figure 27.

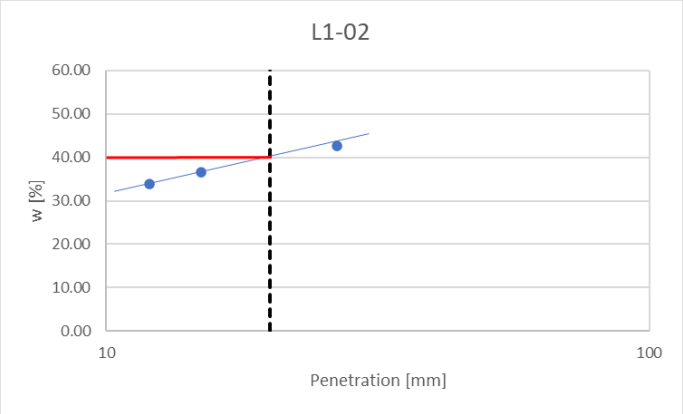

Figure 26: Graphical determination of the LL from fall cone test (Lining 1, Sample 2)

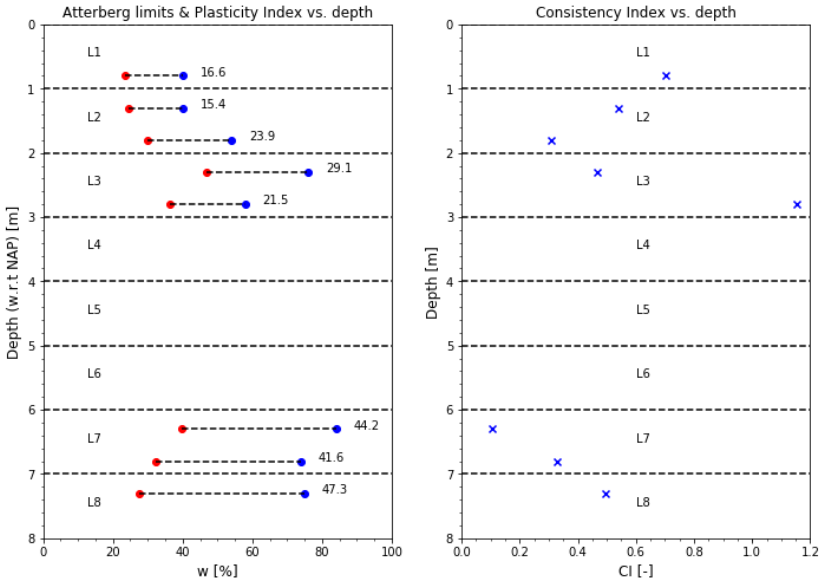

Figure 27: Atterberg Limits and PI vs depth (left), and CI vs depth (right)

4.2.4 Oedometer tests

Three oedometer tests were performed on the Westeremden borehole samples in order to determine the reference oedometer stiffness (E_{oed}^{ref}) of the terp soil layers. It should be noted that these tests were performed after the delivery of the RCE project, and thus served as a model validation exercise.

A total of 3 oedometer tests were performed on the terp soils, 2 of which were made on samples taken from clay layers, and 1 on a sample of one of the peat layers (see note on peat classification in the borehole log presented in subsection 3.1.4). The properties of the specimens tested are summarized in Table 6. The sample labels (A, B, and D) are those corresponding to the Oedometer apparatus used in the TU Delft laboratory. All samples were subjected to a 48h saturation period, during which the samples were fully immersed in water within the consolidation cell, with an applied seating pressure of 2.5 kPa.

Table 6: Oedometer tests sample properties.

Sample	Soil	D [mm]	H [mm]	D/H [-]	Depth (NAP) [m]
A	Clay	65	20	3.25	+3.3
B	Peat	65	20	3.25	+2.4
D	Clay	65	20	3.25	+0.5

The loading sequence applied to the samples contained 9 total stages, 2 of which consisted in unloading steps, as listed below.

1. 2.5 kPa
2. 5 kPa
3. 10 kPa
4. 5 kPa (unloading)
5. 25 kPa
6. 50 kPa
7. 100 kPa
8. 200 kPa
9. 100 kPa (unloading)

The objective of these tests was to obtain values for the reference oedometer stiffness (E_{oed}^{ref}) used for the Hardening Soil model on PLAXIS (see section 5). This corresponds to a tangent stiffness obtained during 1D primary compression, at a reference pressure of 100 kPa. An illustration of this definition is shown in Figure 28, taken directly from the PLAXIS Material Models manual, and in which p_{ref} is the reference pressure of 100 kPa.

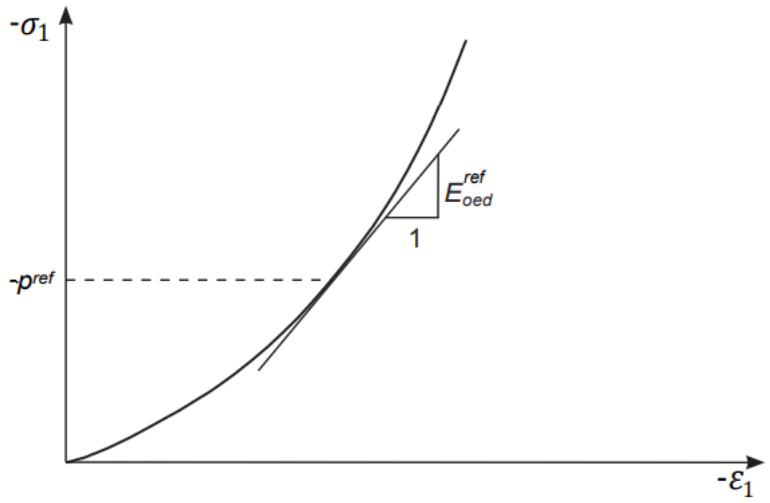

Figure 28: Definition of E_{oed}^{ref} (Bentley, 2021)

In the figure above, the negative sign assigned to stress and strain are due to the modelling convention in which compression is defined as negative and tension as positive.

The results obtained from oedometer tests performed on the three samples are shown in Figure 29, Figure 30, and Figure 31. The left graph in each figure displays the displacement vs. time readings taken directly from the oedometer apparatus, with the applied pressure indicated via the dotted lines (black for loading, red for unloading). The right graph in each figure shows the determination of E_{oed}^{ref} for each sample. The obtained values of E_{oed}^{ref} are listed in Table 7.

Table 7: Values of E_{oed}^{ref} for each sample, determined from the Oedometer tests.

Sample:	**Soil:**	**E_{oed}^{ref} [kPa]**
A	NA Clay Terp	4150
B	NA Peat Terp	4050
D	NA Clay Terp	4600

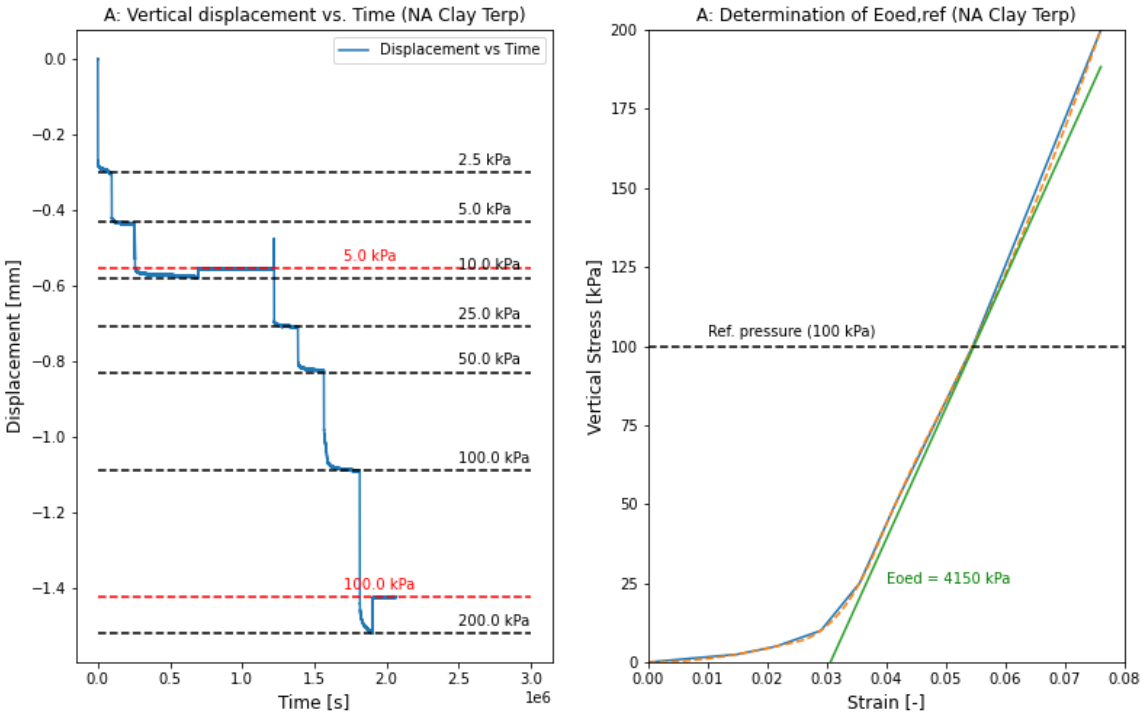

Figure 29: Sample A oedometer test readings (left) and E_{oed}^{ref} determination (right).

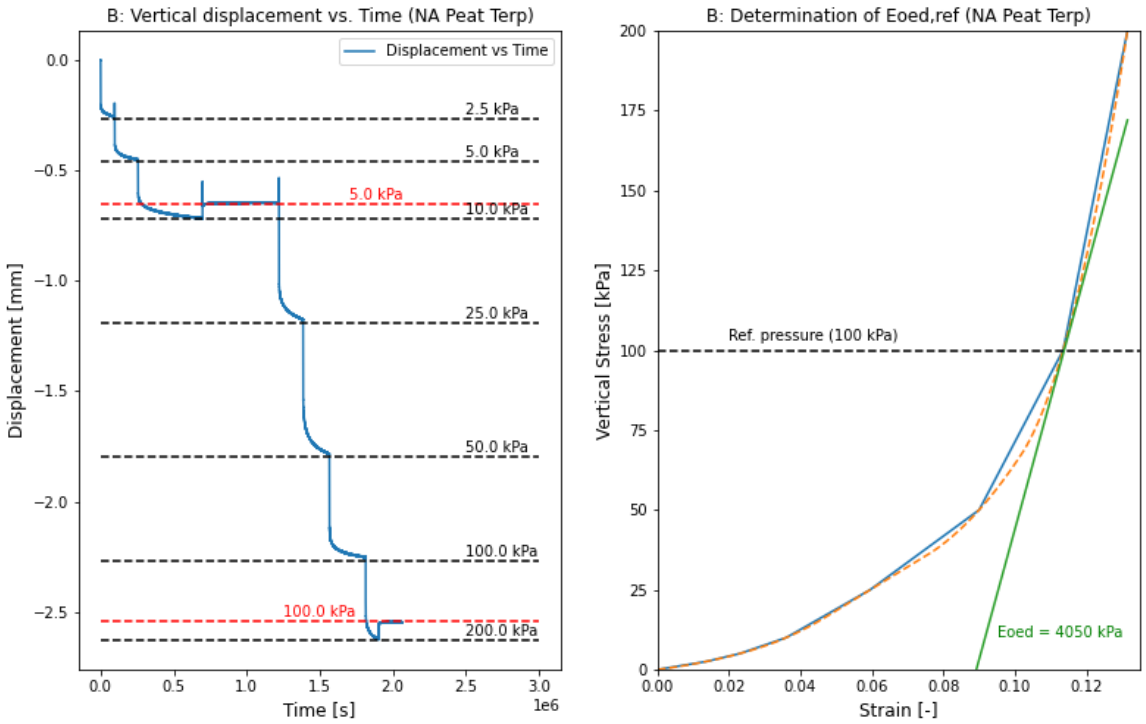

Figure 30: Sample B oedometer test readings (left) and E_{oed}^{ref} determination (right).

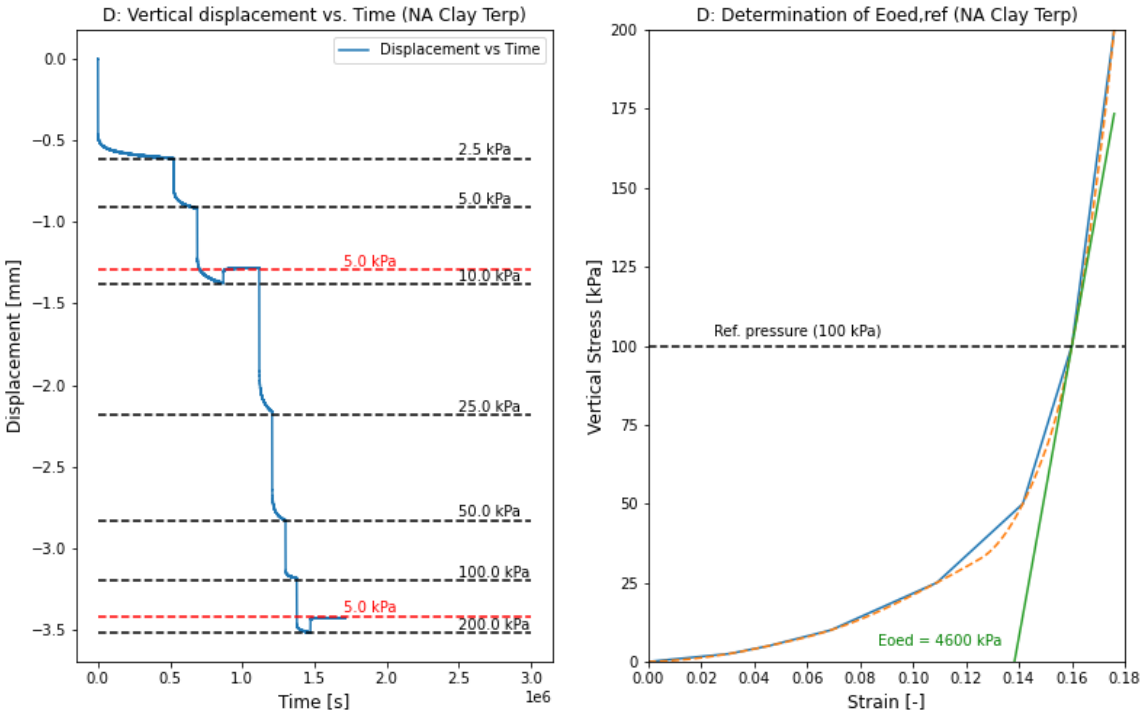

Figure 31: Sample D oedometer test readings (left) and E_{oed}^{ref} determination (right).

The stress vs. strain curves with stress expressed in logarithmic scale are shown in Figure 32. Compared to the results expected from oedometer test theory, the following can be noticed:

- The degree of overconsolidation decreases steadily with depth, with sample A being the most overconsolidated, sample B the second, and sample C seeming almost normally consolidated.
- Sample A displayed a larger settlement than expected during the first 3 loading steps (i.e., until the 10 kPa applied load).

- Sample B exhibited less settlement than expected during the last two loading steps (i.e., passed the 100 kPa applied load).
- Sample D showed less settlement than expected during the last 2 loading steps (i.e., passed the 50 kPa applied load).
- The unloading stiffnesses of the

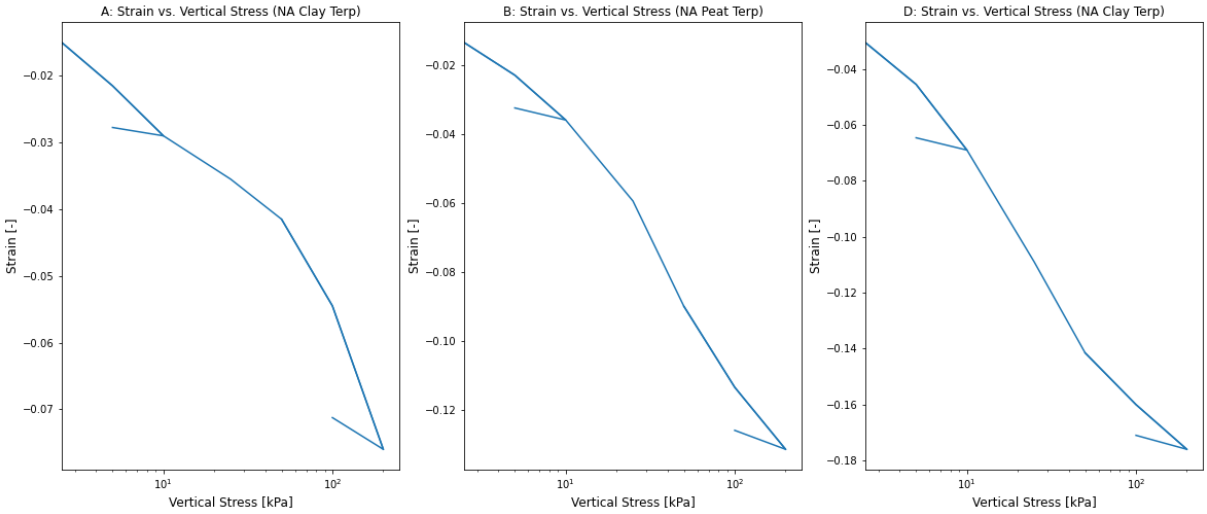

Figure 32: Stress vs. strain graphs for all samples, with stress expressed in log scale.

There are several explanations for the behaviour exhibited by the three samples, and the manner in which the results deviated from the expected theory to some degree. The unexpectedly higher settlement observed during the first 3 loading steps in sample A could be explained by the sample not reaching full saturation before loading. Despite the 48h saturation period to which all samples were subjected to (as suggested in literature), it is possible that more time was required for the clay sample A to reach full saturation. As unsaturated samples are expected to display an increased compressibility due to the presence of air within the pores, this would explain the initially lower stiffness displayed during the first 3 loading steps, which ended when full saturation was achieved.

The lower settlement than expected displayed by samples B and D during the last loading steps can be explained by the presence of foreign material within the samples. As discussed in subchapter 3.1.4, pieces of textiles, wood, ceramic, and masonry debris were found to be present within the soil throughout the borehole core. Although attempts were made to avoid these during sampling, it is very possible that small pieces of such objects were still present within the samples, decreasing the compressibility of the specimens as settlement increased and these interacted with the loading plate.

The fact that the degree of overconsolidation is shown to decrease with depth, however, is a trend that was expected based on conventional theory. Superficial layers are generally subjected to greater variations in loads, which do not affect deeper lying soils. Furthermore, deeper layers are subjected to a greater, constant weight of the overlying soil, thus contributing to a state of normal consolidation.

The oedometer tests were performed as a model validation exercise, and thus the obtained stiffness parameters will be referenced to in section 8.1 of this report, containing post-analysis considerations.

4.3 Empirical formulae

The empirical formulae presented in this subsection were used to obtain reference values for various geotechnical parameters required for the modelling phase.

4.3.1 Unit weight

The soil unit weight can be estimated based on the following formula proposed by Robertson & Cabal (2010):

$$\frac{\gamma}{\gamma_w} = 0.27\left(logR_f\right) + 0.36\left[log\left(\frac{q_t}{p_a}\right)\right] + 1.236 \qquad \text{(Robertson \& Cabal, 2010)}$$

In this formula, γ is the soil unit weight [kN/m^3], γ_w is the unit weight of water [kN/m^3], and R_f is the friction ratio [%]. Parameter q_t is the corrected cone resistance ($q_t = q_c + u2(1 - a)$) [MPa], q_c is the cone resistance [MPa], a is the net area ratio of the CPT cone, and p_a is the atmospheric pressure [MPa]. In absence of parameter a, the measured cone resistance (q_c) [MPa] can also be used.

4.3.2 Angle of internal friction

Campanella and Robertson (1983) proposed a correlation for estimating the peak friction angle for sands based on CPT readings:

$$\phi' = arctan\left(\frac{1}{2.68} * \left[log\left(\frac{q_c}{\sigma'_{v0}}\right) + 0.29\right]\right) \qquad \text{(Campanella \& Robertson, 1983)}$$

Mayne (1990) suggested an alternative relationship for estimating the friction angle in clean sands:

$$\phi' = 17.6 + 11 * logQ_{tn} \qquad \text{(Kulhawy \& Mayne, 1990)}$$

Mayne (2006) proposed a correlation for fine-grained materials, valid for $B_q > 0.1$:

$$\phi' = 29.5 * B_q^{0.121} * \left[0.256 + 0.336 * B_q + logQ_t\right] \qquad \text{(Mayne, 2006)}$$

In the formulae above, φ' is the angle of internal friction [°], σ_{v0}' is the effective vertical in-situ stress [MPa], Q_t is the normalized cone resistance (for non-varying stress exponent) [-], Q_{tn} is the normalized cone resistance (for varying stress exponent) [-], and B_q is the pore pressure ratio [-].

In absence of a reliable estimate of the stress exponent (n), Q_t can be applied instead of Q_{tn} in the formula proposed by Kulhway & Mayne (1990).

Robertson & Cabal (2010) also propose an assumed value of 28 ° for clays and 32 ° for silts, deemed sufficient estimates for many low-risk projects.

Initial estimates of the friction angle for each layer are provided in Figure 33. The left graph in the figure provides the calculated friction angle for each data point of the Fugro CPT DKMP1, from which a layer average value is determined and shown in the right graph.

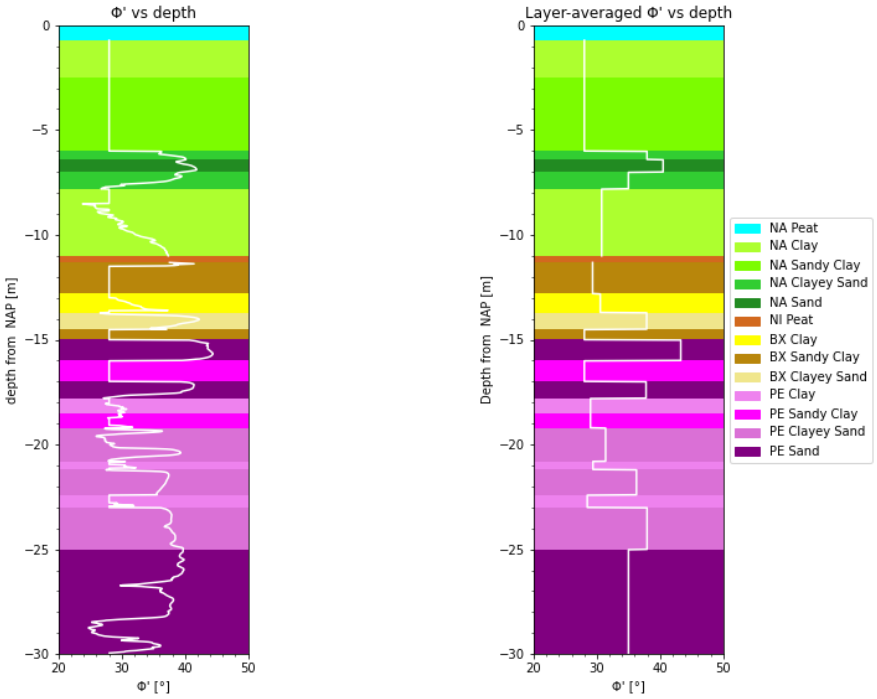

Figure 33: Friction angle vs. depth based on Campanella & Robertson (1983), Mayne (2006), and Robertson & Cabal (2010). Shown for each data point (left) and as a layer-averaged value (right).

The values were obtained by applying the formula proposed by Campanella & Robertson (1983) for layers in which sand is the dominant soil type, and that by Mayne (2006) for layers dominated by clay and for which $B_q > 0.1$. Layers for which clay is the dominant soil type, but $B_q \leq 0.1$, a value of 28 ° was applied as suggested by Robertson & Cabal (2010).

By observing the graphs presented Figure 33, it seems that application of the Campanella & Robertson (1983) formula results in particularly high friction angles for the sandy layers, with some even surpassing 40 °. Such high friction angle values are typically only observed in very dense sands.

Consequently, the same process was therefore repeated, but this time using the formula proposed by Kulhawy & Mayne (1990) for layers dominated by sand. The results are shown in Figure 34. Once again, the left graph shows the calculated value for the friction angle for each data point, while layer-averaged values are shown on the right graph.

While the range of values observed in Figure 34 seem more appropriate, one should still note that the use of empirical relationships should always be paired with adequate engineering judgement. In this case, for example, the use of formulae developed for clean sands should be applied with particular caution as all sand layers considered are in reality mixed with a silt or clay fraction at least to some degree. The obtained values therefore only serve as an initial reference in the parameter determination process.

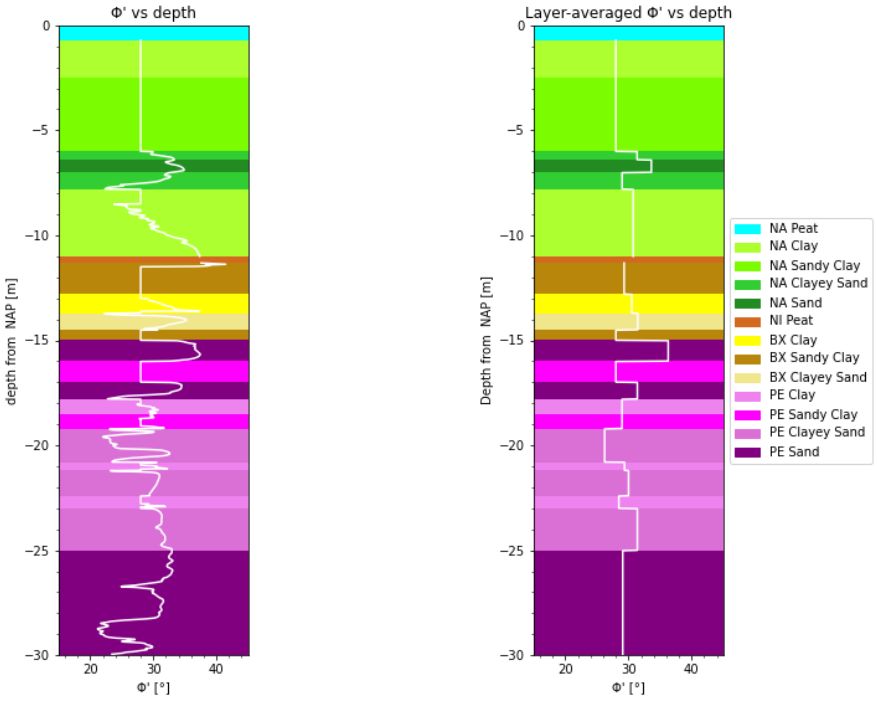

Figure 34: Friction angle vs. depth based on Kulhawy & Mayne (1990), Mayne (2006), and Robertson & Cabal (2010). Shown for each data point (left) and as a layer-averaged value (right).

The layer-averaged friction angle values plotted in Figure 33 and Figure 34 can be found listed in Appendix H.1 and Appendix H.2, respectively.

4.3.3 Shear wave velocity & stiffness modulus

The shear wave velocity (V_s) was estimated based on the formula proposed by Kruiver et al. (2021):

$$V_s = V_s = 359.0 \cdot qc^{0.119} \cdot f_s^{0.100} \cdot {\sigma'_{v0}}^{0.204} \qquad \text{(Kruiver et al., 2021)}$$

In this formula, f_s is the sleeve resistance (in MPa).

The shear stiffness modulus (G_0) was determined via the following relationship, based on shear wave velocity (V_s) and material density (ρ):

$$G_0 = \left(\frac{\gamma}{g}\right) \cdot V_s^2 = \rho \cdot V_s^2$$

This parameter was of particular importance not only for the modelling of the hysteretic behaviour of the soil, relevant for the dynamic analyses performed which are beyond the scope of this report, but also for the model calibration process described Appendix J.

4.4 Dutch Eurocode (NEN 9997-1)

In order to obtain a wider selection of reference geotechnical parameters, Table 2b from the Dutch annex of the Eurocode (NEN 9997-1) was also applied to the DKMP1 CPT. A copy of the Table 2b from NEN 9997-1 is provided in Appendix I.1.

The resulting values of the internal friction angle and cohesion are shown in Figure 35 and Figure 36, respectively. As shown in Figure 35, the obtained values of internal friction angle are significantly lower than those computed via the empirical formulae presented in the previous subsection, due to the more conservative nature of the Eurocode methods. This is also reflected in the cohesion values presented in Figure 36.

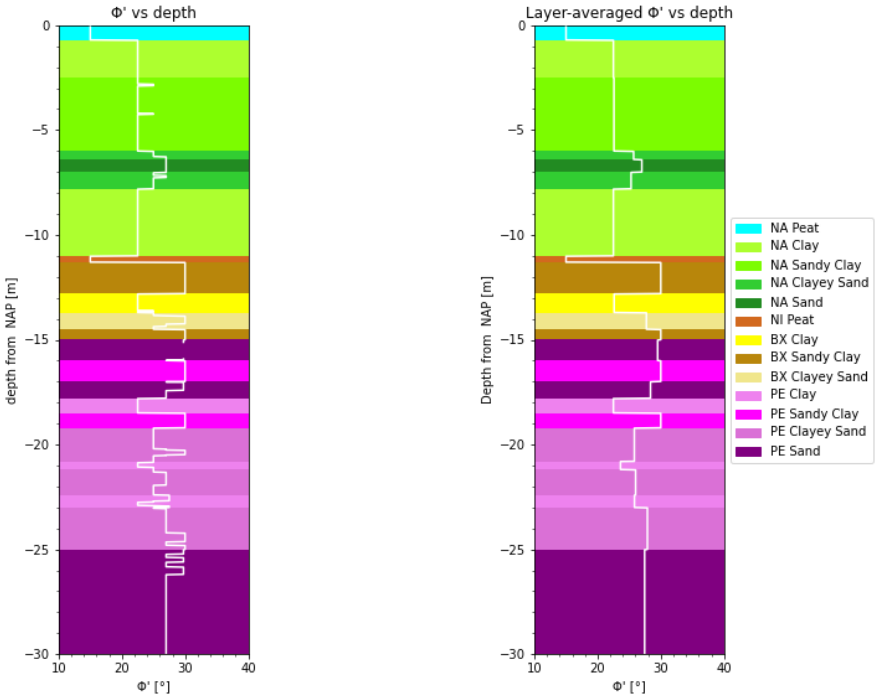

Figure 35: Friction angle for each layer, determined via Table 2b of NEN 9997-1.

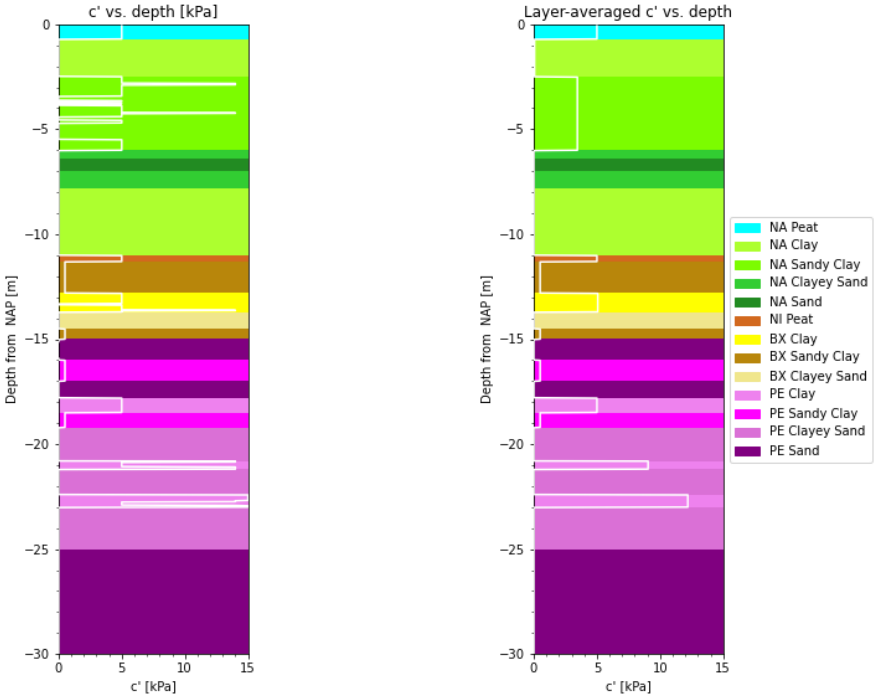

Figure 36: Cohesion for each layer, determined via Table 2b of NEN 9997-1.

The application of Table 2b from NEN 9997-1 also provided reference values for soil stiffness, in the form of the E-Modulus (E_{100}) for each layer, shown in Figure 37. This version of the E-modulus represents the stiffness of a soil subjected to a vertical effective stress of 100 kPa.

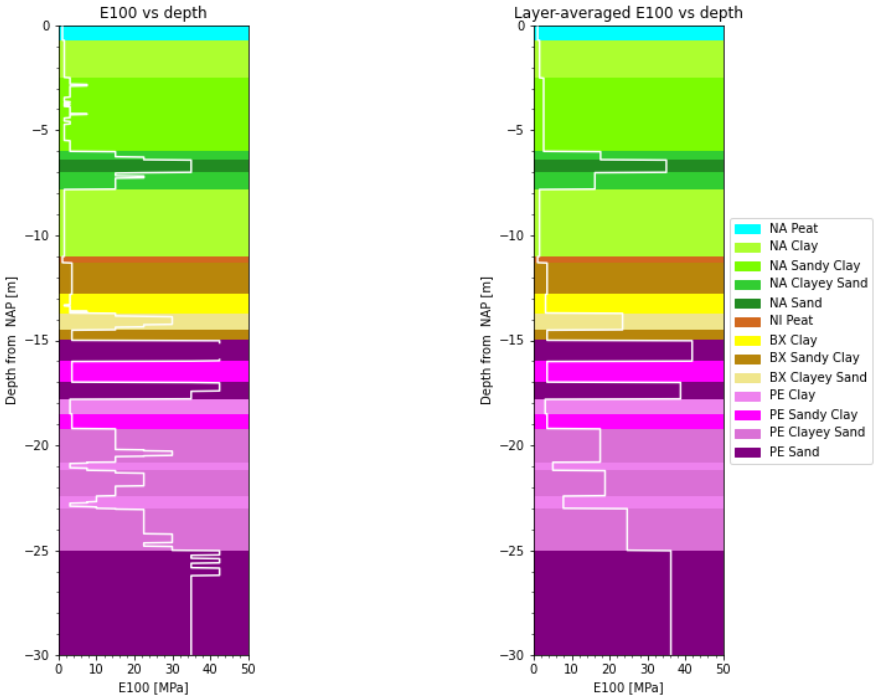

Figure 37: E-modulus (E_{100}) for each layer, determined via Table 2b of NEN 9997-1

This E_{100} form of the E-modulus, however, is not directly applicable in the Hardening Soil (HS) model used for the analyses in this project. In an attempt to obtain at least a rough estimate for the magnitude of the stiffness parameters applicable in the HS model, the E_{100} values were equated to the E_{oed}^{ref} parameter of the HS model, being the oedometer stiffness at a reference vertical effective stress of 100 kPa. From this, the other HS model-specific stiffness parameters E_{50}^{ref} and E_{ur}^{ref} were estimated based on the rule-of-thumb formulae proposed in the PLAXIS Material Models manual (see section 5). The layer-averaged HS model stiffness values obtained from this process are shown in Figure 38.

It is important to note that, in reality, E_{100} and the E_{oed}^{ref} stiffness moduli are not directly interchangeable, despite both being values of stiffness at a reference vertical effective pressure of 100 kPa. While the E_{100} parameter is intended to represent the stiffness of a soil in in-situ conditions, the E_{oed}^{ref} is an oedometer stiffness and therefore represents the stiffness of a laterally constrained soil. Consequently, the E_{oed}^{ref} should be larger than the E_{100} for the same vertical effective stress, and equating the two would results in a conservative estimate of the E_{oed}^{ref}. The degree to which the two forms of E-moduli differ should increase with the increasing compressibility of the (surrounding) soils.

The stiffness parameters presented in Figure 38 should therefore only be seen as reference lower bound values.

The layer-averaged values of all parameters determined using Table 2b from NEN9997-1 are listed in Appendix I.2

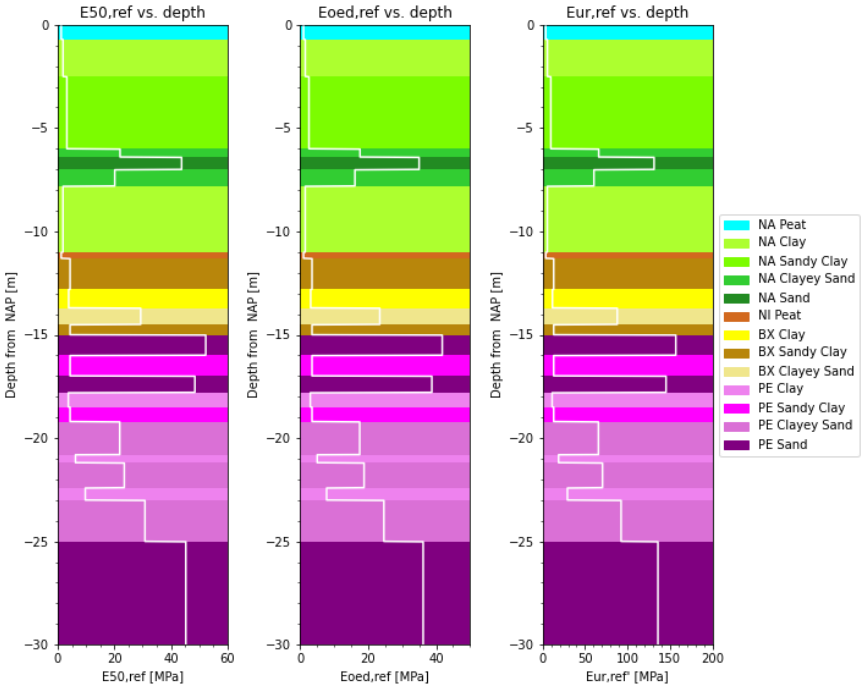

Figure 38: Lower bound estimates of the HS stiffness parameters.

5 Computational models

The software used for all computational models in this project was PLAXIS Connect Edition V21. Depending on the specific model, PLAXIS 2D or PLAXIS 3D was used. A total of 6 models were made, through which 16 scenarios were analysed.

Out of the 6 total models, 5 were designed in 2D and 2 were designed in 3D.

5.1 2D Models

The models used for the 2D static stability analyses contained 2 terp and subsoil characterizations (Westeremden & Toornwerd) and 4 different terp geometries, combined into 5 total models exploring 14 scenarios (see subsection 5.7 for an overview of all scenarios).

For all 2D models, plane-strain conditions were applied. In such conditions, the analysis assumes an infinite length in direction normal to the plane section of the model, and strains in this direction are zero.

5.1.1 Subsoil models

The subsoil in the computational models was defined up to the same maximum depth as that measured by the Westeremden CPTs. Although considering a smaller depth would have made no difference for static analyses, these same subsoil models were used for dynamic analyses (outside the scope of this report), for which larger depths were required. Consequently, the soil layers were modelled from +0 m NAP to -30 m NAP, plus an additional 3 m of high stiffness, linear elastic material representing the bedrock. One should note that this modelled bedrock is not the actual geological bedrock, but rather one based on the assumption that the soil found 30 m below ground has a very high stiffness and is almost non-deformable compared to the soil above. Including this 'bedrock', the subsoil models were thus defined from +0 m NAP to -33 m NAP. The soil layers in all models were designed as horizontal layers, and the +0 m ground level was obtained from the digital elevation map Actueel Hoogtebestand Nederland (AHN).

The stratigraphic arrangement of the soil layers for the Westeremden subsoil models is that of the soil profile provided in subsection 4.1.3, which itself was based on the DKMP1 CPT provided by Fugro.

The Toornwerd subsoil profile was made based on the DINOloket borehole (B07B0119) interpretation and CPT (S07B00261), and followed the soil profile provided in Appendix E.3.

It should be noted that the single CPT available for the Toornwerd terp only reached a depth of approximately -21 m NAP. However, based on the information obtained from the stratigraphic cross-sections presented in subsection 3.2.2, the bottom layer of PE clay was extended to -30 m NAP, once again based on requirements related to the dynamic analyses.

The two subsoil models, and the data used as reference, are listed in Table 8.

Table 8: Reference data for the final subsoil models.

Subsoil Model Label	**Reference source data**
Westeremden "ref"	Fugro CPT (1317-0440-000_DKMP1_000)
Toornwerd "new"	DINOloket CPT (S07B00261) & borehole (B07B0119)

The resulting final subsoil models are shown in Figure 39, in which the Westeremden model stratigraphy is given on the left, and the Toornwerd model stratigraphy on the right. These are screenshots of the soil profiles defined in PLAXIS.

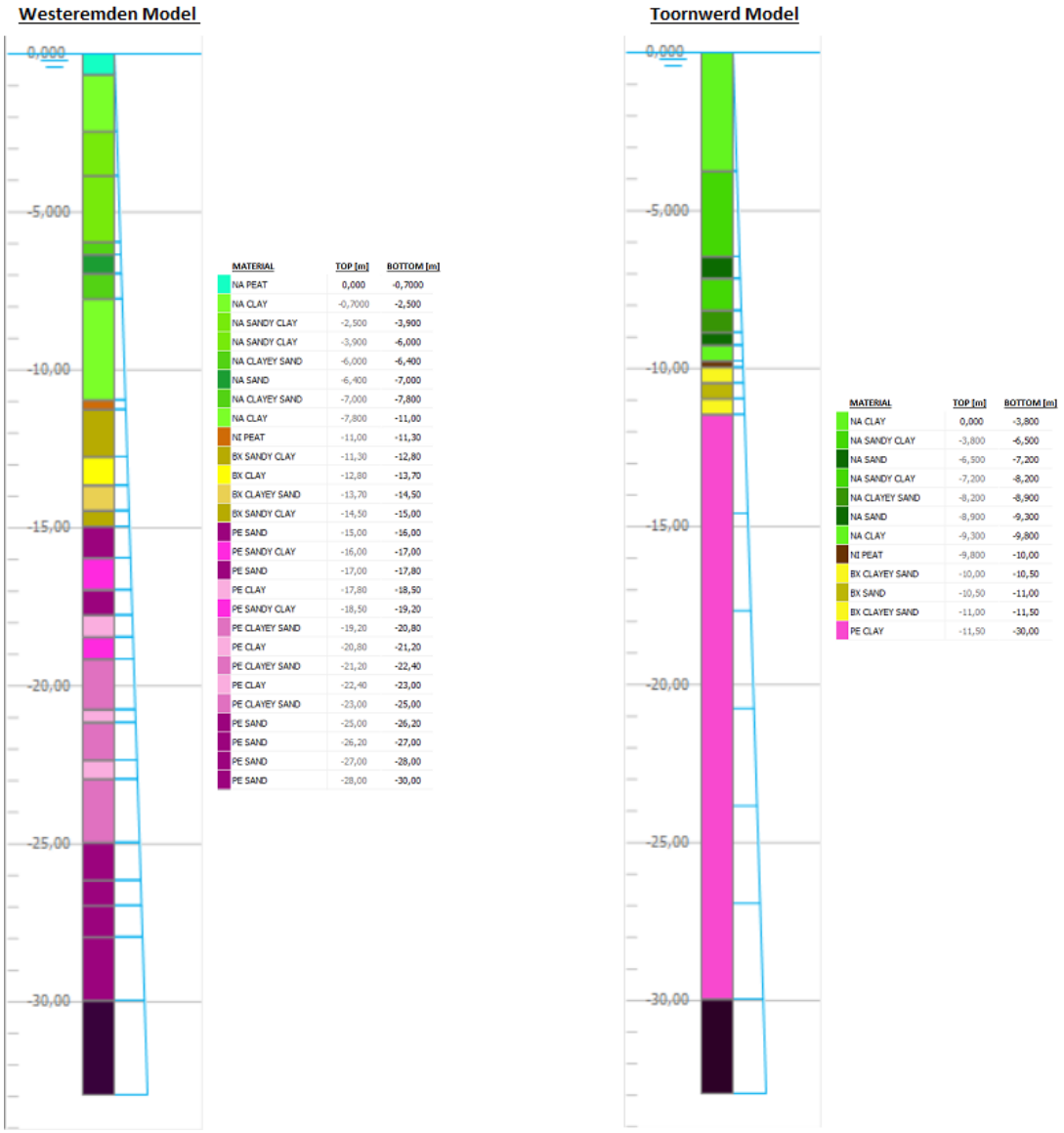

Figure 39: Soil stratigraphy for Westeremden "ref" model (left), and the Toornwerd "new" model (right)

The groundwater level in the model was estimated graphically from the pore pressure readings provided in the Fugro CPTs and was determined to be in proximity of the ground surface. In absence of field data, the most conservative scenario was considered, setting the ground water level equal to the ground surface level in all models.

The lateral extension of the subsoil was set such that free field conditions could be reproduced, meaning that the location of the boundaries do not affect the results of the analyses performed on the slopes. As a conservative estimate, the model was extended by 100 m on both sides of the terp, measured from the toe of each slope. Including the added 70 m separation between the terp slopes (see subsection 5.2.2), the total lateral extension of the subsoil amounted to 270 m.

The material properties assigned to the various soil layers, and the manner in which these were determined, are outlined in section 5.5.

5.1.2 Terp models

For the terp itself, various geometries, applied to multiple subsoil compositions, were considered. Following the selection of Westeremden and Toornwerd as reference terps, four different slope

geometries were defined and applied to the subsoil models as indicated in Table 9. As the ground level was defined at +0 m NAP, the slope heights also indicate their peak elevation with respect to the NAP.

Table 9: Reference geometries of the 2D PLAXIS models

Reference Terp Model Label	Reference geometry	Height [m]	Inclination [°]
Westeremden "ref"	Large height, medium slope	5	35
Westeremden "ref"	Medium height, steep slope	4	45
Toornwerd "new"	Medium height, medium slope	4	36
Westeremden "ref"	Large height, quasi-vertical cut	5	80

The first reference geometry was established by considering the steepest slope of the Westeremden terp (M900 #1 in Figure 6 of this report), but then increasing the slope height to 5 m in order represent the most unfavourable terp conditions that can realistically be found in practice. The less steep slopes at the crest of the steep parts of Westeremden terp edges were also covered in this height overestimation.

A similar concept was applied to the second reference geometry, although the slope inclination was increased to 45°, while the slope height was reduced to 4 m.

The third reference geometry was based on the steepest slopes of the Toornwerd terp (M884 #4 and M884 #6 in Figure 13 of this report).

The fourth geometric case involved a quasi-vertical slope, applied to the Westeremden terp. This geometry was added due to evidence suggesting that such slopes have been cut into existing terps during archaeological studies, and thus an analysis of the stability of these was considered relevant.

For each of the reference geometries, 2D static analyses were performed, each with multiple scenarios involving long-term stability, the presence of loads, ditches (see next subsection) and in some cases, different modelling of the subsoil (see the definition of scenarios presented in subsection 5.7 of this report).

The actual terp layer compositions are shown in Figure 40, with the Westeremden "ref" terp shown on the left, and the Toornwerd "new" model shown on the right. Regarding this characterization of the terp layers, the following should be noted:

- The Westeremden terp layers were based on the borehole sample interpretation provided in subsection 4.1.3. The layer of undefined soil separating two peat layers was characterized as peat of the same composition as the layers around it.
- The Toornwerd terp layers were defined based on the information available from the archaeological investigations mentioned in subsection 3.2.4, which provided a basic description of the soils found within the terp. This model therefore does not provide a reliable representation of the Toornwerd terp soil composition, but only serves as a comparative tool to observe the effects of a different geometry and soil composition compared to the more reliably modelled Westeremden terp.

The specific properties of the soil materials shown are provided in subsection 5.4.

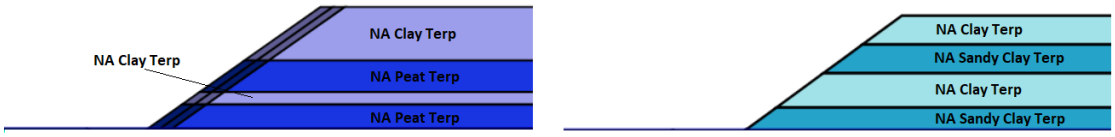

Figure 40: Terp layer composition in the Westeremden "ref" (left), and Toornwerd "new" models

Finally, the characterization of the water table inside the terp is shown in Figure 41, below.

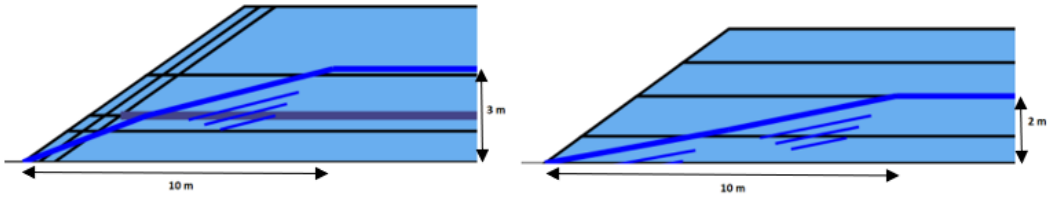

Figure 41: Water table characterization in the Westeremden "ref" (left), and Toornwerd "new" models

For each model, the terp itself was shaped as a symmetric hill, featuring identical slopes on each side. In order to isolate the mechanisms of each slope, and thus ensure that the two did not interact with one another, these were separated by a distance of 70 m.

Note that the diagonal structures adjacent to the terp slope in the Westeremden models were initially made to allow for the characterization of the stabilizing effects of grass, roots and generic small vegetation present on the slope. In the end, however, these effects were not included and thus soil properties were kept the same within layers, resulting in more conservative models.

5.1.3 Ditches

Based on the presence of ditches adjacent to the terp slopes, as observed in subsections 3.1.1 and 3.2.1, these were explicitly inserted into the computational models in order to evaluate their influence on the stability of the slopes. Figure B.4 shows the geometries of the ditches represented in the models.

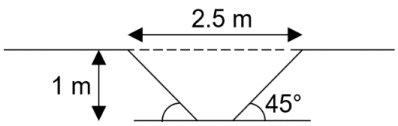

Figure 42: Geometry of modelled ditches.

5.2 3D Models

The 3D models made only concerned the Westeremden subsoil and terp layers, for which 2 models were made analysing 2 total scenarios.

5.2.1 Subsoil models

The 3D computational models feature the same subsoil composition as the 2D, Westeremden “ref” models. Since the 3D models involve static analysis only, however, the maximum depths requiring to be considered are significantly reduced. Consequently, the extension of the subsoil for the 3D models was cut to NAP – 22.4 m, in order to reduce the computational time and memory used, while maintaining a large enough domain to allow for unaffected results and a consistent definition of the water table throughout the models.

For the lateral extension of the 3D models, a domain 100 m x 100 m was applied. This was considered sufficiently large in comparison to the size of the modelled slopes, given that no dynamic calculations were performed for these models. Symmetry was used to only feature one slope in the 3D models.

In this case too, the scenarios have been constructed with the assumption of parallel and horizontal subsoil layers.

5.2.2 Terp models

The terps modelled in the 3D scenarios consist of two types, one with a convex circular slope, and another with a concave circular slope. A geometrical configuration similar to the former one was encountered in Westeremden. While concave flanks have also been observed in Westeremden, these are more angular than circular. Both models feature a slope height of 5 m and inclination of 35°, and the same subsoil definition (see previous subsection). The described convex and concave slopes are shown in Figure 43.

The circular shape of the two slopes is defined by a top and a base radius. The models were made in such a way that the base radius of the concave model is equal to the top radius of the convex model, and vice versa. The properties of the two slopes are summarized in Table 10.

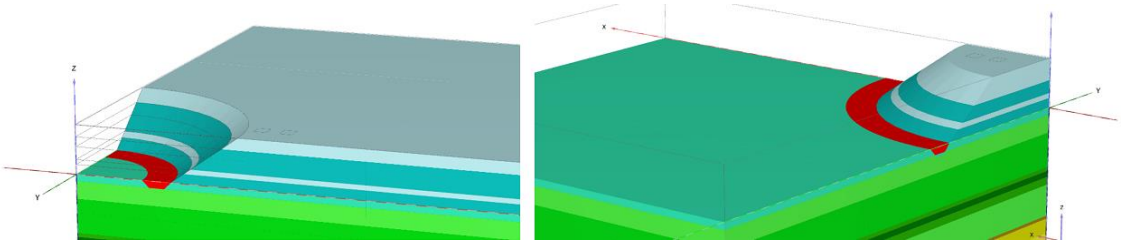

Figure 43: Concave (left) and convex (right) 3D models of terp slope, with highlighted ditches (red)

Table 10: Reference geometries of the 3D PLAXIS models:

Reference Terp Model Label	Reference geometry	Slope base radius [m]	Slope top radius [m]	Height [m]	Inclination [°]
Westeremden “ref1”	Convex	17	10	5	35
Westeremden “ref2”	Concave	10	17	5	35

5.2.3 Ditches

The ditches defined in the 3D models have the same cross sections as those for the 2D models but are extended along the circumference of the base of the 3D slope, defined by the base radii. This can be seen in Figure 43, in which the ditches have been highlighted in red.

5.3 Boundary conditions

The boundary conditions applied to all models consisted in displacement and hydraulic head fields conditions, applied to the lateral and two vertical boundaries (top and bottom) of the models. The number of lateral boundaries depends on whether it is a 2D, for which 2 lateral boundaries are present, or a 3D model being considered, for which the total number of lateral boundaries amounts to 4.

On the lateral boundaries, the following displacement and hydraulic conditions were set:

- Displacements in horizontal direction were set to zero (normally fixed) for both the left-most and right-most nodes.
- Open boundaries were set for the left-most and right-most nodes alike, allowing for hydraulic flow in both horizontal and vertical directions.

The vertical boundaries featured the following displacement and hydraulic conditions:

- Displacements in both horizontal and vertical directions were set to zero (fully fixed) for all nodes on the bottom edge.
- A closed boundary was set for all nodes on the bottom edge, allowing for no hydraulic flow.
- Displacements in both horizontal and vertical direction were unrestricted for all nodes on the top edge (free surface).
- An open boundary was set to all nodes on the top edge, allowing for hydraulic flow in both horizontal and vertical directions.

5.4 Materials

5.4.1 Material model

All analyses in this project were performed using the Hardening Soil model with small-strain stiffness (HSsmall). This a modification of the Hardening Soil model that accounts for increased stiffness of soils at small strains (Bentley, 2021). This model was chosen in favour of the traditional Hardening Soil model as it also accounts for hysteretic material damping in dynamic analyses. For the types of static analyses this model also allows to better represent the behaviour in zones of low strain levels but high stiffnesses (e.g., at a distance from loading), although the difference in results between the two should be minute.

The Hardening Soil model is an advanced model which integrates all the parameters describing limiting states of stress as described by the basic Mohr Coulomb (MC) model (friction angle, ϕ, cohesion, c, and dilatancy angle, ψ), while also accounting for the stress-dependency of stiffness moduli (Bentley, 2021).

Unlike the linear elastic perfectly-plastic MC model, the HS model also incorporates hardening plasticity theory to account for plastic deformations, allowing the yield surface to expand as a result of plastic straining (Bentley, 2021). This results in a much more realistic characterization of soil behaviour. All input parameters required for the HSsmall model are presented in Table 11, as listed in the PLAXIS Material Models manual.

Table 11: Parameters for the Hardening Soil with small strain stiffness model (Bentley, 2021)

Symbol	Description	Units
c'	(Effective) cohesion	$[kN/m^2]$
ϕ'	(Effective) angle of internal friction	[°]
ψ	Angle of dilatancy	[°]
σ_t	Tension cut-off and tensile strength	$[kN/m^2]$
$E_{50,ref}$	Secant stiffness in standard drained triaxial test	$[kN/m^2]$
$E_{oed,ref}$	Tangent stiffness for primary oedometer loading	$[kN/m^2]$
$E_{ur,ref}$	Unloading / reloading stiffness from drained triaxial test	$[kN/m^2]$
m	Power for stress-level dependency of stiffness	$[-]$
$G_{0,ref}$	Reference shear modulus at very small strains ($\epsilon < 10^{-6}$)	$[kN/m^2]$
$\gamma_{0.7}$	Threshold shear strain at which $G_s = 0.722\ G_0$	$[-]$
ν_{ur}	Poisson's ratio for unloading / reloading (default $\nu_{ur} = 0.2$)	$[-]$
p_{ref}	Reference stress for stiffnesses (default $p_{ref} = 100\ kPa$)	$[kN/m^2]$
$K_{0,NC}$	K0 -value for normal consolidation (default $K_{0,NC} = 1 - \sin\phi'$)	$[-]$
R_f	Failure ratio q_f/q_a (default $R_f = 0.9$)	$[-]$
$\sigma_{tension}$	Tensile strength (default $\sigma_{tension} = 0$)	$[kN/m^2]$
c_{inc}	Increase of cohesion with depth (default $c_{inc} = 0$)	$[kN/m^3]$
POP	Pre-Overburden Pressure	$[kN/m^2]$

The PLAXIS Material Models manual also provides the following rules of thumb regarding the stiffness parameters (E_{50}^{ref}, E_{oed}^{ref}, E_{ur}^{ref}) and the stress-dependency of stiffness exponent (m):

$m = 0.5\ (sands)$

$m = 1.0\ (clays)$

$E_{50}^{ref} = 1.25 * E_{oed}^{ref}$

$E_{ur}^{ref} = 3 * E_{50}^{ref}$

5.4.2 Subsoil materials

The material properties assigned to the subsoil layers were determined based on a combination of the reference values produced in section 4, reference values from literature, and engineering judgement. Piunno (2021) also proposed a calibration method with which to estimate a number of HS model parameters from a shear stiffness modulus (G_0) profile, derived from CPT readings (see Appendix J).

The resulting material model input parameters obtained from this process are presented in Table 12 and Table 13 for Westeremden and Toornwerd subsoils, respectively. For convenience, only the parameters relevant for the static analyses are given. Stiffness values have been rounded to the nearest hundred. All parameter units are as defined in Table 11.

Table 12: HSsmall model parameters applied to the Westeremden subsoil model.

Material	γ	E_{50}^{ref}	E_{oed}^{ref}	E_{ur}^{ref}	m	c'	φ'	ψ	G_0^{ref}	ν_{ur}	POP
NA Peat	12	3800	3000	11400	1.00	5	35	0	35000	0.3	20
NA Clay	12.9	5000	4000	14900	1.00	5	23	0	40000	0.3	20
NA Sandy Clay	16.2	8670	7000	26000	0.85	2	26	2	50000	0.3	20
NA Clayey Sand	16.2	18420	14700	55300	0.70	1	28	2	85000	0.3	20
NA Sand	21	34700	27700	104000	0.55	0	32	6	120000	0.3	20
NI Peat	14.1	9900	8000	29700	1.00	5	35	0	80000	0.3	20
BX Clay	14.4	7400	6000	22300	1.00	5	25	0	60000	0.3	-
BX Sandy Clay	16.9	32500	26000	97500	0.80	2	27	2	150000	0.3	-
BX Clayey Sand	16.9	43300	34700	130000	0.70	1	29	2	200000	0.3	-
PE Clay	17.6	6900	5500	20800	1.00	5	27	0	40000	0.3	-
PE sandy Clay	18.1	23800	19100	71500	0.70	2	28	2	110000	0.3	-
PE Clayey Sand	18.1	32500	26000	97500	0.60	1	30	2	150000	0.3	-
PE Sand	21	72200	57800	216700	0.50	0	36	6	250000	0.3	-

Table 13: HSsmall model parameters applied to the Toornwerd subsoil model.

Material	γ	E_{50}^{ref}	E_{oed}^{ref}	E_{ur}^{ref}	m	c'	φ'	ψ	G_0^{ref}	ν_{ur}	POP
NA Clay	12.9	3800	3100	11500	1.00	6	24	0	31000	0.3	20
NA Sandy Clay	16.2	5800	4600	17300	0.85	2	26	2	40000	0.3	20
NA Sand	21	28900	23100	86700	0.55	0	32	6	100000	0.3	20
NA Clayey Sand	16.2	13000	10400	39000	0.70	1	28	2	60000	0.3	20
NI Peat	14.0	9900	7900	29700	1.00	5	35	0	80000	0.3	0
BX Clayey Sand	16.9	32500	26000	97500	0.80	2	27	2	150000	0.3	0
BX Sand	20.0	54200	43300	162500	0.60	0	29	6	250000	0.3	0
PE Clay	17.6	6900	5500	20800	1.00	5	27	0	40000	0.3	0

5.4.3 Terp layer materials

As mentioned in subsection 4.2, a series of laboratory and index tests were performed along an 8 m borehole core taken on top the Westeremden terp. Among these, those used to estimate the undrained shear strength at various depths were of particular use for the characterization of the terp layers modelled in PLAXIS. With the use of PLAXIS SoilTest, a function which allows to simulate standard soil tests, it was in fact possible to reverse-engineer drained parameters from the undrained ones obtained in the laboratory.

Specifically, this involved the following process for each of the two terp layer materials:

1. Assign initial drained parameters for the layer considered, being:
    a. Friction angle (ϕ')
    b. Cohesion (c')
2. Simulate undrained triaxial and direct simple shear tests using PLAXIS SoilTest, which allows for the simulation of undrained tests using the provided drained parameters and the default bulk density of water automatically considered in PLAXIS.
3. Compare the simulated undrained shear strengths to those obtained in the laboratory.
4. Modify the initial drained parameters and repeat the process.

The cell pressure and initial stress used for the undrained triaxial and DSS tests simulations, respectively, were those calculated in the middle of each layer considered. Screenshots of the PLAXIS SoilTest interfaces can be found in Appendix G.

The results, however, suggested values of effective friction angle and cohesion that were unrealistically high for the soil types considered. For precaution, values for drained parameters were taken such that the corresponding simulated undrained shear strengths approached the lab values as much as possible, while still being limited to what was considered a reasonable maximum. The assigned values resulting from this process are shown in Table 14. The table also includes the stiffness values assigned to the terp layers, which were based on reference values for the soil types concerned (and later validated as discussed in section 8.1).

Table 14: Assigned drained parameters from undrained shear strength

Layer name	**Lab Cu [kN/m^2]**	**ϕ' [°]**	**c'$_{ref}$ [kN/m^2]**	**E_{50}^{ref} [kN/m^2]**	**E_{oed}^{ref} [kN/m^2]**	**E_{ur}^{ref} [kN/m^2]**
NA Peat Terp	50	35	12	4000	3500	12000
NA Clay Terp	30	25	11	5000	4000	15500

The high values of undrained shear strength measured in the lab tests can be explained by the heterogeneity of the anthropogenic soil. The real soil material present in the Westeremden cores is considerably more mixed and heterogeneous than the idealized clay and peat layers represented in the model, with plenty of debris and foreign objects as described in subsection 3.1.4.

5.5 Agricultural machine loads

Based on the information presented in subsection 2.3, the loading scenarios included in the static analyses involved simulating the presence of heavy agricultural machinery operating in proximity of the slope top edges. The derivation of the loads applied in the models can be found in Appendix A.1.

In the PLAXIS models, the application of the machine loads was applied in such a way as to simulate a combine harvester operating parallel to the terp edge along the slope, at a distance of 0.5 m from the edge. The applied distributed loads for the 2D models can be seen in Figure 44, and the discussed characteristics are summarized in Table 15.

The load distribution width of 1.3 m is a result of the 45% increase in contact area, and the 1.4 m spacing follows from subtracting twice this amount (2 wheels) from the total width of the combine harvester wheel span (see Appendix A.1).

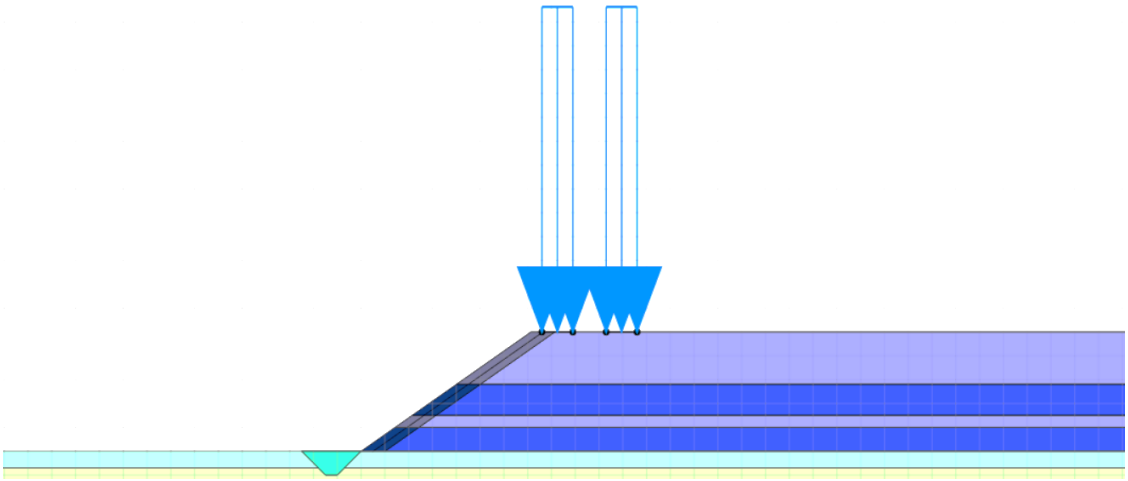

Figure 44: Distributed loads applied to all 2D models.

Table 15: Summary of distributed loads characteristics (2D)

Load magnitude	40 kN/m/m
Distance from slope edge	0.5 m
Load distribution width	1.3 m
Spacing between loads	1.4 m

For the two 3D models, a combine harvester length of 9 m was used, as given by the technical specifications of the John Deere S790 model. For the modelling of the 4 wheels themselves, symmetry was used in such a way that only two wheel loads had to be modelled, as these were placed 4.5 m (centre-line) from the axis of symmetry of the 3D model (y = 0 m). The opposite two wheels are thus implicitly accounted for by the FEM program. The applied distributed loads for the 3D models can be seen in Figure 45.

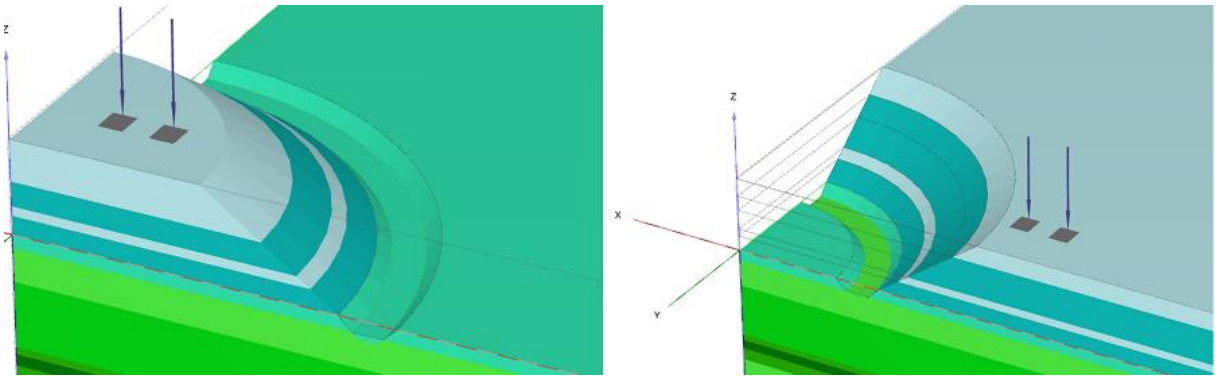

Figure 45: Distributed loads applied to the 3D models (convex left, concave right)

5.6 Construction stages

The static stability analyses performed on all models involved multiple construction stages, the stability of each of which is verified during the calculation phase. For the construction stages for which the degree of stability needs to be quantified, a safety calculation is initiated in order to determine the related safety factor by means of the shear strength reduction method (ϕ & c reduction).

Each construction stage can be performed under drained or undrained conditions. Drained conditions were applied to all stages representing long-term processes, thus for which any excess pore pressures developed during said stage would be dissipated by the beginning of the next stage.

The construction stages applied to all models were the following:

1. Terp construction: layer 1 (drained).
2. Terp construction: layer 2 (drained).
3. Terp construction: layer 3 (drained).
4. Terp construction: layer 4 (drained).
5. New ground water conditions (drained).

All or some of these additional construction stages were then performed, depending on the specific scenarios defined for each model:

- Excavation of the ditch (drained).
- Agricultural vehicle loading (undrained).
- Excavation of a steep slope (undrained).

Safety calculations were performed for all of the additional construction stages, thus determining the safety factors. In the case of the undrained excavation of the steep slope, a 30-day consolidation period was also added, followed by another strength reduction calculation. This allowed to assess both the short-term and the long-term stability of the steep excavation.

5.7 Overview of scenarios

The stability analyses in this project were performed for several scenarios, which differed in some or all of the following properties:

- Model dimensions: 2D and 3D scenarios were considered.
- Subsoil composition: Westeremden vs. Toornwerd subsoil models (see subsections 5.1.1 for 2D and 5.2.1 for 3D models).
- Terp soil composition: Westeremden vs. Toornwerd terp models (see subsections 5.1.2 for 2D and 5.2.2 for 3D models).
- Terp slope geometry: different slope heights and inclinations (see subsections 5.1.2 for 2D and 5.2.2 for 3D models).
- Presence of a ditch: presence or absence of a ditch at the toe of the slope (see subsections 5.1.3 for 2D and 5.2.3 for 3D models).
- Loading conditions: presence or absence of agricultural vehicle loads (see subsection 5.5).
- Unsaturated conditions: accounting or not for the unsaturated zone above the groundwater level.

Unsaturated conditions enhance stability due to favourable suction stresses in the unsaturated zone, provided by surface tension of the groundwater. In PLAXIS, this effect can easily be modelled by unchecking the “Ignore suction” option.

As specified in section 5, a total of 16 scenarios were considered for static analyses, distributed among 6 models. Of these, 4 models were made for 2D calculations, analysing 14 scenarios, and 2 were made for 3D analyses, involving 2 scenarios. These are summarized in Table 16. For convenience, the scenario numbering is consistent with that of the report delivered to RCE. As only static stability analyses are considered in this thesis, the scenarios dedicated to dynamic analyses are marked in grey.

Table 16: Overview of all scenarios considered.

N°	Dimensions	Subsoil	H [m]	Slope [°]	Ditch	Vehicle Loads	Terp	Unsaturated conditions	Type
1	2D	ref	5	35	no	no	ref	no	static
2	2D	ref	5	35	no	yes	ref	no	static
3	2D	ref	5	35	no	no	ref	no	dyn.
4	2D	ref	5	35	yes	no	ref	no	static
5	2D	ref	5	35	yes	yes	ref	no	static
6	2D	ref	5	35	yes	no	ref	no	dyn.
7	2D	ref	5	80	no	no	ref	no	static
8	2D	ref*	5	35	yes	no	ref	no	dyn.
9	2D	ref**	5	35	yes	no	ref	no	dyn.
10	2D	simp.	5	35	no	no	ref	no	dyn.
11	2D	simp.	5	35	no	no	simp.	no	dyn.
12	2D	ref	4	45	no	no	ref	no	static
13	2D	ref	4	45	yes	no	ref	no	static
14	2D	ref	4	45	yes	yes	ref	no	static
15	2D	ref	4	45	yes	no	ref	no	dyn.
16	2D	new	4	36	no	no	new	no	static
17	2D	new	4	36	no	yes	new	no	static
18	2D	new	4	36	yes	no	new	no	static
19	2D	new	4	36	yes	yes	new	no	static
20	2D	new	4	36	yes	no	new	no	dyn.
21	2D	ref	5	35	yes	no	ref	yes	static
22	2D	ref	5	35	yes	yes	ref	yes	static
23	3D	ref	5	35	yes	yes	ref1	no	static
24	3D	ref	5	35	yes	yes	ref2	no	static

The labels assigned to the subsoil and terp types are as defined throughout section 5, but listed below for convenience (for the static analyses only):

- Subsoil:
  - “ref”: Westeremden subsoil model derived from the interpretation of the Fugro DKMP1 CPT.
  - “new”: Toornwerd subsoil model derived from the interpretation of the DINOloket CPT S07B00261 and borehole B07B0119.
- Terp:
  - “ref”: Westeremden terp soil model based on the borehole sample provided by RCE.
  - “new”: Toornwerd terp soil model based on the soil layers described in literature.

6 Results

The results of every scenario are presented in this chapter through Figures 46 to Figure 61. For each scenario, a table containing the summary of its characteristics and computed Safety Factor is provided, followed by an image indicating the most critical failure mechanism.

The failure mechanism is portrayed by shading of displacement increments over the domain, in which larger displacements are represented by an increasingly warmer hue (i.e., red). For each scenario, the points of maximum displacements at failure are indicative of the failure mechanism.

All discussions related to the results presented here are found in section 7.

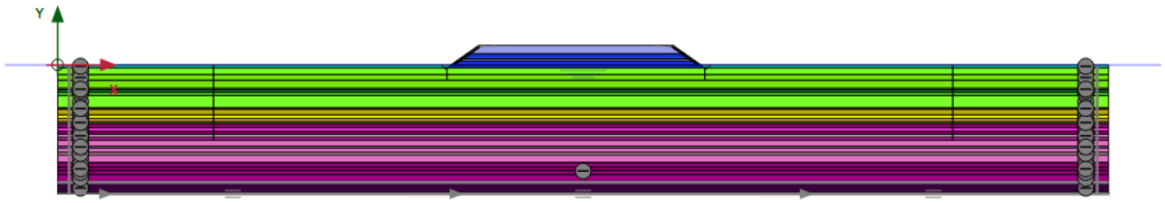

Scenario 1 summary	
Spatial dimensions	2D
Subsoil model	Ref
Terp model	Ref
Slope height	5 m
Slope inclination	35 °
Ditches	No
Agricultural machinery loads	No
Analysis type	Static
Consideration of unsaturated conditions	No
Calculated Safety Factor (FS)	**1.312**

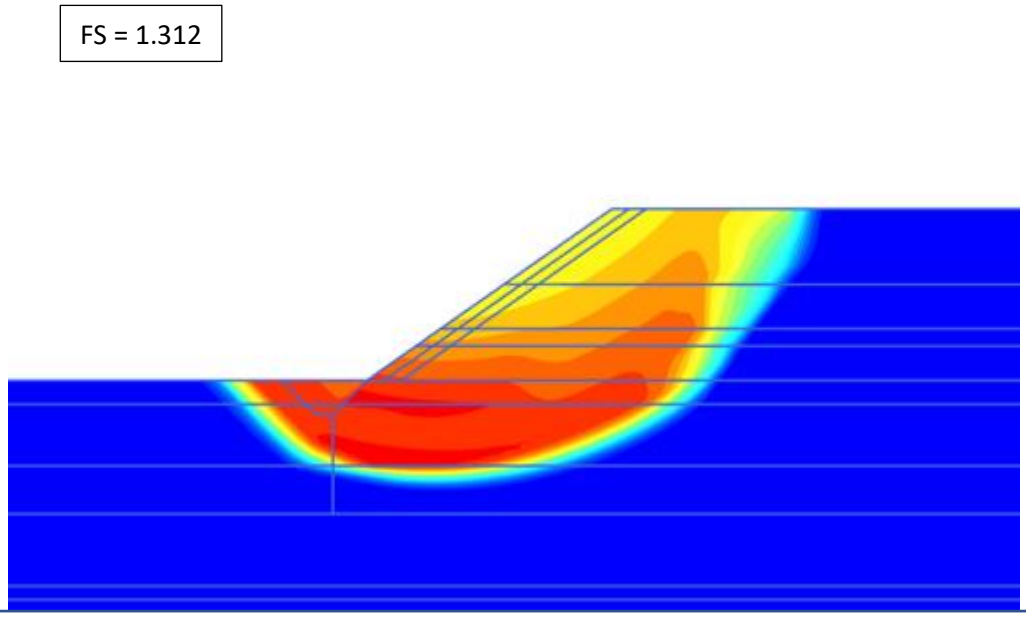

Figure 46: Scenario 1 results.

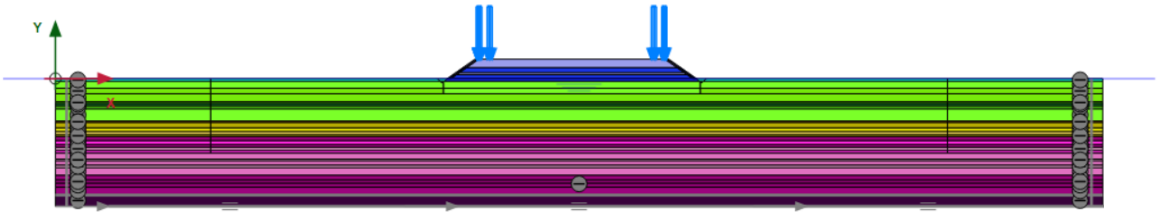

Scenario 2 summary	
Spatial dimensions	2D
Subsoil model	Ref
Terp model	Ref
Slope height	5 m
Slope inclination	35 °
Ditches	No
Agricultural machinery loads	Yes
Analysis type	Static
Consideration of unsaturated conditions	No
Calculated Safety Factor (FS)	**1.026**

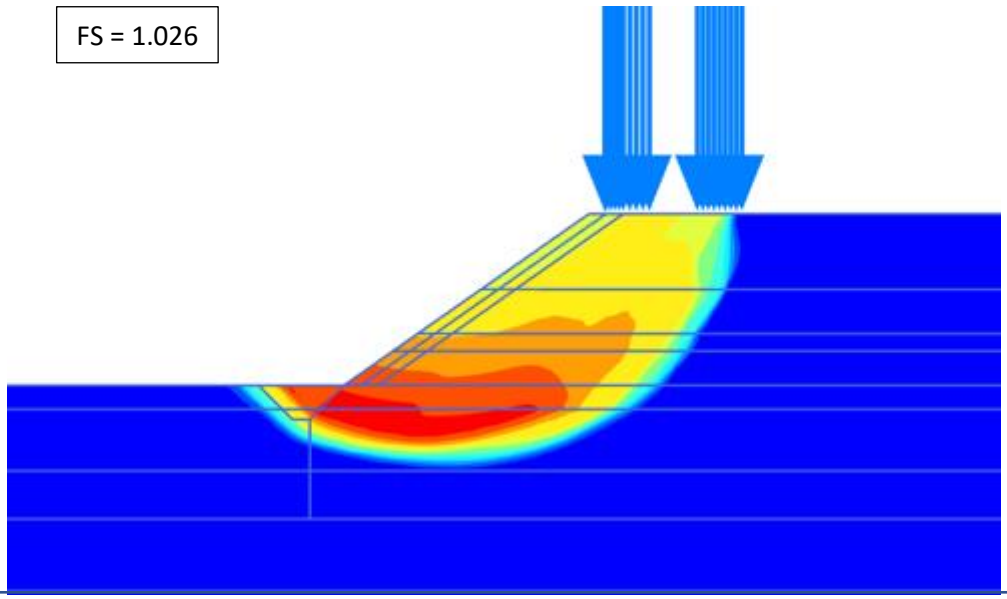

Figure 47: Scenario 2 results.

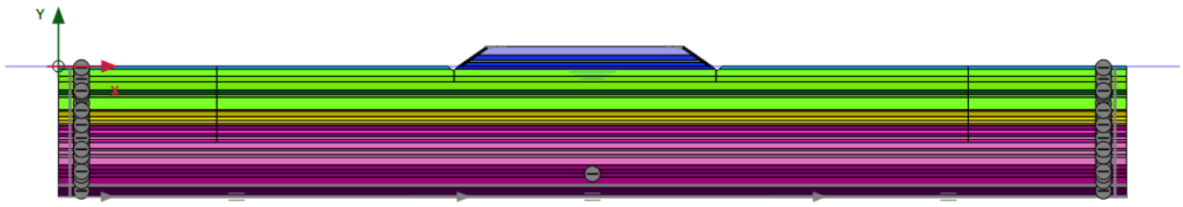

Scenario 4 summary	
Spatial dimensions	2D
Subsoil model	Ref
Terp model	Ref
Slope height	5 m
Slope inclination	35 °
Ditches	Yes
Agricultural machinery loads	No
Analysis type	Static
Consideration of unsaturated conditions	No
Calculated Safety Factor (FS)	**1.227**

FS = 1.227

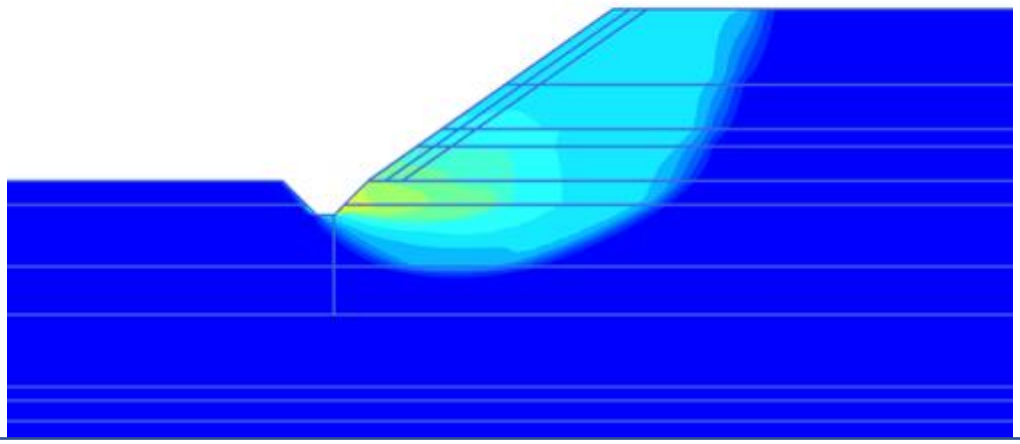

Figure 48: Scenario 4 results.

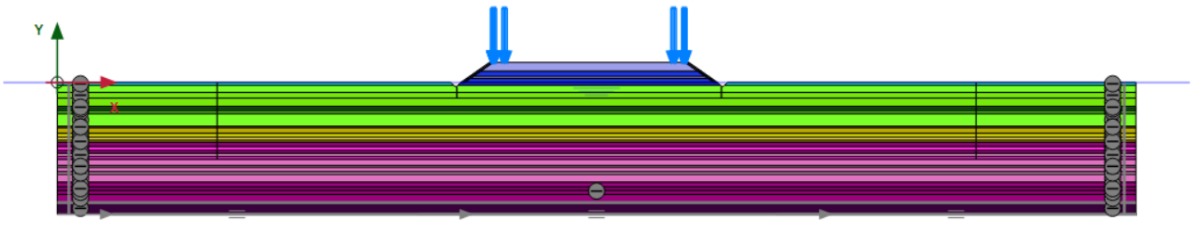

Scenario 5 summary	
Spatial dimensions	2D
Subsoil model	Ref
Terp model	Ref
Slope height	5 m
Slope inclination	35 °
Ditches	Yes
Agricultural machinery loads	Yes
Analysis type	Static
Consideration of unsaturated conditions	No
Calculated Safety Factor (FS)	**< 1.0 (unstable)**

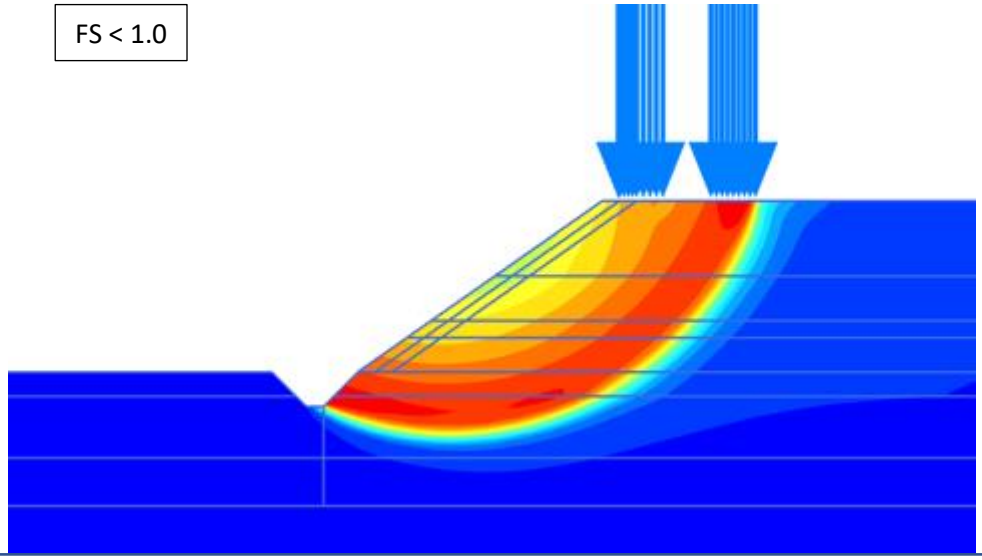

Figure 49: Scenario 5 results.

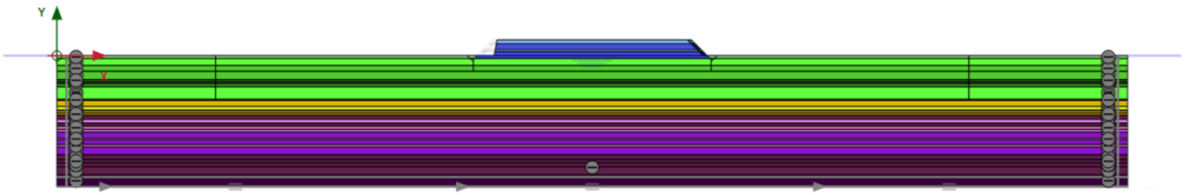

Scenario 7 summary	
Spatial dimensions	2D
Subsoil model	Ref
Terp model	Ref
Slope height	5 m
Slope inclination	80 °
Ditches	No
Agricultural machinery loads	No
Analysis type	Static
Consideration of unsaturated conditions	No
Calculated Safety Factor (FS) [t = 0]	**1.269 (only short term!)**
Calculated Safety Factor (FS) [t = 1 month]	**< 1.0 (Unstable)**

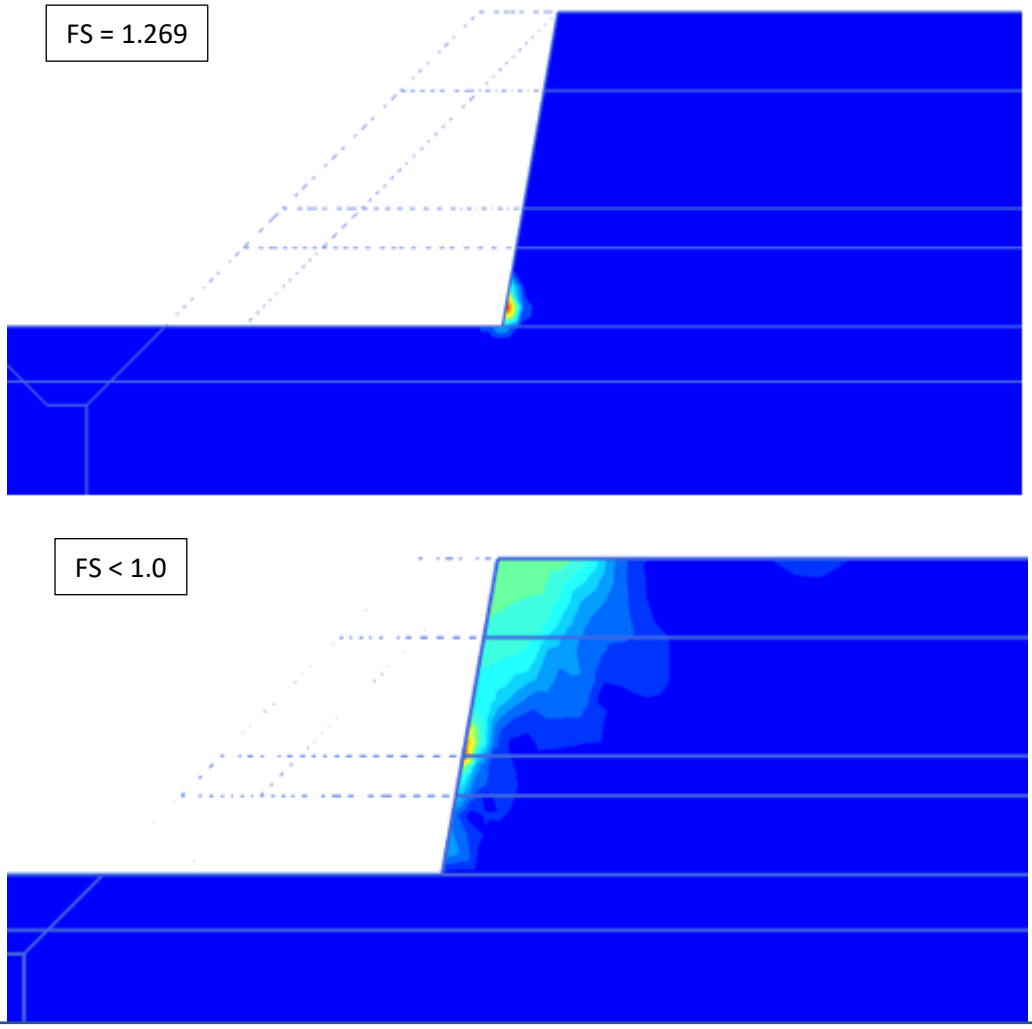

Figure 50: Scenario 7 results. Short term (above) and long term (below).

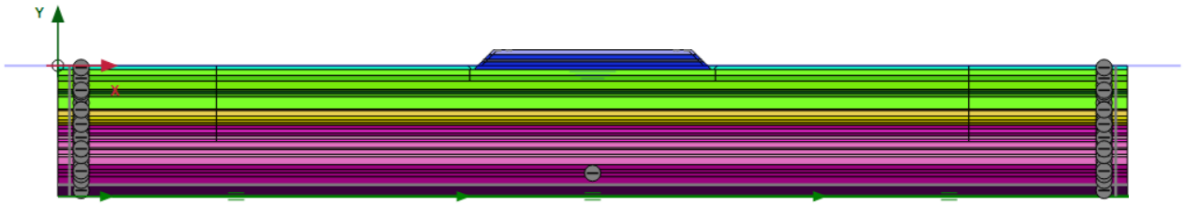

Scenario 12 summary	
Spatial dimensions	2D
Subsoil model	Ref
Terp model	Ref
Slope height	4 m
Slope inclination	45 °
Ditches	No
Agricultural machinery loads	No
Analysis type	Static
Consideration of unsaturated conditions	No
Calculated Safety Factor (FS)	**1.532**

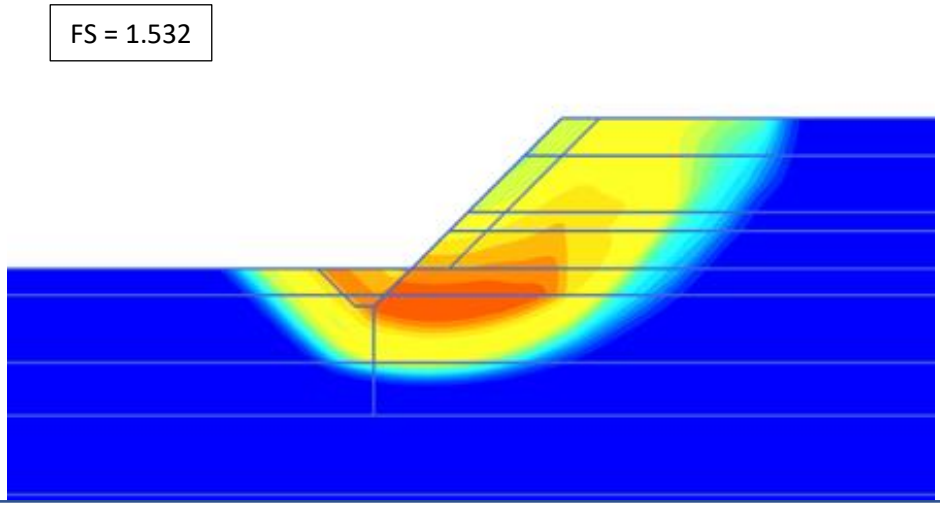

Figure 51: Scenario 12 results.

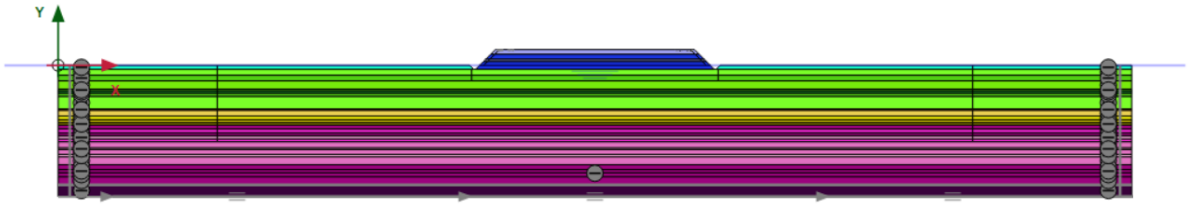

Scenario 13 summary	
Spatial dimensions	2D
Subsoil model	Ref
Terp model	Ref
Slope height	4 m
Slope inclination	45 °
Ditches	Yes
Agricultural machinery loads	No
Analysis type	Static
Consideration of unsaturated conditions	No
Calculated Safety Factor (FS)	**1.351**

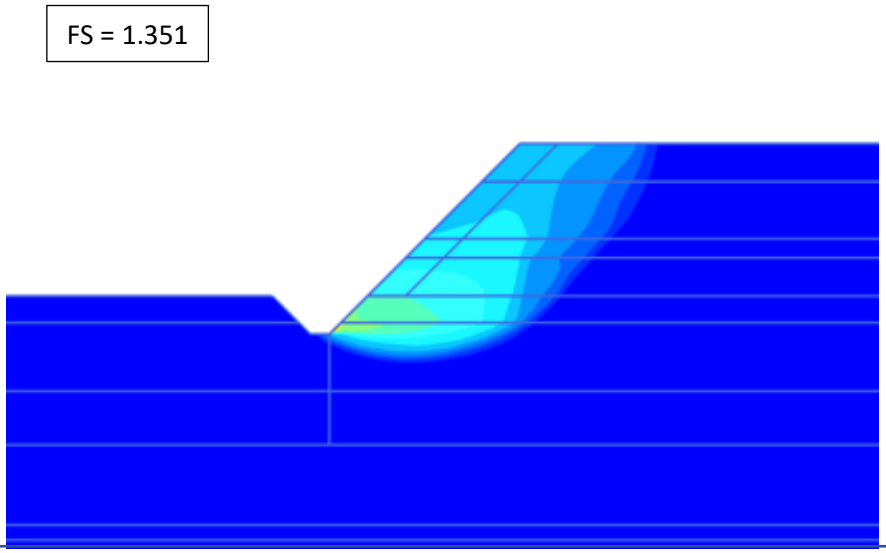

Figure 52: Scenario 13 results.

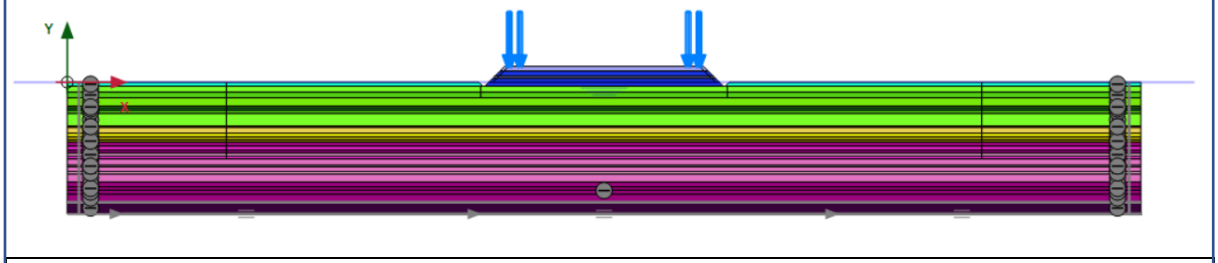

Scenario 14 summary	
Spatial dimensions	2D
Subsoil model	Ref
Terp model	Ref
Slope height	4 m
Slope inclination	45 °
Ditches	Yes
Agricultural machinery loads	Yes
Analysis type	Static
Consideration of unsaturated conditions	No
Calculated Safety Factor (FS)	**1.007**

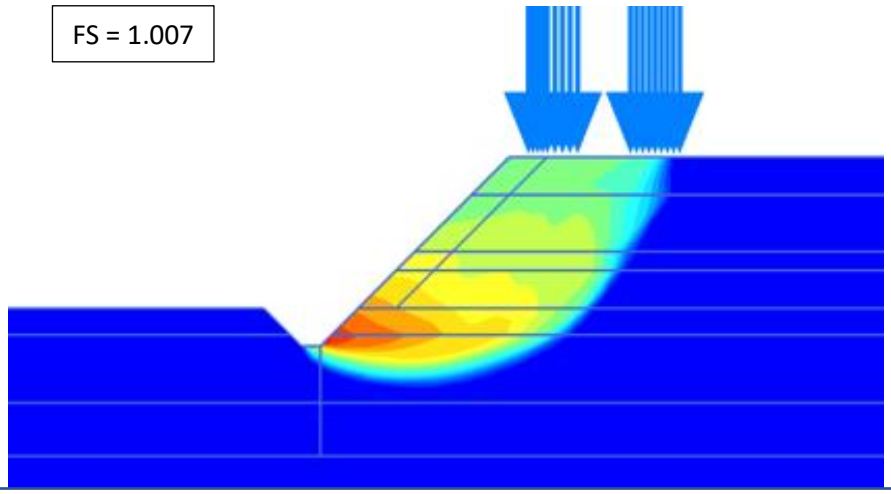

Figure 53: Scenario 14 results.

Scenario 16 summary	
Spatial dimensions	2D
Subsoil model	New
Terp model	New
Slope height	4 m
Slope inclination	36 °
Ditches	No
Agricultural machinery loads	No
Analysis type	Static
Consideration of unsaturated conditions	No
Calculated Safety Factor (FS)	**1.511**

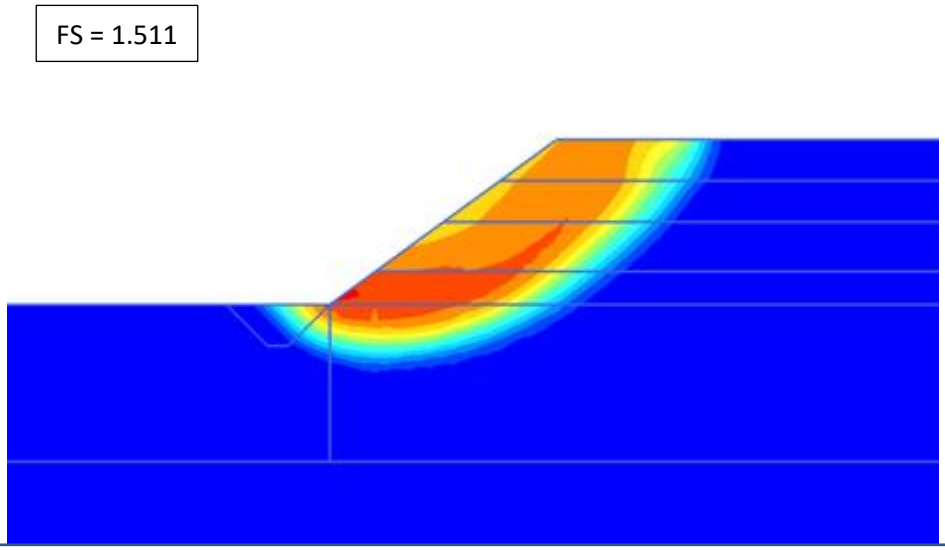

Figure 54: Scenario 16 results.

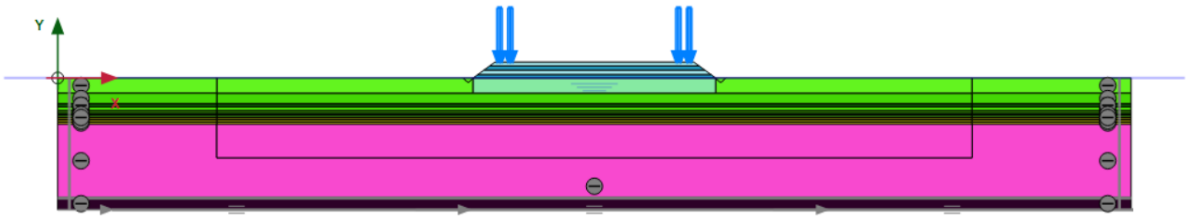

Scenario 17 summary	
Spatial dimensions	2D
Subsoil model	New
Terp model	New
Slope height	4 m
Slope inclination	36 °
Ditches	No
Agricultural machinery loads	Yes
Analysis type	Static
Consideration of unsaturated conditions	No
Calculated Safety Factor (FS)	**1.004**

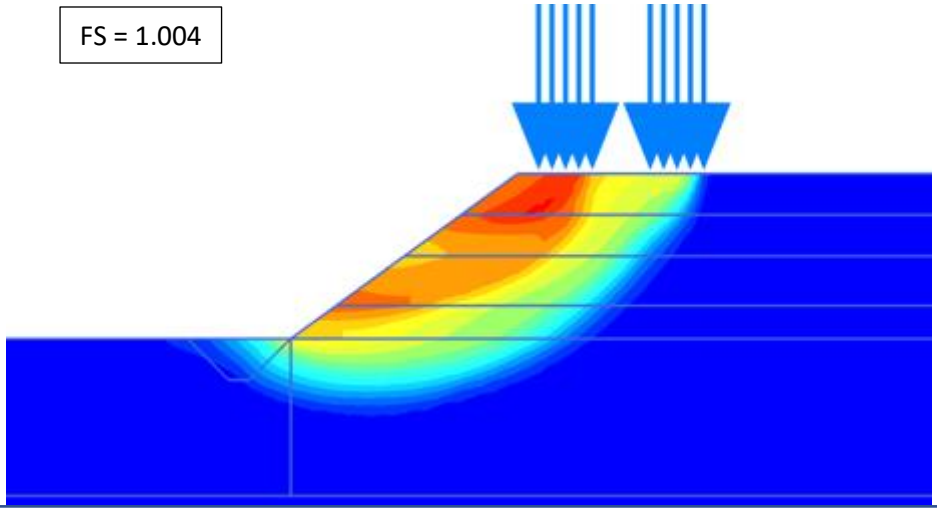

Figure 55: Scenario 17 results.

Scenario 18 summary	
Spatial dimensions	2D
Subsoil model	New
Terp model	New
Slope height	4 m
Slope inclination	36 °
Ditches	Yes
Agricultural machinery loads	No
Analysis type	Static
Consideration of unsaturated conditions	No
Calculated Safety Factor (FS)	**1.300**

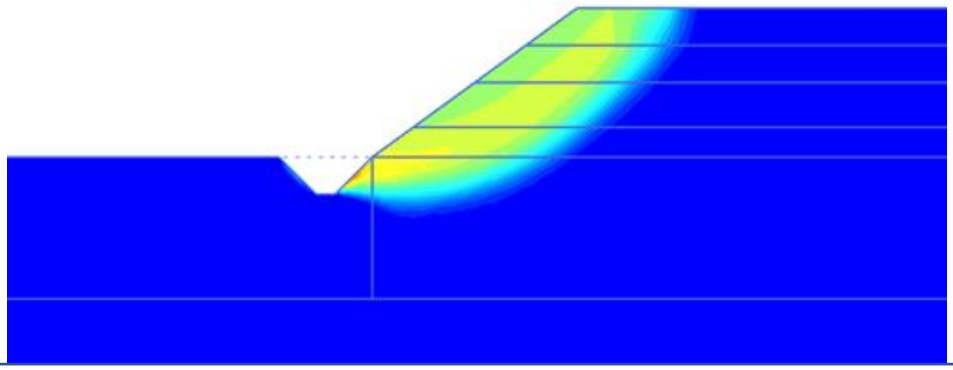

Figure 56: Scenario 18 results.

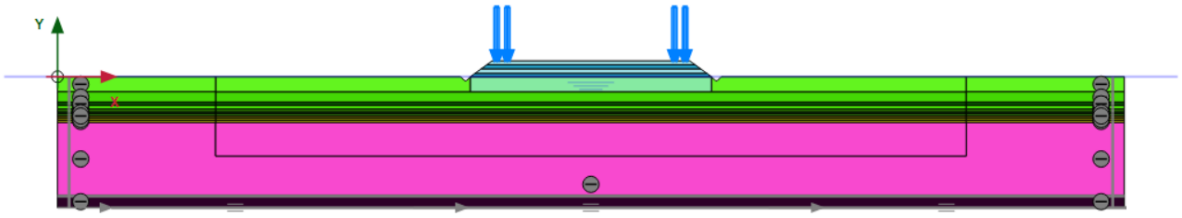

Scenario 19 summary	
Spatial dimensions	2D
Subsoil model	New
Terp model	New
Slope height	4 m
Slope inclination	36 °
Ditches	Yes
Agricultural machinery loads	Yes
Analysis type	Static
Consideration of unsaturated conditions	No
Calculated Safety Factor (FS)	**1.001**

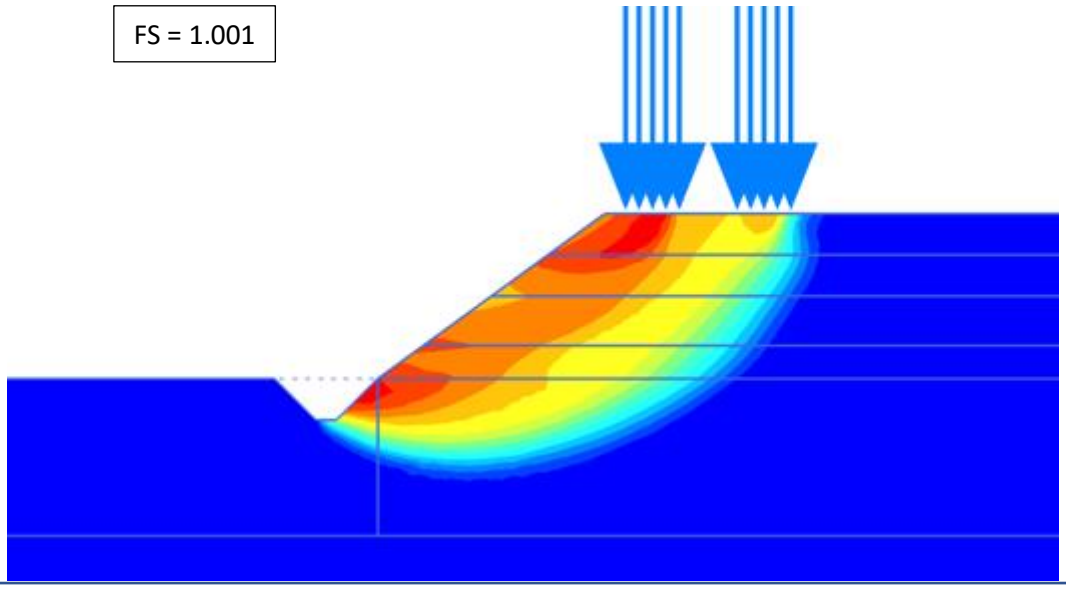

Figure 57: Scenario 19 results.

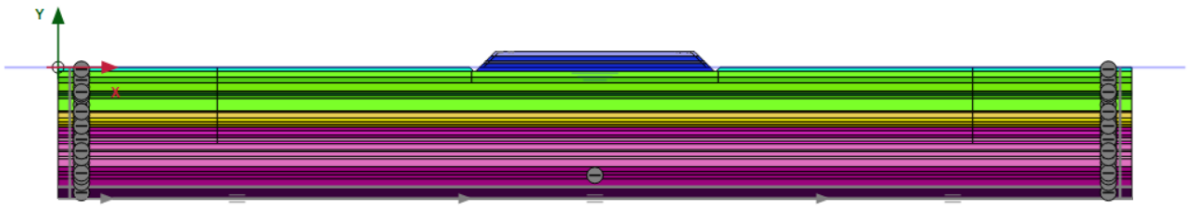

Scenario 21 summary	
Spatial dimensions	2D
Subsoil model	Ref
Terp model	Ref
Slope height	4 m
Slope inclination	36 °
Ditches	Yes
Agricultural machinery loads	No
Analysis type	Static
Consideration of unsaturated conditions	Yes
Calculated Safety Factor (FS)	**1.286**

FS = 1.286

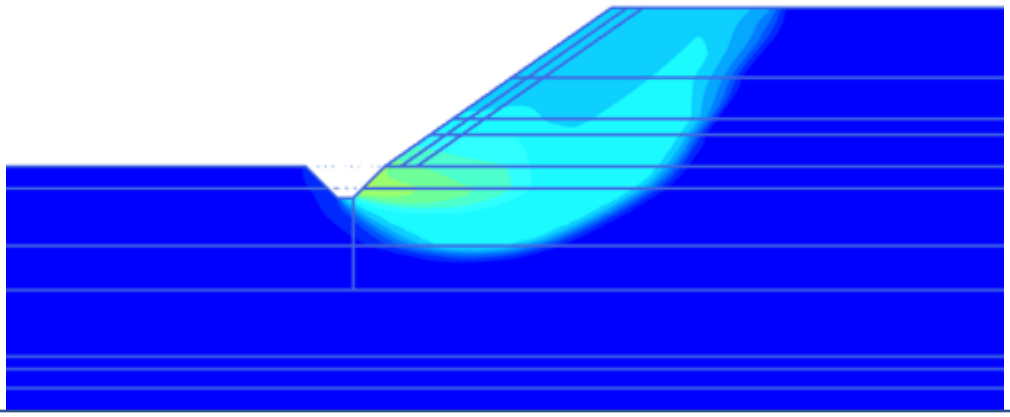

Figure 58: Scenario 21 results.

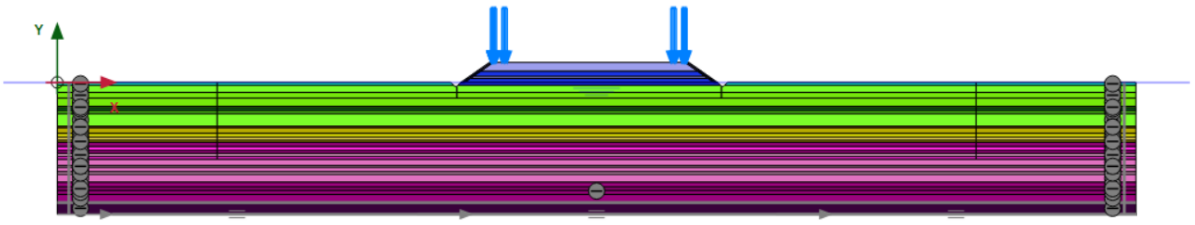

Scenario 22 summary	
Spatial dimensions	2D
Subsoil model	Ref
Terp model	Ref
Slope height	4 m
Slope inclination	36 °
Ditches	Yes
Agricultural machinery loads	Yes
Analysis type	Static
Consideration of unsaturated conditions	Yes
Calculated Safety Factor (FS)	**1.001**

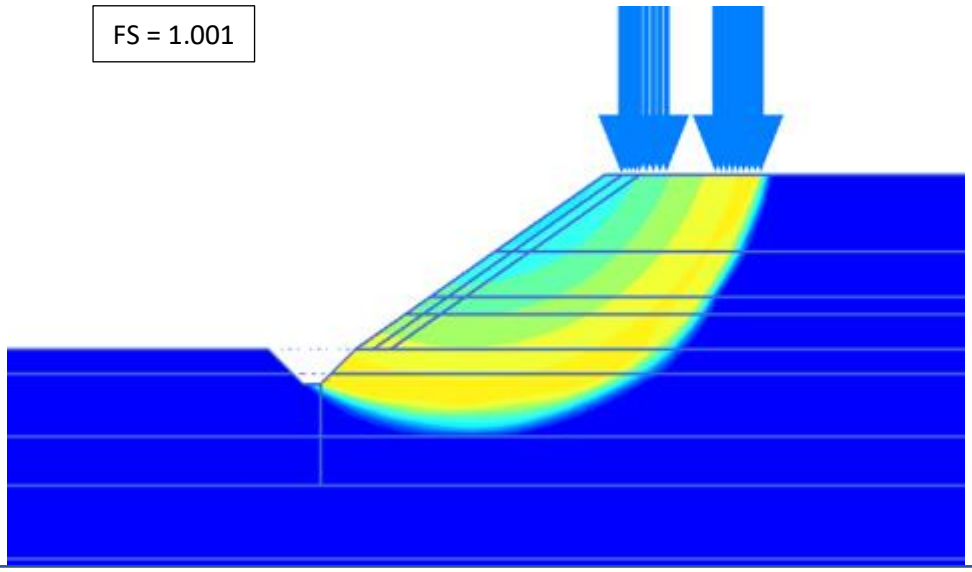

Figure 59: Scenario 22 results.

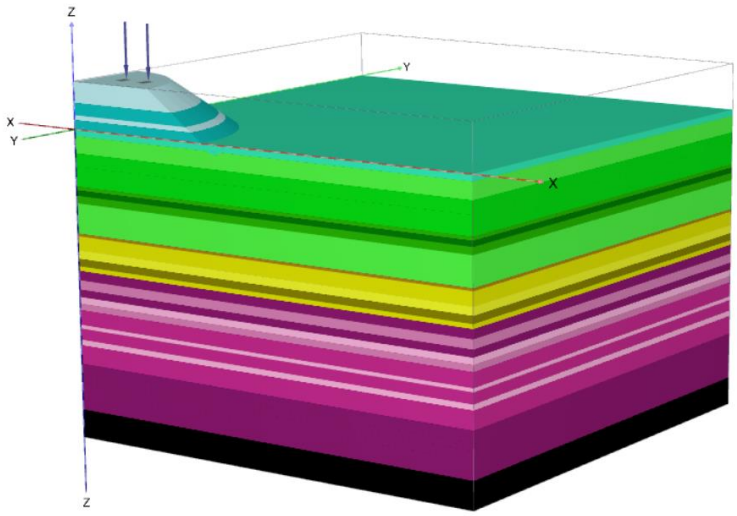

Scenario 23 summary	
Spatial dimensions	3D
Subsoil model	Ref
Terp model	Ref - Convex
Slope height	4 m
Slope inclination	36 °
Ditches	Yes
Agricultural machinery loads	Yes
Analysis type	Static
Consideration of unsaturated conditions	No
Calculated Safety Factor (FS)	**1.254**

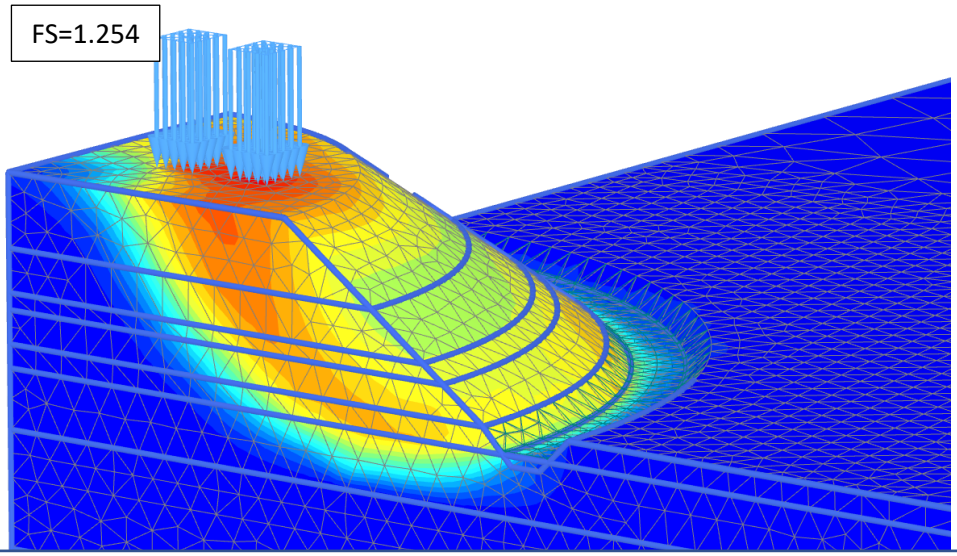

Figure 60: Scenario 23 results.

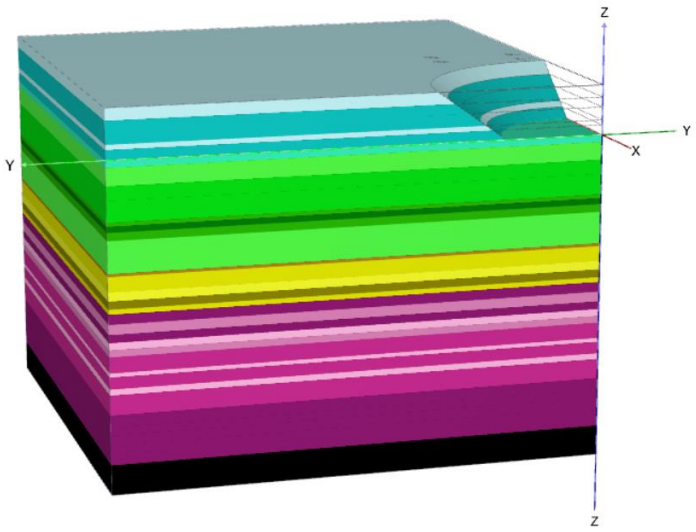

Scenario 24 summary	
Spatial dimensions	3D
Subsoil model	Ref
Terp model	Ref - Concave
Slope height	4 m
Slope inclination	36 °
Ditches	Yes
Agricultural machinery loads	Yes
Analysis type	Static
Consideration of unsaturated conditions	No
Calculated Safety Factor (FS)	**< 1.0 (Unstable)**

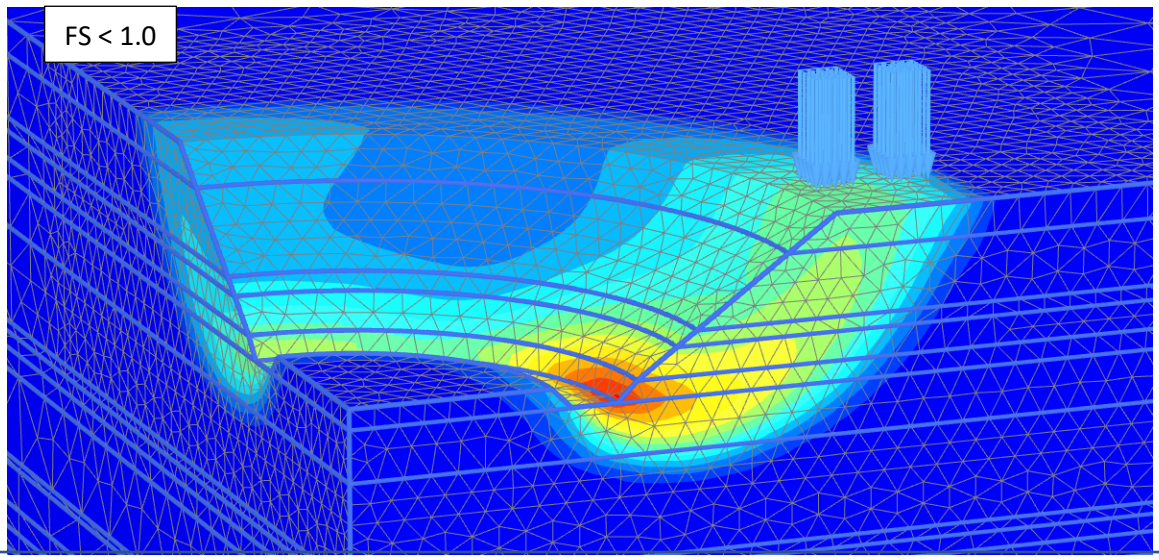

Figure 61: Scenario 24 results.

7 Discussion of the results of the analyses

In this section, the results presented in section 6 are discussed. As context for the interpretation of results, the following should be noted:

- The application of the vehicle loads is always assumed to occur at a much faster rate than the hydrodynamic period of the terp layers, and is thus always modelled as an undrained loading step.
- The ditches included in certain scenarios are pre-existing, and are thus modelled as a drained excavation step.
- Any cut excavated into the existing terp slope is also considered to occur at a much faster rate than the hydrodynamic period of the terp layers, and is thus modelled as an undrained excavation step. In the case of scenario 7, this is also followed by a consolidation calculation.
- All strength reduction steps for the determination of safety factors were carried out as drained procedures. This follows a comparative investigation in which it was determined that applying undrained strength reduction for these scenarios leads to an overestimation of the safety factor. This is due to the suction stresses that develop during the undrained strength reduction process itself, which alter the scenarios and compromise the resulting safety factor.

7.1 Analysis of results

The results of the static analysis will be discussed for each model, by comparing the safety factors and failure mechanisms related to the multiple scenarios featured therein. The safety factors discussed are those presented in section 6 and, for convenience, repeated in the Table 17 below.

Table 17:Summary of the static analyses results per scenario.

N°	Dimensions	Subsoil	H [m]	Slope [°]	Ditch	Vehicle Loads	Terp	Unsaturated conditions	Safety factor
1	2D	ref	5	35	no	no	ref	no	1.312
2	2D	ref	5	35	no	yes	ref	no	1.026
4	2D	ref	5	35	yes	no	ref	no	1.227
5	2D	ref	5	35	yes	yes	ref	no	< 1.0
7	2D	ref	5	80	no	no	ref	no	1.269*
12	2D	ref	4	45	no	no	ref	no	1.532
13	2D	ref	4	45	yes	no	ref	no	1.351
14	2D	ref	4	45	yes	yes	ref	no	1.007
16	2D	new	4	36	no	no	new	no	1.511
17	2D	new	4	36	no	yes	new	no	1.004
18	2D	new	4	36	yes	no	new	no	1.300
19	2D	new	4	36	yes	yes	new	no	1.001
21	2D	ref	5	35	yes	no	ref	yes	1.286
22	2D	ref	5	35	yes	yes	ref	yes	1.001
23	3D	ref	5	35	yes	yes	ref1	no	1.254
24	3D	ref	5	35	yes	yes	ref2	no	< 1.0

In Table 17, scenarios are colour-coded based on the safety factor obtained by the static analyses. Stable scenarios are shaded green, unstable scenarios are shaded red, while scenarios with low and critical safety factors (i.e., SF ≈ 1.0) are indicated in yellow and orange, respectively.

(*) Scenario 7 is considered as unstable due to the stability implied by the safety factor is only valid in the short term. A one-month consolidation period resulted in a SF < 1.0 (see subsection 7.1.2)

7.1.1 Scenarios 1, 2, 4, and 5

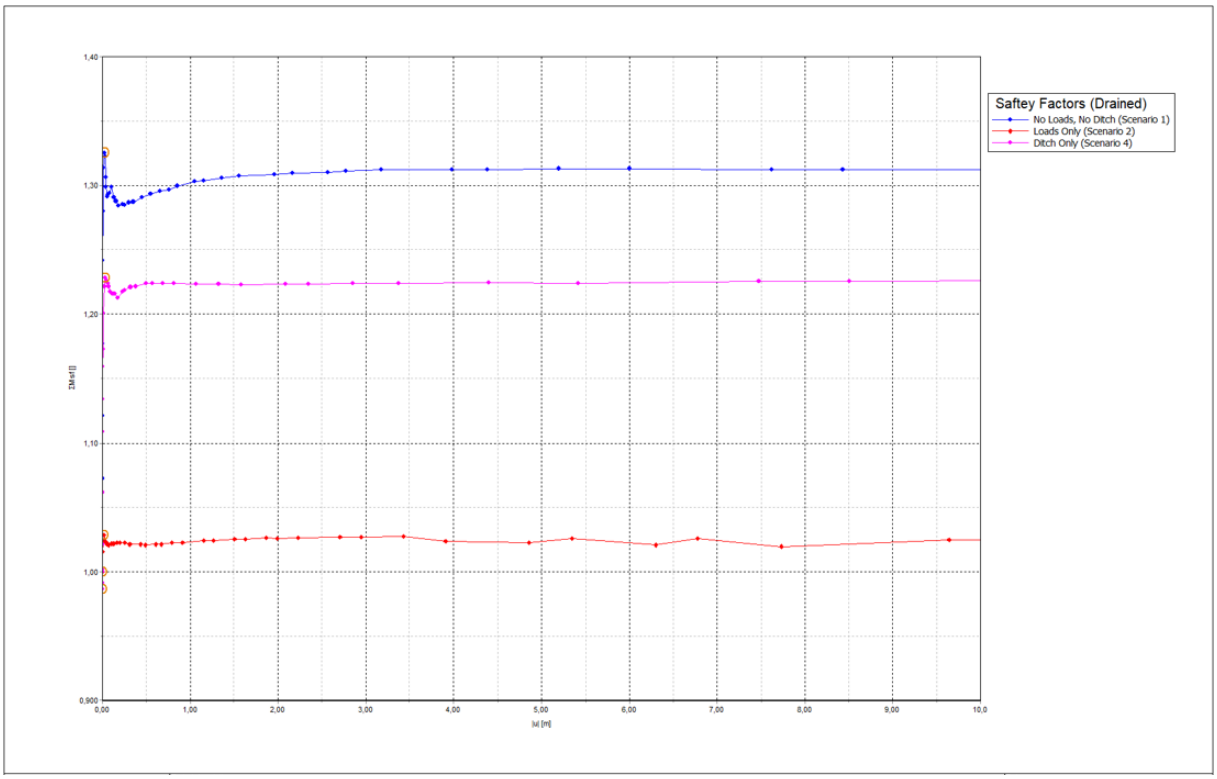

Figure 62: Factors of safety for scenarios 1, 2, 4, and 5.

The graph above shows the obtained Safety Factors for scenarios 1, 2, 4, and 5. One should note that this is a purely numerical process, in which the shear strength parameters of the soil are reduced in proportion to the ΣMsf parameter on the vertical axis. The horizontal axis indicates the simulated (fictitious) displacement that would occur on the relevant node considered in the FE model (selected to be within the failing soil mass), as a result of the reduction of shear strength. The value at which ΣMsf remains approximately constant with increasing displacement is considered as the Safety Factor.

The stability of the Westeremden reference slope model, with no added loads or ditches, was investigated via scenario 1. As one would expect, this first scenario featured the largest Safety Factor of the four, with an FS = 1.312. The failure mechanism resulting from the strength reduction process is one of base failure, with a clearly visible circular sliding plane running from the slope base to behind its crest.

The vertical loads introduced in scenario 2, which simulate the presence of agricultural machinery on the terp edge, lead to a significant decrease in Safety Factor to a value of 1.026. This scenario therefore indicates a case of limit stability, in which only a slight reduction in soil strength is required to induce failure of the slope. The failure mechanism itself remains similar to the previous scenario, as the loads seem to further accentuate the observed circular sliding plane, but with no overall change in type of failure.

The introduction of the ditch in scenario 4, without the vertical external loads, results in a computed Safety Factor of 1.227 compared to the 1.312 Safety Factor obtained without it. This clearly suggests that the ditch has a destabilizing effect. Additionally, the observed failure mechanism changes to that of toe failure. This is logical, as the excavation of the ditch leads to a weakening of the slope toe, causing a localized failure that anticipates the previously encountered circular sliding plane.

The combined effect of the vertical external loads with the excavation of the ditch in scenario 5 leads to direct failure of the slope (i.e., FS < 1.0). This is not surprising, given the already very low Safety Factor obtained in scenario 2, while the presence of the ditch makes the situation even worse. The failure mechanism is once again that of toe failure, caused by the weakening of the toe and the applied external loads.

7.1.2 Scenario 7

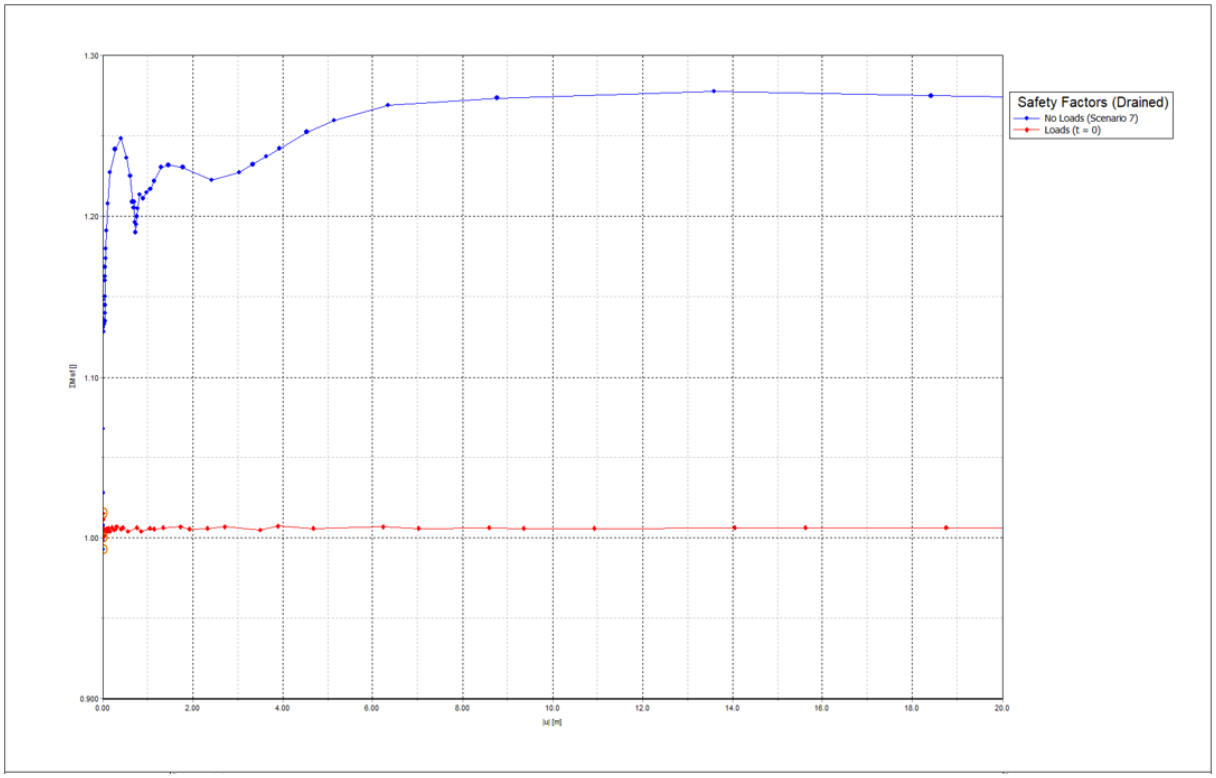

Figure 63: Factors of safety for scenario 7.

The seventh scenario presented in this report featured the excavation of a quasi-vertical slope from the Westeremden reference model. The excavation of the slope itself was reasonably assumed to occur quickly compared to the hydrodynamic period of the terp layers, and was thus modelled as an undrained excavation. The resulting static analysis indicated a stable situation, with a computed Safety Factor of 1.269.

This apparent stability, however, is only valid in the very short term and is a result of suction provided by the undissipated (negative) excess pore pressures, which develop during excavation. Further simulations, in which a 1-month consolidation period was introduced with no other changes, resulted in direct failure of the slope, with no strength reduction process required (i.e., FS < 1.0).

The extent to which suction forces contribute to the (short-term) stability of the slope becomes apparent when introducing vehicle loads. As shown in the graph above, immediately after the excavation of the steep slope, the terp remains (barely) stable even with the addition of vehicle loads, despite the same slope failing with no external loads present after just 1 month of pore pressure dissipation.

These results are of particular significance, as there are records of such quasi-vertical slopes being excavated in existing terps, and although these may seem stable when first excavated, a serious risk of instability is still present in the longer term.

7.1.3 Scenarios 12, 13, and 14

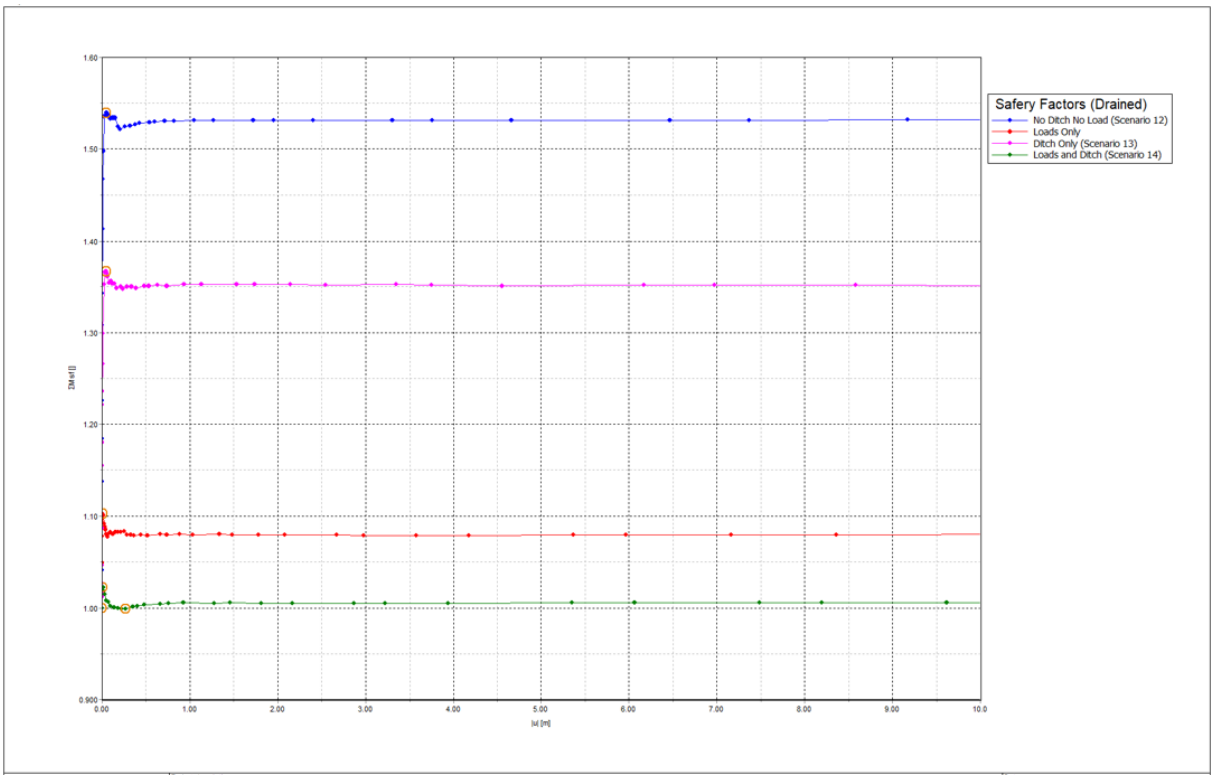

Figure 64: Factors of safety for scenarios 12, 13, and 14.

These scenarios are comparable to those discussed in subsection 7.1.1, but involve a steeper slope of 45 ° and lower height of 4 m. Once again, the largest Safety Factor resulted from the scenario involving no ditch or external loads, being scenario 12 with FS = 1.532. The resulting failure mechanism seems to once again be that of base failure, but with proportionately larger displacements occurring on the slope toe, caused by the steeper slope.

The excavation of the ditch introduced in scenario 13 once again results in a lowering of the Safety Factor, to FS = 1.351, and causes a change in failure mechanism to that of toe failure. This same failure mechanism is then further accentuated by the introduction of the external loads in scenario 14, which however significantly lowers the Safety Factor to FS = 1.007. Scenario 14, in which both the external loads and ditch are included, therefore represents a critical situation of borderline stability.

These results, when compared to those from scenarios 1, 2, 4, and 5, suggest that, for the Westeremden terp model, a 1 metre increase in slope height is more detrimental to slope stability than a 10 ° increase in inclination. This can be directly deduced from the larger Safety Factors, which are summarized in the table and the graph above.

In order to provide a complete comparison with the scenarios 1, 2, 4, and 5, the “Loads Only” case for this model was also included.

7.1.4 Scenarios 16, 17, 18, and 19

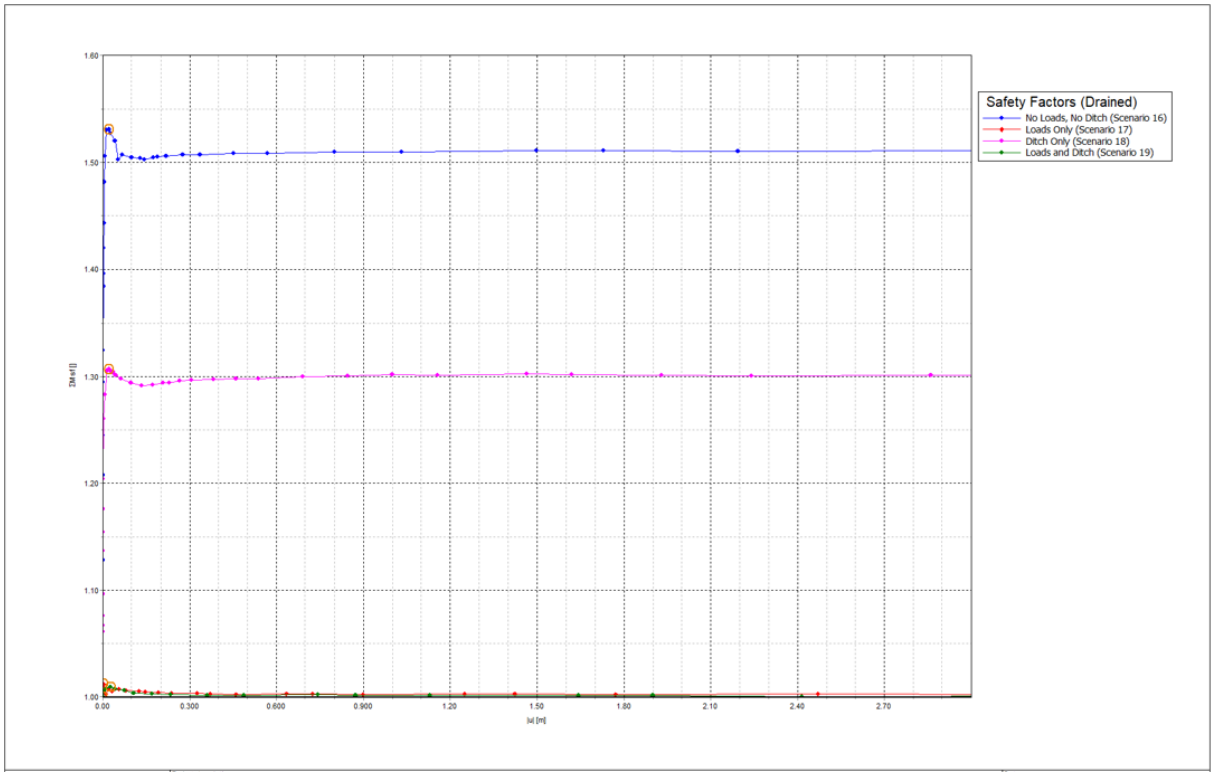

Figure 65: Factors of safety for scenarios 16, 17, 18, and 19.

These scenarios were the first involving a different subsoil and terp composition model, being the Toornwerd reference model.

Scenario 16, featuring no external loads or ditch, resulted in a Safety Factor of 1.511, and a base failure mechanism.

The introduction of the external loads in scenario 17 has the expected effect of significantly lowering the Safety Factor, resulting in a FS = 1.004 (critical). Unlike previous scenarios, however, the introduction of the loads significantly changed the failure mechanism. It was in fact observed that a comparatively larger proportion of displacements occurred on top edge of the slope, in proximity of the loads. This can be explained by the weaker top clay layer present on the top of the terp, compared to the same layer in the Westeremden reference model, which causes a local failure in direct proximity of the vehicle loads, preceding the failure along the sliding plane observed in the previous models.

As was the case with the other models, however, the excavation of the ditch alone does result in a weakening of the toe of the slope, and a consequent shift in failure mechanism. This is reflected in the results of scenario 18, in which the predicted failure mechanism clearly indicates failure at the toe, as was the case with other scenarios involving a ditch with no external loads. The computed Safety Factor for this scenario, being FS = 1.300; lower than the situation without ditch.

Scenario 19 featured both the excavated ditch and external agricultural vehicle loads. Results from this scenario are very similar to those from scenario 17, both in terms of critical stability, with a FS = 1.001, and failure mechanism, in which the largest displacements are observed on the top edge of the slope. This can once again be explained by the weaker terp topsoil layer, which fails locally in proximity of the loads, before failure can occur elsewhere. Consequently, the effect of the ditch is almost negligible in terms of stability, due to the much more pronounced effects of the external loads.

By comparing the Safety Factors from scenarios 16 and 18, with those from scenarios 12 and 13, one can conclude that the Toornwerd reference model (H = 4 m, θ = 36 °) and the Westeremden steep reference model (H = 4 m, θ = 45 °), are approximately equally stable when the vehicle loads are not considered.

This is despite the Westeremden steep model having a less favourable geometry, which suggests that its soil material composition, which differs from that of the Toornwerd model, must be having a compensating effect. The higher strength parameters of the terp layers featured in the Westeremden model, as can be seen in subsection 5.4, present a reasonable explanation for this.

When the vehicle loads are introduced, however, while the Safety Factors for both models are very close to 1, it is the Toornwerd model which results in less stable scenarios. This was explained by the local failures occurring on the top (weaker) terp layer in the Toornwerd model.

The presence of the sandy clay terp layers in the Toornwerd model, compared to the peat terp layers present in the Westeremden model, further explain the results for scenarios 17 and 19. This is due to the much larger stiffness of the sandy clay compared to peat, which "forces" a larger proportion of the displacements to take place in other layers, such as the weak clay layer upon which the loading occurs.

7.1.5 Scenarios 21 and 22

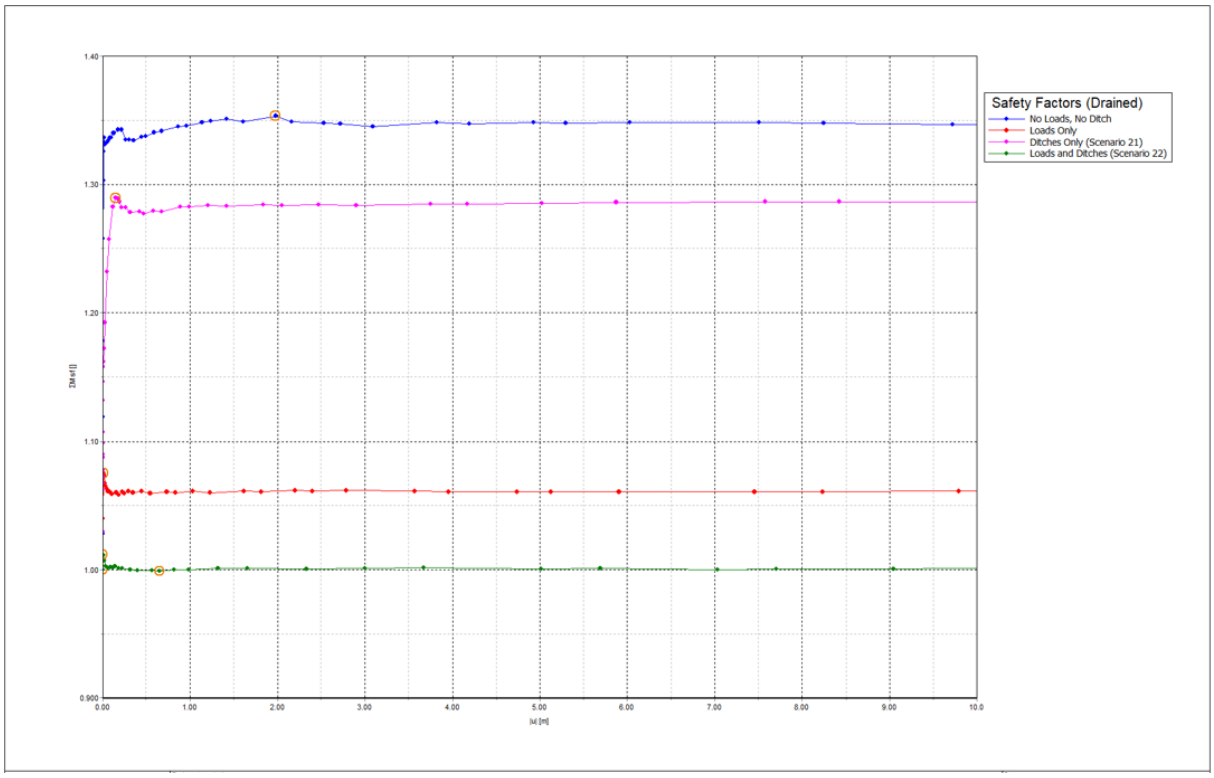

Figure 66: Factors of safety for scenarios 21 and 22.

These two scenarios include the effect of unsaturated soil in the Westeremden terp reference model. Scenario 21, featuring the inclusion of a ditch, but not of external loads, results in a Safety Factor of 1.286, and a slope toe failure mechanism that can be considered characteristic of the models with the presence of a ditch.

Scenario 22, which included both ditch and agricultural vehicle loads, resulted in a Safety Factor indicating critical stability, with a value of FS = 1.001.

For the sake of completeness, stability analyses for this model were also performed for cases with no loads or ditch, and with the loads alone (see image above). From all four static analyses performed, and after comparing these with scenarios 1, 2, 4, and 5, it is clear that the inclusion of unsaturated conditions comes with an increase in computed Safety Factors and thus increased slope stability. However, since the suction stresses as a result of unsaturated behaviour are non-sustainable during periods of heavy rainfall, they may not be relied upon and resulting calculated safety factors of these scenarios are not reliable.

7.1.6 Scenarios 23 and 24

The last two scenarios considered in the static analyses were for two distinct 3D geometries, one being convex (scenario 23), and the other a concave slope (scenario 24). Both scenarios featured the external vertical loads and ditch, and both were based on the same subsoil characterization. Thus, any differences in results should stem from the difference between the convex and concave geometry.

The static analysis of the convex slope in scenario 23 resulted in a Safety Factor FS = 1.254. Interestingly, although the formation of a circular slipping plane can be seen, the resulting failure mechanism is that of a slope failure, rather than a toe, or base failure, which was characteristic of all other scenarios. This can only be related to the 3D effects from a convex geometry, which are absent in all of the other analyses.

Scenario 24, featuring a concave slope, on the other hand, resulted in failure when both the loads and ditches are applied, and thus a Safety Factor < 1.0. The difference in response can only be attributed to the geometry of the 3D terp considered in this scenario.

The failure mechanism resulting from this scenario, however, was much more in line with those observed in 2D analyses featuring external vertical loads and ditch, as a slope toe failure mechanism can clearly be identified.

7.2 Summary and comparison of static analyses results

From the results presented in subsections 7.1.1 – 7.1.6, the following can be concluded:

- The results suggest that all considered terp slopes are stable for all scenarios involving no added external loads or ditches.
    - FS = 1.31 for scenario 1 (H = 5 m, θ = 35 °, "Westeremden ref")
    - FS = 1.53 for scenario 12 (H = 4 m, θ = 45 °, "Westeremden ref")
    - FS = 1.51 for scenario 16 (H = 4 m, θ = 36 °, "Toornwerd ref")
- The addition of the external loads, representing possible agricultural vehicles, significantly reduces the safety factor and leads to critical or unstable conditions in all models.
    - FS = 1.03 for scenario 2 (H = 5 m, θ = 35 °, "Westeremden ref")
    - FS < 1.01 for scenario 17 (H = 4 m, θ = 36 °, "Toornwerd ref")
    - Although not marked as a scenario, the steep version of the Westeremden reference model (H = 4 m, θ = 45 °, "Westeremden ref") with added external loads resulted in an FS = 1.07 (see subchapter 0)
- The inclusion of possible existing ditches at the slope toe of the terp (with no external loads) resulted in a reduction in safety factors for all models:
    - FS = 1.23 for scenario 3 (H = 5 m, θ = 35 °, "Westeremden ref")
    - FS = 1.35 for scenario 13 (H = 4 m, θ = 45 °, "Westeremden ref")
    - FS = 1.30 for scenario 18 (H = 4 m, θ = 36 °, "Toornwerd ref")
- The combination of vehicle loads and presence of a ditch creates a critical or unstable condition for all models tested.
    - **FS < 1.0** for scenario 5 (H = 5 m, θ = 35 °, "Westeremden ref")
    - FS < 1.01 for scenario 14 (H = 4 m, θ = 45 °, "Westeremden ref")
    - FS < 1.01 for scenario 19 (H = 4 m, θ = 36 °, "Toornwerd ref")
- The vehicle loads alone negatively affect stability to a much larger degree than the ditch alone, for all models tested.
- Results for all scenarios from the two geometry variants of the Westeremden reference terp suggest that a shorter, steeper slope (H = 4 m, θ = 45 °) is more stable than a taller, gentler slope (H = 5 m, θ = 35 °).
- The Toornwerd terp model was observed to be more stable overall when compared to the Westeremden terp model, but was slightly more susceptible to local failure in proximity of the loads.
    - FS for scenarios 16, 18, and 19 > FS for scenarios 1, 4, and 5
    - FS for scenario 17 < FS for scenario 2
- The inclusion of unsaturated conditions in the Westeremden reference terp results in an increase in stability for all scenarios considered, due to the favourable suction stresses provided in the unsaturated zone. Due to the fact that unsaturated conditions are prone to change, however, one should not rely on such an increase of the safety factors.
- Results from the quasi-vertical slope model indicate a deceptively large safety factor for a newly excavated, 80 ° steep slope. This stability, however, is entirely provided by suction resulting from newly developed, negative excess pore pressures which, as these dissipate in time, quickly lead to a deterioration of stability and eventual failure of the slope.

8 Post-analysis considerations

In this section of the report, post analysis considerations are made regarding model validation, the topic of drained versus undrained safety analysis calculations, as well as the differences observed in 2D and 3D safety analyses.

8.1 Model validation via oedometer tests

As outlined in subsection 4.2.4, oedometer tests were performed to 3 samples of soil obtained from a borehole performed on the Westeremden terp. From these tests, values for the HS stiffness parameter E_{oed}^{ref} were determined for clay and peat layers present within the terp. Provided in Table 18 are the values obtained for each sample, together with those that had been applied to the model, and the difference between the two expressed as a percentage.

Table 18: E_{oed}^{ref} values obtained from oedometer tests, compared to those applied in the models.

Sample:	Soil:	E_{oed}^{ref} [kPa] (oedometer tests)	E_{oed}^{ref} [kPa] (models)	Difference [%]
A	NA Clay Terp	4150	4000	+3.75
B	NA Peat Terp	4050	3500	+15.71
D	NA Clay Terp	4600	4000	+15.00

As shown in the table above, the values used in the models were reasonably similar to those obtained from laboratory testing. In all 3 cases, the values used in the models were lower in magnitude, by a maximum of 15.71 %.

Considering that the stiffness values applied to the Westeremden terp layers during modelling were based on those suggested in literature and engineering judgement, performing the oedometer tests was important to obtain a degree of model validation.

Furthermore, the drained strength parameters for the same layers were obtained by combining the undrained shear strength values obtained in the laboratory with the PLAXIS SoilTest tool (see subsection 5.4.3). Since the PLAXIS SoilTest tool itself required values of E-modulus as input, the use of reference values for these was the most significant source of uncertainty related to the drained strength parameters determination process, given the relation between soil strength and stiffness in non-linear models (particularly the $E_{50}^{ref}/E_{oed}^{ref}$ ratio). Thus, the E_{oed}^{ref} values obtained by the oedometer tests also provide an indirect validation for the drained strength parameters.

To understand this indirect validation, one should not that, unlike in linear elastic perfectly plastic models, strength and stiffness are not independent of each other in non-linear models such as the HS (small). Specifically in undrained loading, the effective stress path of a soil, and thus the point at which this meets the failure line, is affected by its stiffness. This is due to how soil stiffness impacts the degree to which pore pressures increase in response to loading, and thus the amount by which effective strength is reduced.

Due to this relation, validation of soil stiffness parameters used in the simulated undrained DSS & Triaxial tests also serve as an indirect validation of the obtained drained strength parameters.

Unfortunately, the parameters assigned to the subsoil beneath the terp could not be validated by laboratory testing. However, as the terp slope layers are the most relevant in a static stability analysis (see failure mechanisms presented in section 6), the validation obtained by the oedometer tests are highly significant for the investigation performed for this thesis.

8.2 Drained vs. undrained safety calculations

In all analyses performed in this project, safety factors were determined via drained safety calculations, regardless of whether a short-term or long-term response was considered. In other words, whether a specific construction stage was modelled as drained (terp construction) or undrained (vehicle loading & quasi-vertical slope excavation), the ϕ-c reduction calculations that followed were set to ignore undrained behaviour.

The physical meaning of a drained or undrained ϕ-c reduction calculation may seem ambiguous, as ϕ-c reduction processes only exist in the context of modelling and do not occur in reality. In fact, there is no agreement among experts regarding the application of drained or undrained safety calculations by means of the ϕ-c reduction method (Brinkgreve, pers. comm., 2021).

In the early stages of this project, safety calculations were performed with the same drainage conditions as the construction stage being considered. The results that emerged, however, showed inconsistencies that were clearly indicated an issue with this method. An example of this were the undrained safety factors obtained for a scenario involving the excavation of a quasi-vertical slope (scenario 7) being higher than those resulting from a drained safety analysis of a much shallower, existing slope, subjected to the same loading conditions, soil properties, and with equal slope height.

By further analysing the model calculations involved, it was observed that negative excess pore pressures developing during the undrained ϕ-c reduction processes were the cause of unrealistically large safety factors. After switching to drained safety calculations, this issue was solved.

One should note that applying a drained safety calculation to an undrained construction stage does not equate to converting the drainage conditions of said scenario to a drained setting. Rather, it simply means that any excess pore pressures that developed during an undrained construction stage will remain during the safety analysis, but will not be increased by the ϕ-c reduction process.

On the other hand, any excess pore pressures present in the beginning of an undrained safety calculation will be altered by the by the ϕ-c reduction process. On the matter, van der Sloot (2013) notes the following:

- For loading problems (for instance embankments) allowing excess pore pressures to change [during safety calculations] often leads to an increase of excess pore pressures. This would therefore lead to a lower factor of safety compared to the case where no change of excess pore pressures would be allowed.
- For unloading problems (for instance excavations) allowing excess pore pressures to change [during safety calculations] often leads to a decrease of excess pore pressures and sometimes even to pore tensions (suction). This would therefore lead to a higher factor of safety compared to the case where no change of excess pore pressures would be allowed.

The latter situation was precisely what occurred when an undrained safety calculation was applied to scenario 7, leading to results which, when compared to the safety factors obtained for other scenarios, were physically impossible.

The argument remains on whether safety calculations should therefore always be applied with drained settings, or whether one should perform both drained and undrained safety calculations, and then consider the results featuring the lowest safety factors.

The latter of the two choices is the most conservative, but which approach is most appropriate depends on the meaning that one attributes to safety calculations. One could argue that a ϕ-c reduction calculation should be applied to specific situations with fixed excess pore pressures, that

should remain unchanged during throughout the calculation, thus resulting in a measure of stability for the exact situation being considered.

On the other hand, one could also argue that, specifically for loading problems, allowing the excess pore pressures to be altered during the ϕ-c reduction process could compensate for the possibility of having over-estimated the strength parameters during modelling, as the excess pore pressures developed during the safety calculation will be a result of the lowering of the ϕ and c values. In this case, the obtained factors of safety would, in theory, be a measure of stability for the situation that would have existed, should lower values of ϕ and c had been used as input for the model. This, however, would need to be verified via an investigative project of its own.

In this thesis, the first of the two theories was applied. However, considering that many of the subsoil parameters used in the models were obtained via empirical relationships and reference values, with no advanced laboratory testing, a case could be made for the use of undrained safety calculations for scenarios involving loading problems, should the argument expressed in the previous paragraph be correct.

8.3 2D vs. 3D static stability analyses

The last post-analysis subject covered in this section concerns possible differences between 2D and 3D static stability analyses. The argument exists that 2D finite element calculations will generally result in higher estimations of displacements compared to 3D analyses, and consequently lower estimations of the safety factors (Brinkgreve, pers. comm., 2022). This is due to two reasons.

Firstly, the accuracy of an FE mesh in 2D is generally higher than in 3D due to it being easier to produce much finer meshes when working on 2D models. This results in more degrees of freedom and higher order elements, compared to a 3D mesh of larger and thus more constrained elements. These increased constraints cause a reduction in the calculated displacements and thus an increase in calculated safety factors.

Secondly, due to 3D effects, an arbitrary body of soil interacts with its surroundings on a larger number of interfaces in a 3D model. Consequently, any load applied is resisted by more soil, thus increasing the overall strength of the system. This increased strength leads to lower displacements.

In order to gain further insight on the consequences of this effect for the analyses performed, the 2D analyses of scenarios 1, 2, 4, and 5 were reproduced in 3D, with the varying lengths for the added third dimension (y-axis) being the only difference between the models. The effects related to the increased mobility of the nodes could then be observed in the difference in safety factors obtained in each version of the model.

Two 3D versions of scenarios 1, 2, 4, and 5 were analysed, with lengths in the 3rd dimension of 0.5 m and 50 m. These models are presented in Appendix K. The resulting safety factors for each scenario are presented in Table 19.

Table 19: Safety Factors comparison between 2D and different 3D models of scenarios 1, 2, 4, and 5.

Scenario	2D Safety Factors	3D (0.5 m) Safety Factors	3D (50 m) Safety Factors
1	1.312	1.320	1.341
2	1.026	1.027	1.327
4	1.227	1.236	1.296
5	< 1.0	< 1.0	1.271

The results listed in Table 19 confirm the argument that increased three-dimensionality leads to an overall increase in safety factor magnitude.

In general, the difference in safety factors observed between the models was minimal, with the exception of scenarios 2 and 5 in the 3D (50 m) model. These two scenarios are those in which vehicle loads are included, and the calculated safety factors were considerably larger than those for the equivalent scenarios in the 2D and 3D (0.5 m) models.

The difference in safety factors resulting from scenarios 2 and 5 in the 3D (50 m) model is too large to be a result of just increased three-dimensionality. One should note that this model was the only one for which the vehicle loads were not represented as 2 distributed loads along the entire width of the model, in direction normal to the plane section (representing plane-strain conditions).

Rather, due to the 3D nature of the model, the vehicle loads were modelled as 4 distributed loads, each representing one wheel of the agricultural vehicle. The dimensions and spacing of the wheel loads were defined as in section 5 for the 2D models, but with an added centreline spacing of 3.8 m in the y-direction separating the front and rear wheels, as illustrated in the technical specifications of the combine harvester considered.

The difference between the full representation of the vehicle loads compared to the plane-strain conditions is the only way to explain the considerable difference in the calculated safety factors. To verify that this is indeed the case, a third 3D model was made, once again extended to 50 m in the y-direction. This time, however, the vehicle loads were modelled to reproduce the plane-strain conditions (thus applying the same 40 kPa pressure across the entire model width). The results are summarized in Table 20.

Table 20: Safety Factors for a 3D (50 m) model of scenarios 1, 2, 4, and 5, simulating plane-strain conditions.

Scenario	1	2	4	5
3D (50 m) – Plane Strain Safety Factors	1.341	1.046	1.298	< 1.0

As indicated above, the safety factors obtained for scenarios 2 and 5 were 1.033 and < 1.0 (unstable), respectively. The obtained results are much more in line with those obtained from the 2D and 3D (0.5 m) models, suggesting that the significant increase in safety factors for scenarios 2 and 5 in the 3D (50 m) model was a direct result of the manner in which the vehicle loads were represented.

Furthermore, the safety factors obtained for the scenarios not featuring external loads were almost identical to those observed in the previous 3D (50 m) model. This is not surprising given that the only differences between the two models was the manner in which the loads were represented, and the trend of slightly higher safety factors with increasing three-dimensionality can once again be observed when comparing this model to the 2D and 3D (0.5 m) versions.

As previously stated, the considerable difference in safety factors observed for scenarios 2 and 5 can understood by considering the interaction boundaries between the soil and the external loads. By modelling the loads in more realistic 3D conditions, in which the 40kPa loads were distributed based on the geometry and spacing of the combine harvester wheels, the number of soil-wheel interfaces were increased, thus increasing the amount of soil resisting the load (compared to the size of the loading area), resulting in significantly larger safety factors.

By analysing these results, two arguments can be made regarding 2D and 3D stability analyses. Firstly, the use of 2D models can be significantly beneficial when considering relatively simple geometries with

no external loads, as these allow for higher degrees of mesh refinement while using significantly less memory space and quicker computation times.

However, when accounting for external loads present on a slope, the plane-strain conditions inherent with 2D modelling may result in a considerable underestimation of the slope stability and consequent safety factors. In such cases, and those considering complex geometries, a 3D slope stability analysis would therefore be more appropriate, provided that the mesh of the model can be refined enough to minimize the aforementioned element constraint effect. Alternatively, a suitable transformation process should be identified to convert the real loads in 3D into equivalent loads in 2D.

9 Conclusion & recommendations

9.1 Conclusion

In conclusion of this thesis, the results obtained from the various analyses are used to provide answers directly addressing the research questions posed in subsection 1.3.

1. **Could terp slopes present a danger of collapse in their current state, without any external loading applied?**

In this study, "steep" edges are defined as terp edges along slopes inclined by at least 35 degrees. To evaluate possible instabilities, information on the slopes must always be associated with that on the height of the terps. From scenarios 1 (5 m height and 35 ° slope angle), 12 (4 m height and 45 ° slope angle), and 16 (4 m height and 36 ° slope angle) it was possible to conclude that such slopes are stable under normal circumstances. The associated Safety Factors for scenarios 1, 12, and 16, were in fact of FS = 1.312, FS = 1.532, and FS = 1.511, respectively.

Furthermore, it was shown that the stability of steep edges is certainly aided by conditions of partial saturation. This cannot be relied on, however, as the effect can easily be lost following sufficient rainfall, which may occur in the area.

Even more so in the case of severe weather conditions, such as heavy rainfall or storms, one can expect the stability of the slopes to decrease further. This would be both due to the increased pore pressures and the erosion caused by surface runoff on the slopes. The degree to which such severe weather conditions would affect the overall stability of the slopes, and if such effects would be enough to cause slope failure with no additional external loads was not investigated in this project and would therefore need further analysis of its own.

2. **What types of external loads can one expect to the terp slopes to be subjected to, and how could these contribute to their instability?**

On the basis of the scenarios analysed, terp slopes with heights larger than 4 m and inclinations greater than or equal to 35 ° present a serious risk of instability when also featuring the presence of heavy vehicles, such as for agricultural activity near the slope crest. For all cases considered, in fact, the inclusion of the vehicle loads alone was enough to reduce the FS by 0.3 – 0.5, with all resulting Safety Factors having values below 1.1.

It is important to note that, although the safety factors associated with these scenarios are, in theory, still above unity, these have been shown to indicate a state of metastability at best, and any further disturbance can cause catastrophic failure. Furthermore, even should failure of the slope itself not occur, the risk remains of the vehicle itself falling down the slope, with potentially fatal consequences for the driver or anyone present below..

Scenarios involving both vehicle loads and a pre-existing ditch were also shown to result in states of metastability (see scenarios 14 and 19), or even instability (see scenario 5). Even when the effects of unsaturated zones are considered, the combined effect of the loads and ditch still presente~~d~~ significant stability risks (see scenario 22).

3. **What magnitude of loading can one expect in proximity of the terp slopes, and at what distance from the slope edges would these lead to potential slope collapse?**

For this project, the weight of heavy agricultural machinery was considered as the most likely unfavourable loading condition present on the terps. A total weight of 343 kN was estimated for a

combine harvester specifically, resulting in a contact pressure of 40 kPa between each wheel and the underlying soil. These loads were placed 0.5 m away from the slope edge.

The considered loading conditions proved to be a serious risk for the stability of the terp slopes, emphasising the danger applying heavy loads in proximity of the slope edges. While the exact distance from the slope edges at which heavy loading would no longer present a stability risk is difficult to quantify, a 1.5 – 2 m safety zone would be a reasonable measure to prevent both slope failure and limit the risk of heavy vehicles falling down the slope.

4. What dangers can be associated to the land use in proximity of the terp slopes, in relation to their potential instability?

Aside from the already discussed effect of vehicle loads tied to agricultural activities being performed near the edge of a terp, it was shown how the excavation of steep slopes at the terp edges also presents serious stability concerns. This is of particular relevance due to the documented cases of slopes with inclinations of 80 ° – 90 ° being excavated within the existing terp slopes, for archaeological studies.

From subchapter 7.1.2, in which scenario 7 was discussed, it was shown that a quasi-vertical slope, with a height of 5 m, excavated within the Westeremden terp can deceivingly appear as stable in the short term, immediately following its excavation. The safety factors associated with this scenario, however, were shown to decrease dramatically with time, due to the dissipation of negative excess pore pressures developed during the undrained excavation. It was in fact shown that the decrease in FS over time was so significant, that a freshly excavated 80 ° slope, which is initially able to remain stable with vehicle loads present, becomes unable to support itself, even without external loads, after just one month.

In this case, exposure of the slope to even slight rainfall would worsen the situation, due to the negative pore pressures dissipating faster and thus causing the stability of the slope to deteriorate more quickly. Heavy rainfall would make matters even worse, also due to the eroding effect of surface runoff.

Consequently, the excavation of such slopes should be considered as a serious stability risk, regardless of any apparent short-term equilibrium.

Furthermore, even if one were to excavate such a slope, but with a short enough height as to minimize stability concerns, it is strongly advised to not do so when agricultural activities are also taking place, as any unforeseen interaction between the slope and the agricultural vehicles (e.g., a crash or fall) could cause a sudden collapse of the slope, and potentially lead to casualties.

9.2 Recommendations

The final remarks for this project come in the form of a number of recommendations regarding both the significance of the obtained results, as well as possible improvements to increase the reliability of these.

Firstly, based on the analyses performed, the argument can be made that even the terp slopes with the most unfavourable geometries should be stable in static conditions, provided that no significant external force is applied in their direct proximity. It should be noted, however, that the terp slopes selected for analysis were chosen primarily based on geometric properties, and then on the availability of geotechnical data (which, in general, was lacking). The possibility remains of the existence of terp slopes that, despite perhaps not displaying the most unfavourable geometries, feature a terp soil composition significantly weaker than those analysed in this report. A more detailed inventory of the

terp slope soil properties, obtainable via further ground investigations and lab testing, would be useful to identify those slopes for which the soil composition presents the greatest risk of instability.

Secondly, it is strongly recommended to avoid situations in which heavy vehicles come into close proximity with steep edges of terp slopes. The results obtained from the static stability analyses clearly indicated that the highest risks of slope collapse occurred when the modelled vehicle loads were applied near the slope edges. To avoid potentially catastrophic incidents, a minimum distance from the slope edges should be clearly marked, within which no motor vehicle should be allowed to be operated. Exceptions could be made for particularly light vehicles, such as basic tractors which present an extremely lower load that those analysed in this report (see Appendix B). Such exceptions, however, should only be made after a thorough analysis of the effect of such small vehicle loads on slope stability.

Thirdly, further excavations performed on the existing terp slopes, such as those excavated during archaeological studies of the terps, should be limited to small heights and mild slopes not exceeding the original inclination. Limiting the slope height in particularly reduces the chance of slope collapse significantly, as well as the potential consequences should one occur regardless. Any apparent stability of freshly excavated slopes should not be taken for granted, as these could be only stable in the short-term, and collapse after a period of consolidation. The excavation of such slopes during and in proximity of activities involving significant loads (such as agricultural vehicles) should absolutely be avoided.

The final recommendation concerns the need for a more thorough ground investigation and laboratory testing of the soil terp layers, as well as the underlying soil. The greatest source of uncertainty in the analyses performed in this project is the geotechnical input parameters used for the models. While the Westeremden terp layers were subjected to laboratory testing with which the model properties were validated to a certain degree, these were applied to specimens obtained from a single borehole. A much bigger sample size would be required for a reliable characterization of the terp soil material.

For the Toornwerd terp, the lack of geotechnical data was even more an issue, and the soil layers had to be modelled based on undetailed information obtained from archaeological investigations and reference strength and stiffness parameter values. Oedometer test, or even more so, triaxial test results with which one could more reliably model the terp layers would have been of great benefit for this project.

Triaxial test or oedometer tests would have also been of great use for the modelling the subsoil layers in all models, due to the lack of other methods with which to estimate the stiffness parameters used in the Hardening Soil model. These were, in fact, the parameters for which the uncertainty was the highest.

It can thus be argued that additional geotechnical data would be the greatest asset for increasing the reliability of results from investigations such as the ones performed in this project.

References

Bentley Systems, Inc., 2021, PLAXIS CONNECT Edition V22.00 Material Models Manual.

Fijma, P., 2009. Archeologisch onderzoek Wierde Toornwerd, Inventariserend veldonderzoek en Archeologische begeleiding, Grontmij Archeologische Rapporten 485, 37 p.

Hielkema, J.B. and Jans, J.E.A., 2009. Plangebied W.J. Dethmerweg 9 te Toornwerd, gemeente Loppersum; een archeologische begeleiding. RAAP-NOTITIE 3183. 30 p.

Kruiver, P., de Lange, G., Kloosterman, F., Korff, M., van Elk, J., Doornhof, D., 2021. Rigorous test of the performance of shear-wave velocity correlations derived from CPT soundings: A case study for Groningen, the Netherlands. Soil Dynamics and Earthquake Engineering (IF 2.637) Pub Date: 2020-10-22, DOI: 10.1016/j.soildyn.2020.106471.

Kulhawy, F.H., and Mayne, P.H., 1990. Manual on estimating soil properties for foundation design, Report EL-6800 Electric Power Research Institute, EPRI, August 1990.

Meijles, E.W., Aalbersberg, G., Groenendijk, H.A., 2016. Terp composition in respect to earthquake risk in Groningen, RUG, Mar 2016.

Nicolay, J., 2019. Een doorsnede door zeven Friese terpen: Rapportage van het 'Terpenproject Steilkantonderzoek Friesland'. Grondsporen, Groninger Instituut voor Archeologie, Rijksuniversiteit Groningen. 77 p. plus appendices.

Postma, D., 2010. De opgraving en toekomstige bescherming van een steilkant. Terpbewoning in oostelijk Friesland. Twee opgravingen in het voormalige kweldergebied van Oostergo. Deel 1 Anjum opgraving. Nicolay (red.), Groningen Archaeological Studies, 10: 33-60.

Robertson, P.K. 2009. Interpretation of cone penetration tests – a unified approach, Canadian Geotech. J., 46(11):1337–1355.

Robertson, P.K., and Campanella, R.G., 1983a. Interpretation of cone penetration tests – Part I (sand). Canadian Geotechnical Journal, 20(4): 718-733.

Robertson, P.K., and Campanella, R.G., 1983b. Interpretation of cone penetration tests – Part II (clay). Canadian Geotechnical Journal, 20(4): 734-745.

Robertson, P.K. and Cabal, K.L., 2010. Estimating soil unit weight from CPT. 2nd International Symposium on Cone Penetration Testing, Huntington Beach, CA, USA, May 2010.

Robertson, P.K. and Cabal, K.L., 2015. Guide To Cone Penetration Testing, 6th Edition, 2015. Gregg Drilling & Testing Inc., Signal Hill, California, USA.

Soil Consolidation and Oedometer Test, THE INTERNATIONAL INFORMATION CENTER FOR GEOENGINEERS, https://www.geoengineer.org/education/laboratory-testing/soil-consolidation

TNO, 2016. DINOloket - Data en Informatie van de Nederlandse Ondergrond. Online. url: https://www.dinoloket.nl/html.

van den Doel, 2016, History of the Terp, https://connect-int.org/connections/2016/08/history-of-the-terp.

van der Kroft, P. and Varwijk, T.W. 2020. Hellend vlak: meetgegevens van steilkanten in het Fries-Groningse kweldergebied archeologisch vooronderzoek: een bureauonderzoek. RAAPrap_4644.

van der Sloot, 2013, March 07, Safety analysis and undrained behaviour, https://communities.bentley.com/products/geotech-analysis/w/plaxis-soilvision-wiki/45955/safety-analysis-and-undrained-behaviour.

Appendix A: Loads

A.1 Agricultural vehicle loads: combine harvester

The definition of the machine loads to be included in the models was based on a review of the agricultural machinery typically used in the region. It was decided to consider combine harvesters of different sizes and weights, and after reviewing the ranges of total forces, the heaviest was chosen as reference for the machine loads in order to produce conservative models.

The quantities involved in the determination of the machine loads can be seen in Table. For the calculation of the fuel and grain load weights, fuel and grain densities of 883 kg/m^3 and 721 kg/m^3 were considered, respectively. Harvester and cutting platform weights were based on technical specifications obtained from the website of the agricultural machinery manufacturing company John Deere. Specifically, the S790 combine and 635F cutting platform (Figure A.1, left) were used as reference, being the largest and heaviest models.

The spatial dimensions of the distributed loads were also determined based on reference values of combine harvester dimensions. As not enough information was available from John Deere regarding harvester width and wheel spacing, the remaining data required to make a reference case was obtained from another agricultural machinery manufacturing company, Claas. The Lexion 780 model was chosen as it is comparable to the John Deere S790 in terms of weight and size, and the total data combined from these two models was sufficient to produce a realistic reference case for the machine loads. The width dimensioning of the Lexion 780 model can be seen in Figure A.1 (right).

It should be noted that the contact area used to convert the force per wheel into distributed load was larger than the actual wheel surface area. This correction was applied to estimate a more realistic distribution of stress on the soil – wheel interface, and essentially entails a 45% increase in contact area compared to the actual wheel surface, an amount obtained from engineering judgement following consults on typical wheel loads simulated in such analyses.

As shown in Table A.1, for the heaviest possible combine harvester, this resulted in a contact pressure of 40 kN/m^2 per wheel. Comparatively, this is considerably higher than the surface pressure commonly attributed to vehicle loads in engineering practice, which is generally around 20 kN/m^2. However, given the type of vehicle being considered, and to maintain a conservative approach, a value of 40 kN/m^2 was deemed appropriate.

Figure A.1: John Deere S790 combine and 635F platform (left). Width dimensions for the Lexion 780, 770 and 670 (780 being the largest) (right).

Table A.1: Determination of reference machine loads.

Machine:	Combine Harvester (including cutting platform)
Combine mass:	20750 kg
Auger platform mass:	3000 kg
Fuel capacity:	1.25 m^3
Grain capacity:	14 m^3
Total mass:	35000 kg
Total weight:	343 kN (35 ton)
Number of wheels:	4
Force per wheel:	86 kN
Wheel length:	1.5 m
Wheel width:	0.9 m
Pressure per wheel:	40 kN/m^2

A.2 Other possible vehicle loads

In addition to the combine harvester considered, an inventory of other possible vehicles, with corresponding wheel surface loads, is provided in Figure A.2 to A.5.

John Deere 6 Series – 230R	
Base machine weight	9.3 tons
Wheelbase	2.9 m
Track	1.7 m
Force per wheel (front)	20 kN
Force per wheel (rear)	25 kN
Pressure per wheel (front)	13 kPa
Pressure per wheel (rear)	26 kPa
Corrected soil pressure per wheel (front)	9 kPa
Corrected soil pressure per wheel (rear)	17 kPa

John Deere 6 Series – 6250R	
Base machine weight	11.4 tons
Wheelbase	2.93 m
Track	1.93 m
Force per wheel (front)	25 kN
Force per wheel (rear)	34 kN
Pressure per wheel (front)	27 kPa
Pressure per wheel (rear)	18 kPa
Corrected soil pressure per wheel (front)	18 kPa
Corrected soil pressure per wheel (rear)	12 kPa

Figure B.11: John Deere 6 Series tractors. Dimensions and loads

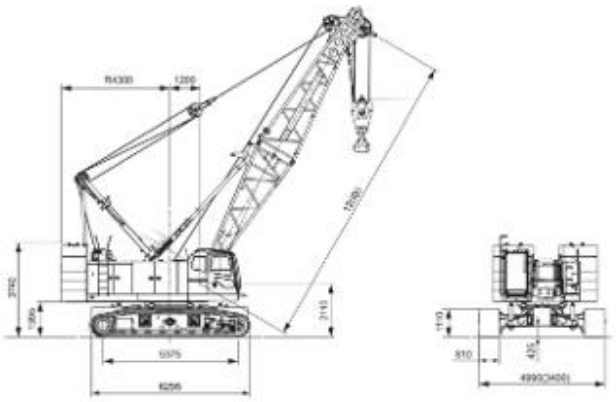

Hitachi SCX1000A-3	
Gross Vehicle Weight	101 tons
Continuous track length	5.375 m
Continuous track width	0.81 m
Force per continuous track	495 kN
Pressure per continuous track	114 kPa

Figure B.12: Hitachi SCX1000A-3 crane. Dimensions and loads

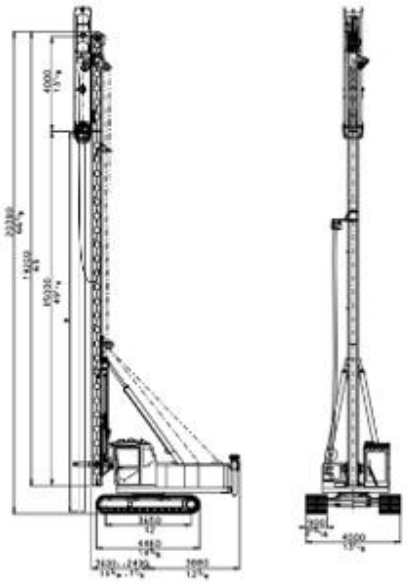

Junttan PM16	
Gross Vehicle Weight	37 tons
Continuous track length	3.65 m
Continuous track width	0.9 m
Force per continuous track	181 kN
Pressure per continuous track	55 kPa

Figure B.13: Junttan PM16 crane. Dimensions and loads

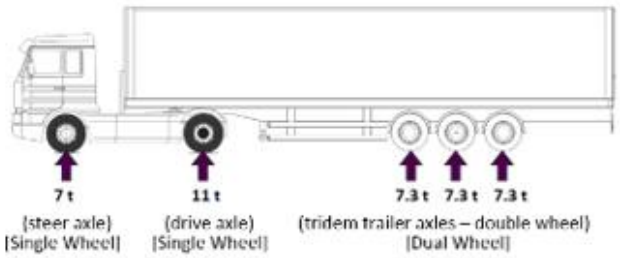

Generic Two-Axle Tractor + Tridem Axle Trailer (2)	
Gross Vehicle Weight	39.9 tons
Trailer length	13.6 m
Force per wheel (steer axle)	34 kN
Force per wheel (drive axle)	54 kN
Force per wheel (trailer)	36 kN
Pressure per wheel (steer axle)	114 kPa
Pressure per wheel (drive axle)	179 kPa
Pressure per wheel (trailer)	59 kPa
Corr. Soil pressure per wheel (steer axle)	76 kPa
Corr. Soil pressure per wheel (drive axle)	119 kPa
Corr. Soil pressure per wheel (trailer)	40 kPa

Tractor + Multi-Axle Bale Trailer (Grasbalen transport)	
Gross Vehicle Weight	24.5 tons
Trailer storage length	8.54 m
Trailer storage width	2.5 m
Force per wheel (steer axle)	25 kN
Force per wheel (drive axle)	43 kN
Force per wheel (trailer)	26 kN
Pressure per wheel (steer axle)	23 kPa
Pressure per wheel (drive axle)	23 kPa
Pressure per wheel (trailer)	64 kPa
Corr. Soil pressure per wheel (steer axle)	15.1 kPa
Corr. Soil pressure per wheel (drive axle)	15.1 kPa
Corr. Soil pressure per wheel (trailer)	42.3 kPa

Figure B.14: Tractor + multi-axle trailer for grass ball transport. Dimensions and loads

Appendix B: DINOloket borehole data

In this appendix, a summary of the DINOloket geological models is provided. All information given is taken directly from the DINOloket website and the TNO (2016) report listed in the references.

B.1 The Digital Geological Model & GeoTop Model

The Digital Geological Model (DGM) is a model of the subsurface geological layers of the Netherlands, defined up to a depth of 500 m NAP. In this model, the geological layers are classified into lithostratigraphic units based on the lithology and rock properties of each, and insight into the spatial relationships of these units is provided.

The DGM layer model is based on approximately 26500 verified, high quality borehole logs, selected from the 430000 available on the DINOloket database. All of the borehole logs used for the DGM are coupled with a validated lithostratigraphic interpretation.

While the DGM provides a representation of the subsurface at the regional level, a smaller-scale model is required when characterizing the subsoil at a local scale.

The GeoTOP model refines the top 50 m of the DGM, providing a detailed view of the Dutch subsurface based on a higher concentration of borehole logs. The model contains as much information on the subsurface as possible, represented in borehole logs with lithostratigraphic interpretations and lithological classes.

GeoTOP is applied when information on the stratigraphy and lithology of the shallow subsurface is of high importance, such as groundwater studies, prediction of land subsidence, foundation design, etc. In this project, it was used to characterize the shallow subsoil relevant for the stability analysis for Dutch terp slopes.

B.2 Quality levels of DINOloket borehole logs

All lithostratigraphic interpretations obtained from DINOloket are authorised by the Geological Survey of the Netherlands, which distinguishes between 3 levels of quality:

- Quality Level 1: The borehole interpretation has been validated during the formation of the DGM subsurface model, and is thus one of the 26500 detailed borehole logs that have been verified during the modelling process.
- Quality Level 2: The borehole interpretation has been made independently from the DGM modelling project, and thus has not been validated.
- Quality Level 3: The borehole interpretation has been generated automatically in the context of the GeoTOP model. Only some of these interpretations have been checked (at random).

The borehole interpretation that has been used to characterize the Toornwerd terp subsoil is of Quality Level 1.

Appendix C: Westeremden CPTs

All CPTs for the Westeremden terp used in this project are presented in this Figure C.1 to C.4.

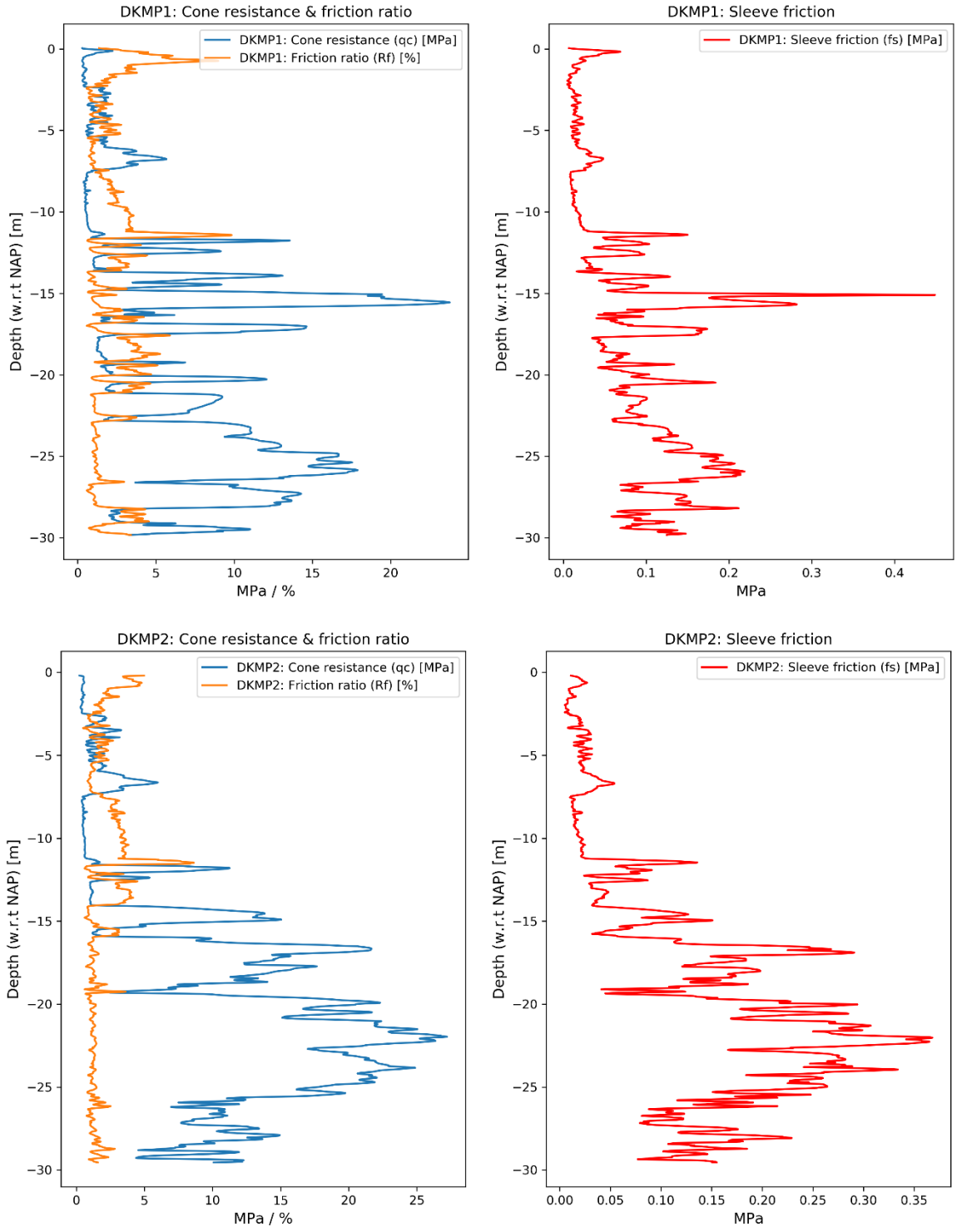

Figure C.1: CPTs DKMP1 & DKMP2 (Fugro).

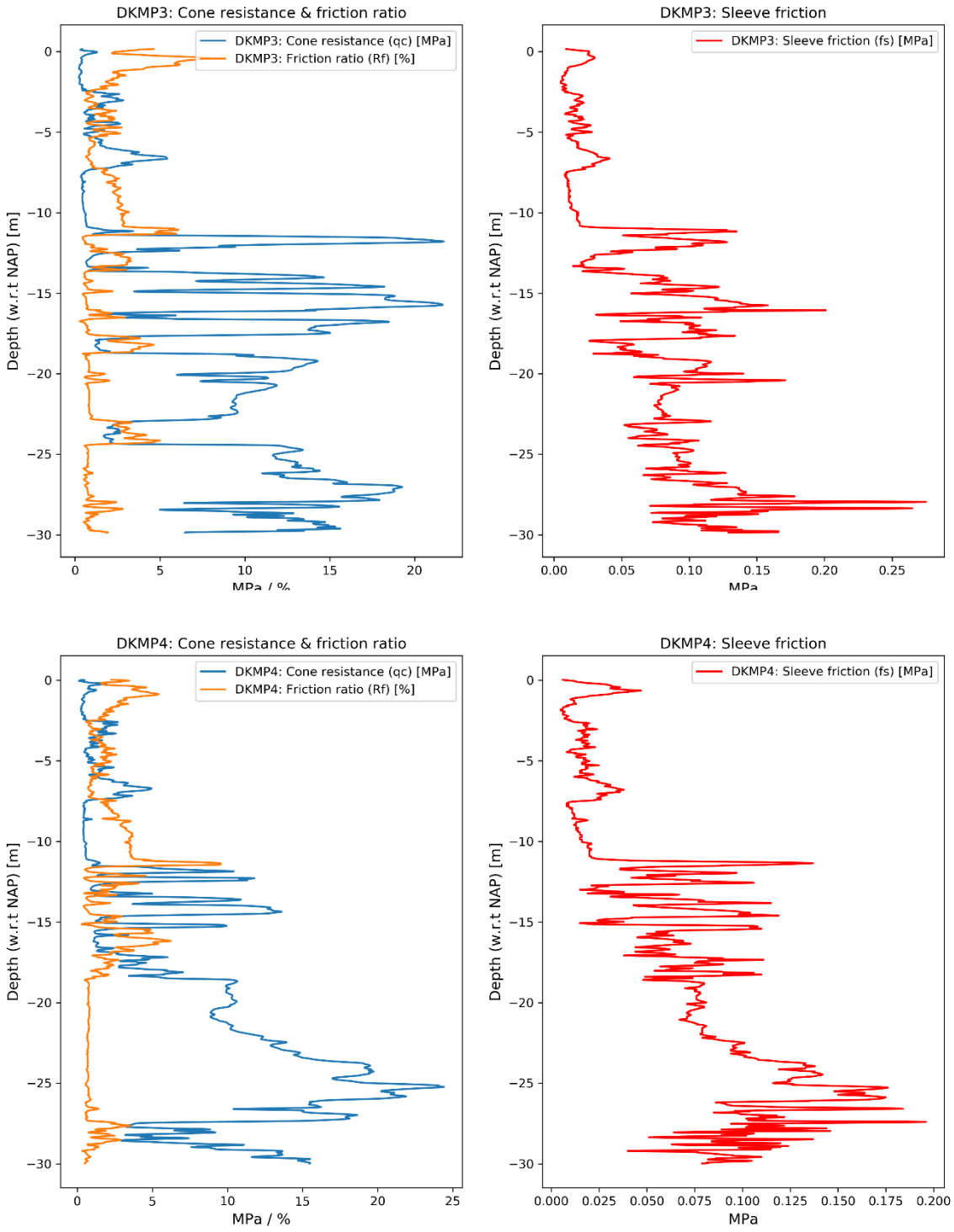

Figure C.2: CPTs DKMP3 & DKMP4 (Fugro).

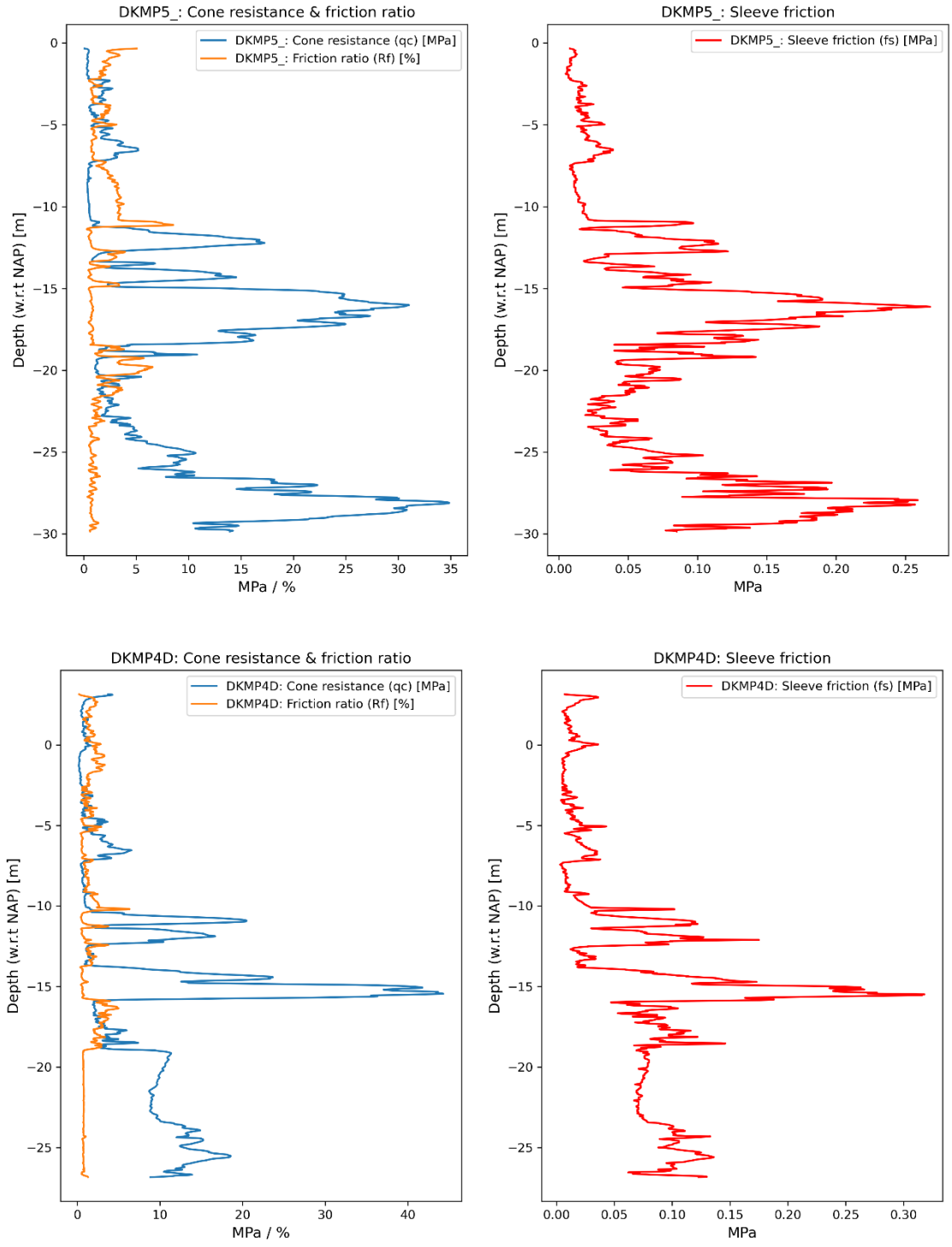

Figure C.3: CPTs DKMP5 & DKMP4D (Fugro).

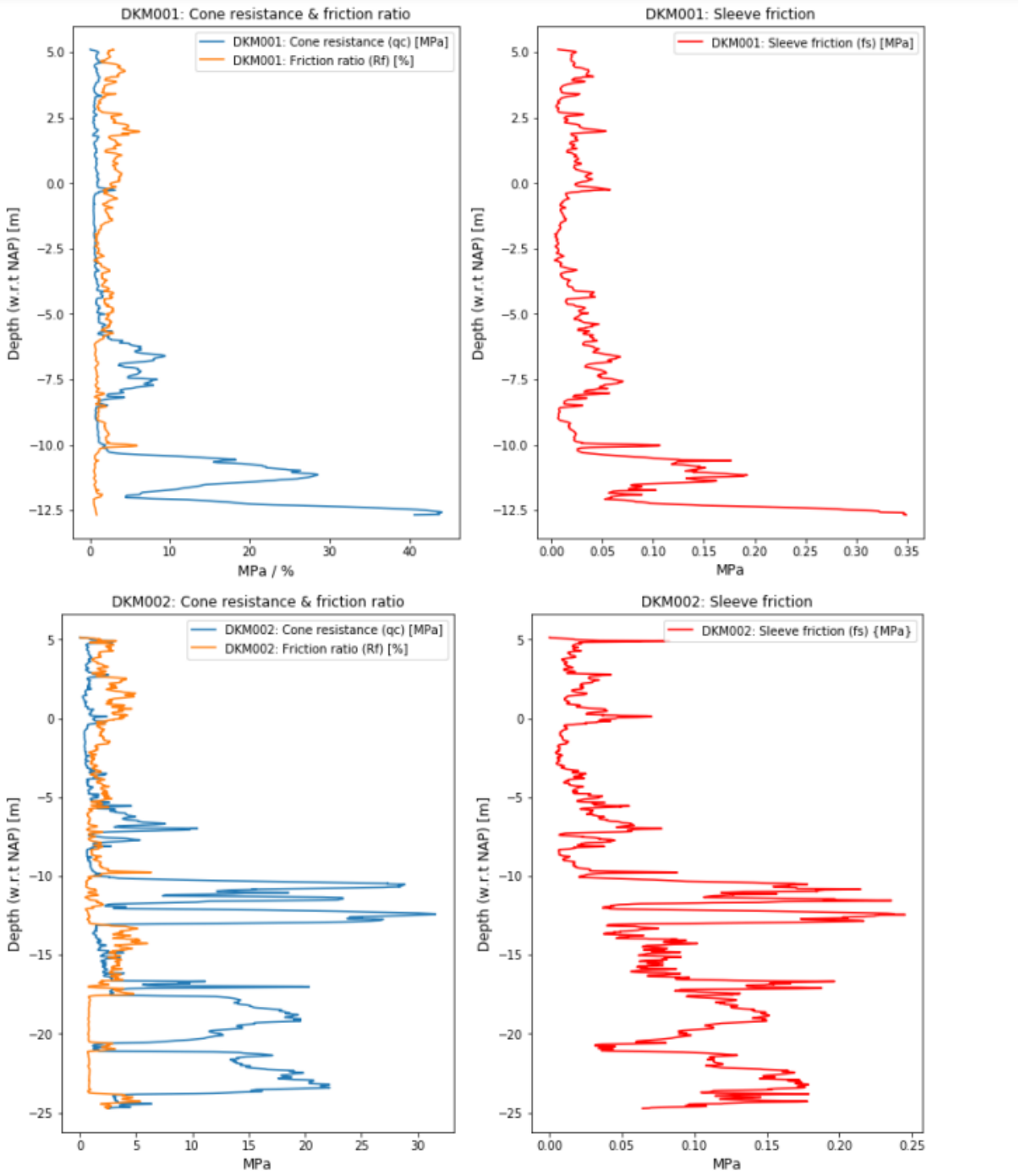

Figure C.4: CPTs DKM001 & DKM002 (Wiertsma & Partners).

Appendix D: Toornwerd

D.1 DINOloket CPT (S07B00261)

The readings from the Toornwerd CPT S07B00261 are shown in Figure D.1, below.

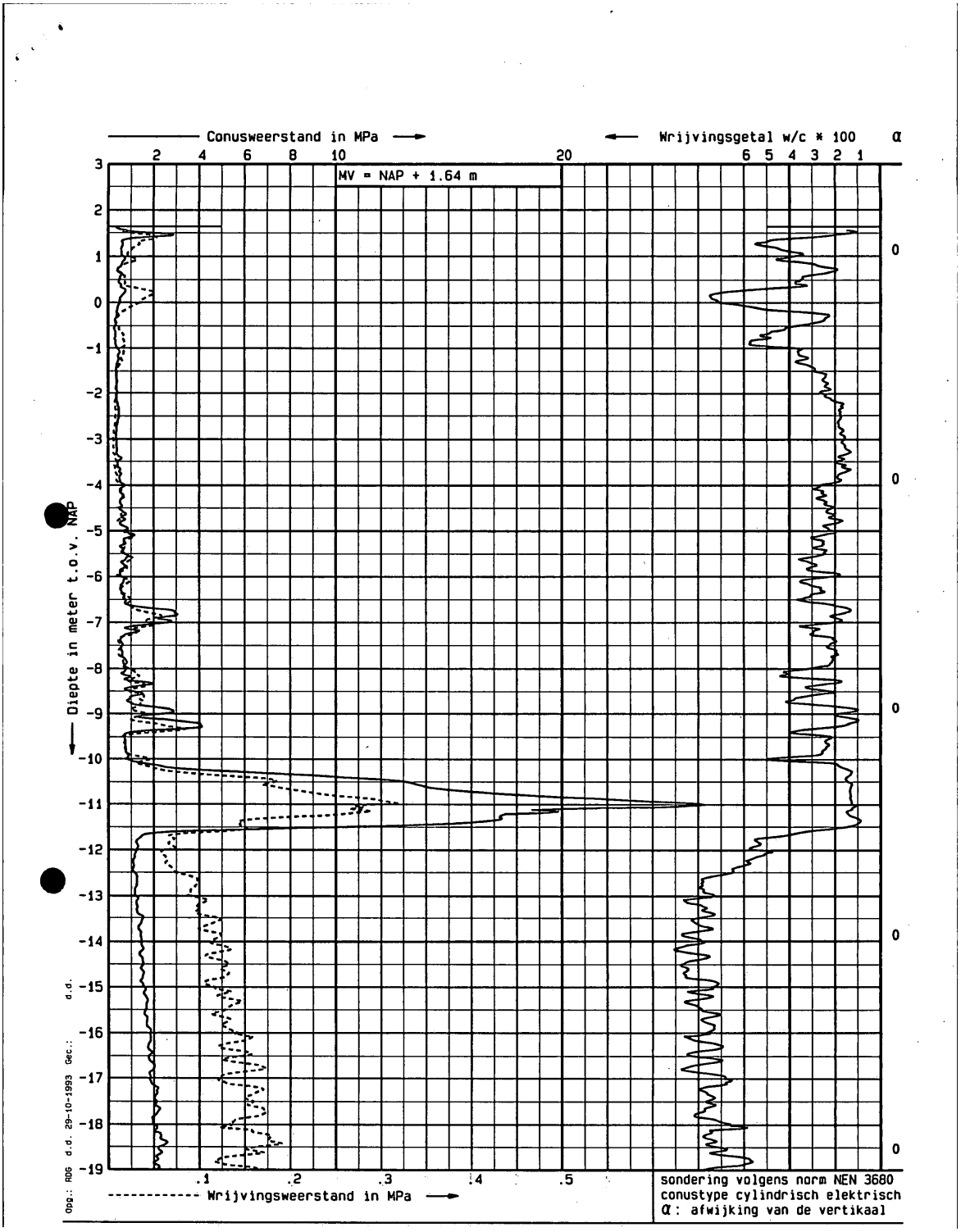

Figure D.1: Toornwerd CPT S07B00261 (DINOloket).

D.2 DINOloket Borehole (B07B0119)

The lithostratigraphic interpretation of the borehole B07B0119 obtained from DINOloket is shown in Figure D.2, below.

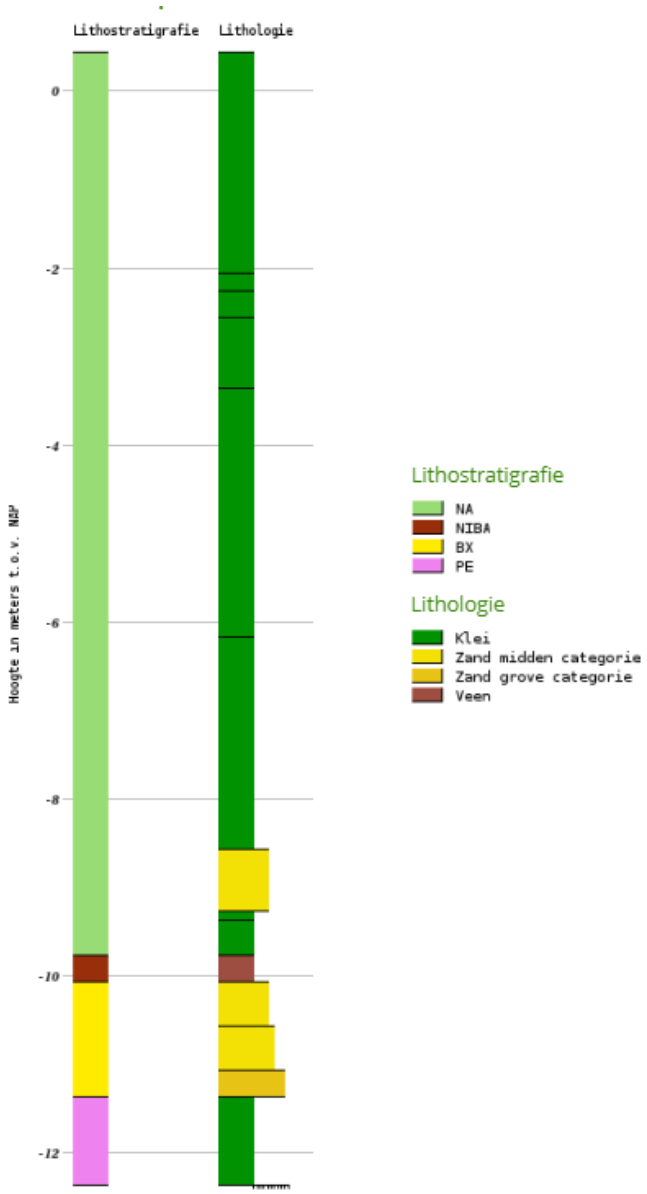

Figure D.2: Stratigraphic model of the Toornwerd borehole (DINOloket).

The borehole interpretation is classified as Quality Level 1 on DINOloket (see Appendix B.2).

D.3 Toornwerd soil profile

The subsoil profile used in the static analyses for the Toornwerd reference terp is shown below.

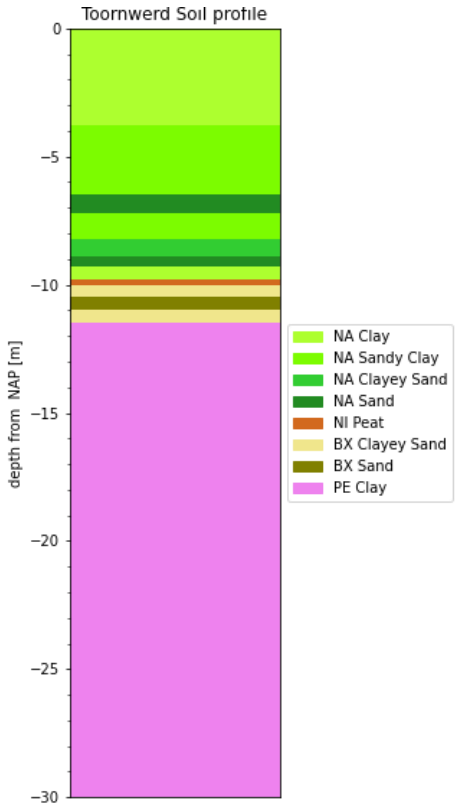

Figure D.3: Toornwerd model subsoil profile (Piunno & Rossetti, 2021)

Appendix E: Soil Behaviour Type (SBT) methods

E.1 Traditional SBT, SBTn, and modified SBT methods

The most common CPT-based methods to estimate soil types are based on the charts suggested by Robertson et al. (1986), Robertson (1990) and Robertson (2010). These charts link cone resistance and friction ratio readings to specific soil behaviour types (SBTs), through which different types of soils are classified. The distinction is made between three versions:

- Non-normalized CPT Soil Behaviour Type (SBT) chart: Robertson et al. (1986).
- Normalized CPT Soil Behaviour Type (SBTn) chart: Robertson (1990).
- Modified non-normalized CPT Soil Behaviour Type (SBT) chart: Robertson (2010).

The original SBT chart is solely based on readings taken directly from performed CPTs, in the form of cone resistance (q_c or q_t) and friction ratio (R_f), as shown in Figure E.1. The distinction between q_c and q_t is made based on the availability of pore pressure readings (u_2), with which the measured cone resistance (q_c) is corrected for pore pressure effects and thus converted to the corrected cone resistance (q_t). A further parameter required for this correction process is the net area ration of the CPT apparatus (a), which is determined from laboratory calibration and has typical values between 0.70 and 0.85 (Robertson et. al, 2014). The formula used to determine the corrected cone resistance (q_t) is shown below.

$$q_t = q_c + u_2(1 - a)$$

In general, the SBT chart can be used with either version of the cone resistance, as the difference between the two is negligible, with the exception of fine-grained soils with a q_c < 1 MPa (Robertson, 2010). As can be seen by Figure E.1, the SBT chart recognizes 12 different soil behaviour types.

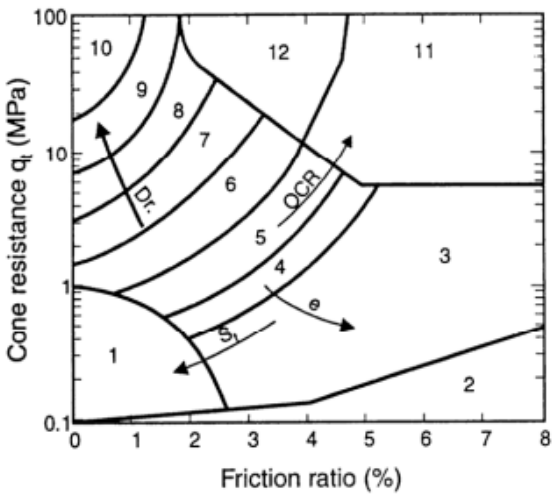

Zone	Soil Behavior Type
1	Sensitive fine grained
2	Organic material
3	Clay
4	Silty Clay to clay
5	Clayey silt to silty clay
6	Sandy silt to clayey silt
7	Silty sand to sandy silt
8	Sand to silty sand
9	Sand
10	Gravelly sand to sand
11	Very stiff fine grained*
12	Sand to clayey sand*

* Overconsolidated or cemented

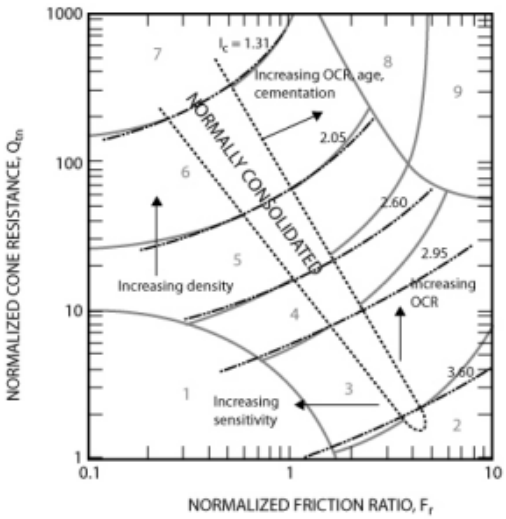

Zone	Soil Behavior Type
1	Sensitive, fine grained
2	Organic soils - clay
3	Clay – silty clay to clay
4	Silt mixtures – clayey silt to silty clay
5	Sand mixtures – silty sand to sandy silt
6	Sands – clean sand to silty sand
7	Gravelly sand to dense sand
8	Very stiff sand to clayey sand*
9	Very stiff fine grained*

* Heavily overconsolidated or cemented

Figure E.1: Left: SBT chart (Robertson et al., 1986). Right: SBTn chart (Robertson, 1990)

The SBTn chart, also shown in Figure E.1, makes use of normalized CPT parameters (Q_{tn} and F_r), as both cone resistance and sleeve friction are known to increase with depth due to the increasing effective overburden stress. This chart distinguishes between 9 soil behaviour types.

The normalization of the cone resistance and friction ratio occurs via the formulae shown below. The normalized cone resistance (Q_{tn}) and normalized friction ratio (F_r) are obtained based on the calculated overburden stress (σ_{vo}), CPT sleeve friction (f_s), atmospheric reference pressure (P_a), and soil-dependent stress exponent (n).

$$Q_{tn} = \left(\frac{q_t - \sigma_{vo}}{P_a}\right)\left(\frac{P_a}{\sigma'_{vo}}\right)^n$$

$$F_r = \left(\frac{f_s}{q_t - \sigma_{vo}}\right) * 100$$

The stress exponent parameter (n) is determined iteratively using the normalized soil behaviour index (I_c), which is based on the normalized cone resistance (Q_{tn}) and normalized friction ratio (F_r), as shown by the equations below (Robertson, 2009).

$$n = 0.381(I_c) + 0.05\left(\frac{\sigma'_{vo}}{P_a}\right) - 0.15$$

$$I_c = [(3.47 - \log(Q_{tn}))^2 + (\log(F_r) + 1.22)^2]^{0.5}$$

In this iteration process, an initial value of n = 1.0 is assumed. The Q_{tn} is then calculated, followed by the I_c, leading to a new value for n. This process is repeated until $\Delta n \leq 0.01$ (Robertson, 2009). Robertson & Wride (1998) linked values of the I_c parameter to specific SBTn zones, as can also be seen in the SBTn chart shown in Figure E.1.

The use of normalized CPT parameters makes soil interpretations based on the SBTn more reliable than the traditional SBT charts. However, these are only applicable when accurate information on soil unit weight and groundwater conditions is available. Furthermore, when the effective overburden stress lies between 50 kPa and 150 kPa, there is often little difference between the SBT and SBTn soil interpretations (Robertson, 2010).

Due to its simplicity and the smaller number of parameters required, the use of the traditional SBT method remained a popular choice despite the existence of the newer, normalized SBTn version. For this reason, Robertson (2010) provided an update on the traditional method in the form of the modified non-normalized SBT chart, combining elements of both SBT and SBTn methods.

Table E.1: Proposed unification between 12 SBT zones and 9 SBTn zones (Robertson 2010).

SBT zone (Robertson et al, 1986)	SBTn zone (Robertson, 1990)	Proposed common modified non-normalized SBT description
1	1	Sensitive fine-grained
2	2	Clay – organic soil
3	3	Clays: clay to silty clay
4 & 5	4	Silt mixtures: clayey silt to silty clay
6 & 7	5	Sand mixtures: silty sand to sandy silt
8	6	Sands: clean sands to silty sands
9 & 10	7	Dense sand to gravelly sand
12	8	Stiff sand to clayey sand (OC or cemented)
11	9	Stiff fine-grained (OC or cemented)

The non-normalized SBT chart uses the cone resistance (q_c or q_t), made dimensionless by dividing by the atmospheric pressure (P_a), and friction ratio (R_f). The 12 soil behaviour types identified by the original SBT chart were reduced to 9 in order to match those from the SBTn method. The unification of the soil behaviour types proposed by Robertson (2010) are shown in Table E.1.

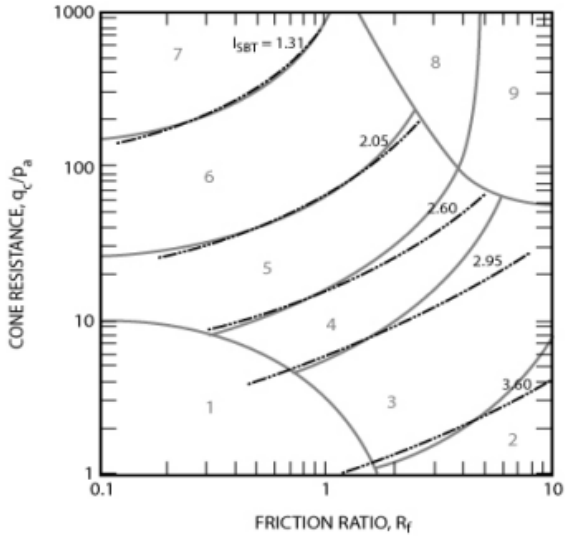

Zone	Soil Behaviour Type (SBT)
1	*Sensitive fine-grained*
2	*Clay - organic soil*
3	*Clays: clay to silty clay*
4	*Silt mixtures: clayey silt & silty clay*
5	*Sand mixtures: silty sand to sandy silt*
6	*Sands: clean sands to silty sands*
7	*Dense sand to gravelly sand*
8	*Stiff sand to clayey sand**
9	*Stiff fine-grained**

** Overconsolidated or cemented*

Figure E.2: Modified (non-normalized) SBT chart (Robertson, 2010).

The resulting modified non-normalized SBT chart is shown in Figure E.2, above. Robertson (2010) also presents a non-normalized soil behaviour index (I_{SBT}) soil behaviour index, which is essentially the same as the normalized version but only involves the basic CPT measurements:

$$I_{SBT} = [(3.47 - \log(q_c/P_a))^2 + (\log(R_f) + 1.22)^2]^{0.5}$$

As shown in Figure E.2, the I_{SBT} parameter can be used to approximate the soil behaviour type of a given soil. This is done as follows:

- $I_{SBT} > 3.60$: SBT zone = 2
- $2.95 < I_{SBT} \leq 3.60$: SBT zone = 3
- $2.60 < I_{SBT} \leq 2.95$: SBT zone = 4
- $2.05 < I_{SBT} \leq 2.60$: SBT zone = 5
- $1.31 < I_{SBT} \leq 2.05$: SBT zone = 6
- $I_{SBT} \leq 1.31$: SBT zone = 7

When applying the modified SBT method for soil classification based on CPT readings, both measured cone resistance (q_c) and the corrected cone resistance (q_t) can be applied. However, the corrected cone resistance should be applied when pore pressure (u_2) measurements are available, as this will lead to more accurate classification, particularly with cohesive fine-grained soils (Robertson, 2010).

E.2 Fugro modified SBTn method

Another version of the soil behaviour type charts is proposed by Fugro, in which the normalized SBTn charts are modified in order to improve their applicability in Dutch soils. The modifications applied by Fugro are the following:

- Soils with a $q_c < 1.5$ MPa and $R_f > 5\%$ as peat.
- A different distribution of SBT zones 4 and 5, aimed at producing improved interpretations of loose sands and shallow clay layers.

The resulting SBTn chart proposed by Fugro is shown in Figure E.3.

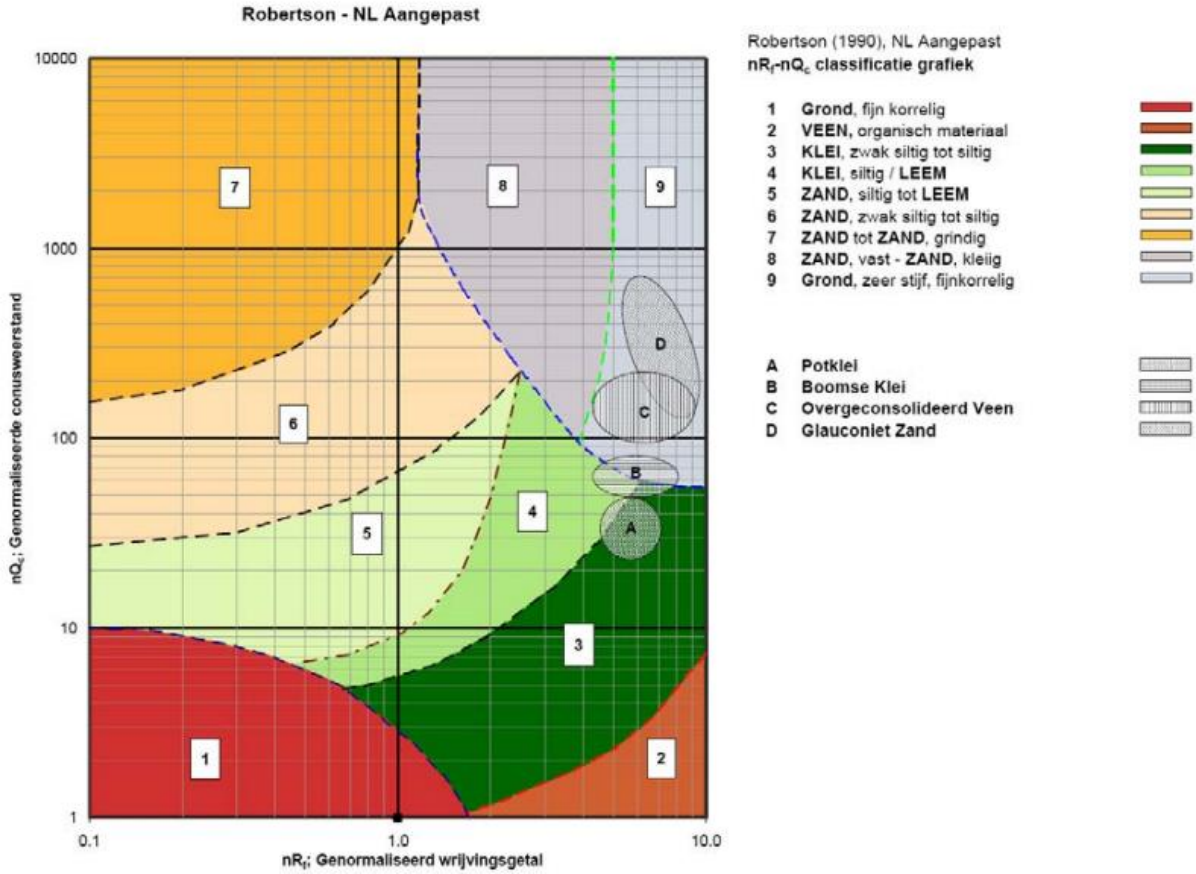

Figure D.3: Modified SBTn chart as proposed by Fugro for CPT-based classifications of Dutch soils.

Appendix F: Liquid Limit determination graphs

The graphs used to estimate the liquid limit of the Westeremden soil samples tested with the liquid limit penetrometer method (see subsection 4.2.3) are shown in Figure F.1, below.

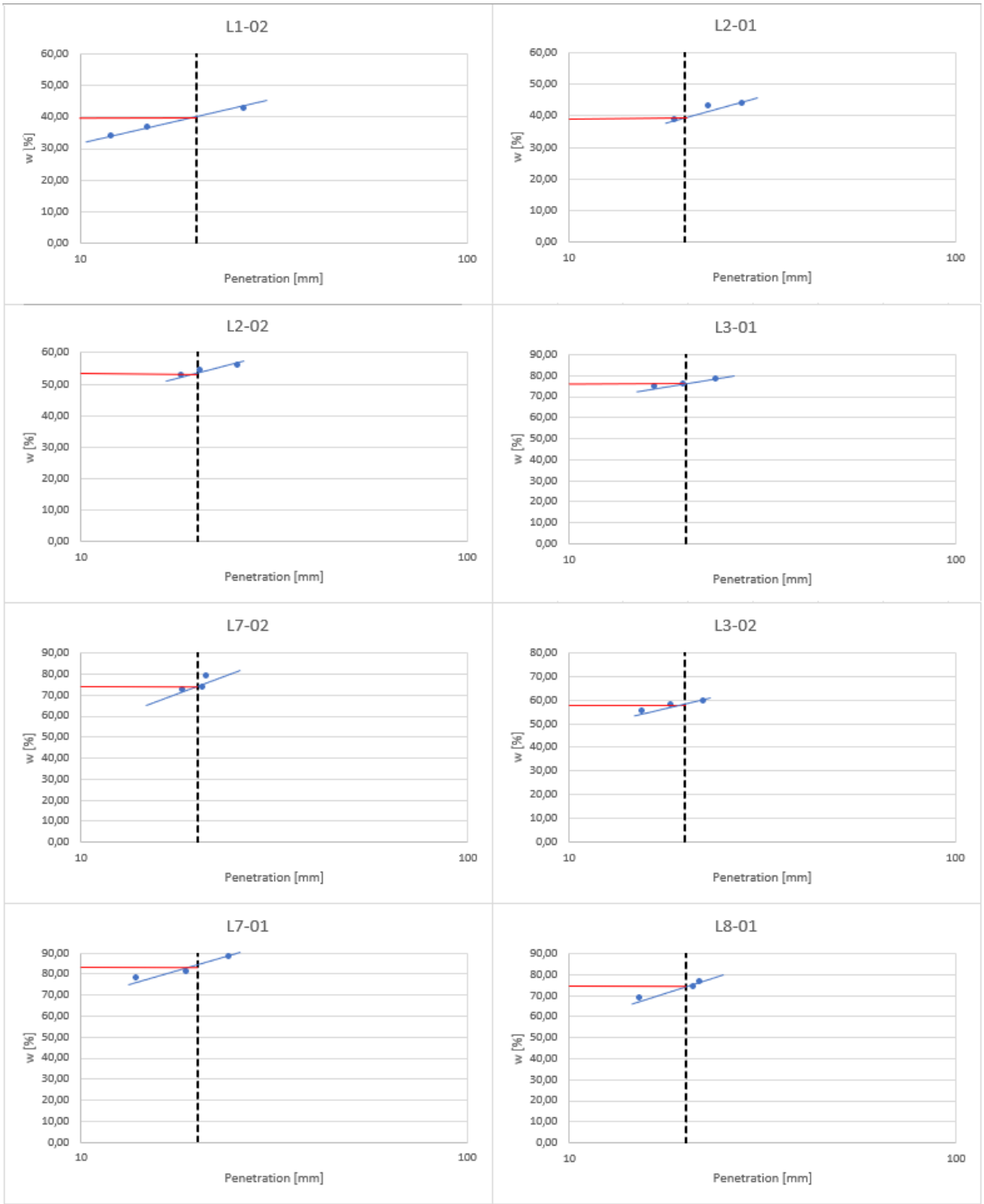

Figure F.1: Graphical estimation of the water content at which the liquid limit cone penetrometer reached a penetration of 20 mm (used to determine the liquid limit of the samples).

Appendix G: Undrained Triaxial & DSS tests (Plaxis SoilTest)

Screenshots of the PLAXIS SoilTest procedures are given in Figure F.1 and Figure F.2 for the NA Peat Terp and NA Clay Terp soils, respectively. For the NA Peat Terp, the cell pressures applied for the two simulated undrained triaxial tests 13.04 kN/m^2 (top left in Figure F.1) and 15.66 kN/m^2 (bottom left in Figure F.1), while the initial vertical stress applied to the two simulated undrained DSS tests were of 30.59 kN/m^2 (top right in Figure F.1) and 36.72 kN/m^2 (bottom right in Figure F.1).

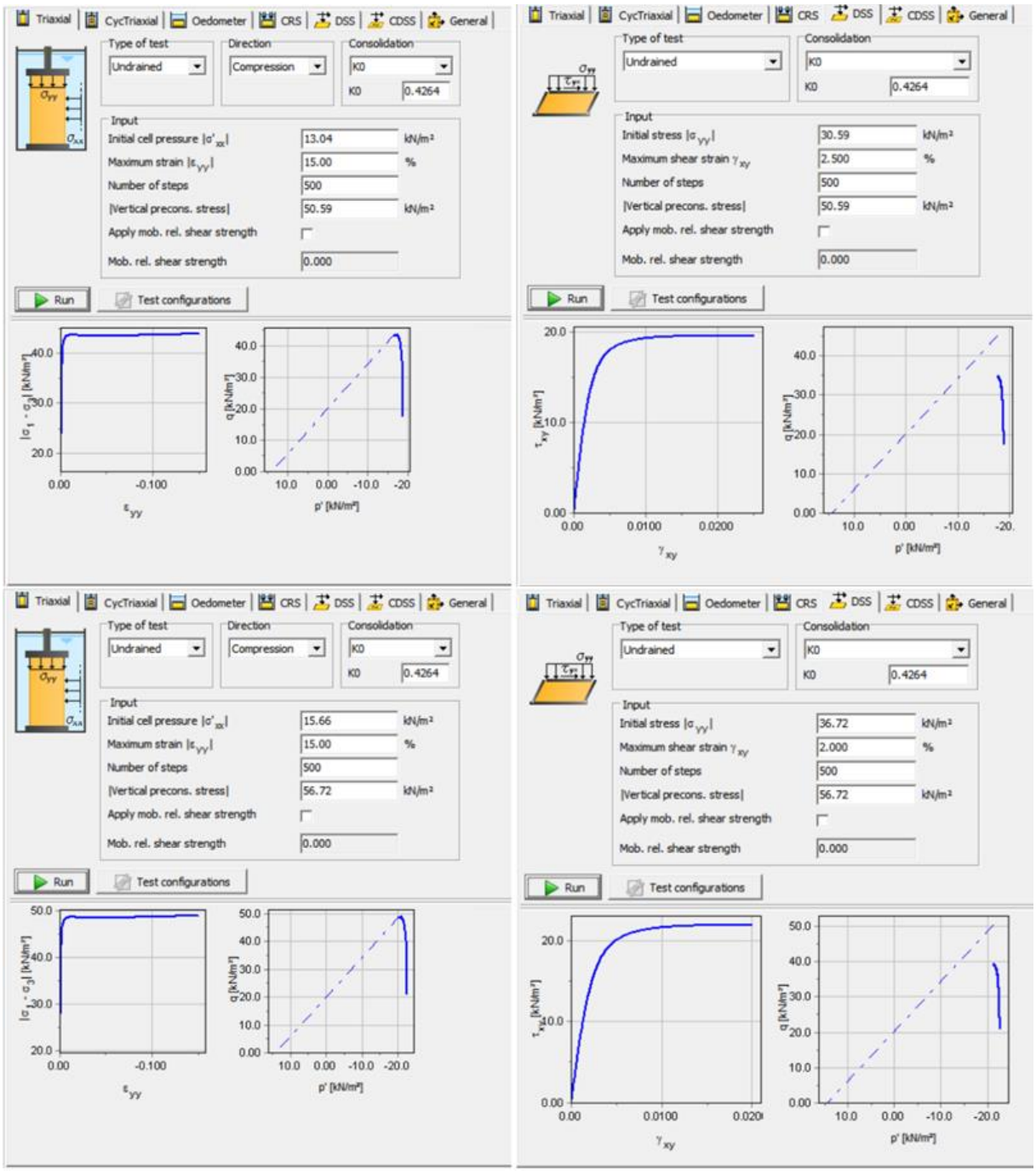

Figure G.1: NA Peat Terp PLAXIS SoilTest results for the upper layer (top) and lower layer (bottom).

For the NA Clay Terp, the cell pressures applied for the simulated undrained triaxial tests were 7.82 kN/m^2 (top left in Figure F.2) and 20.12 kN/m^2 (bottom left in Figure F.2), while the initial vertical stress applied to the simulated undrained DSS tests were 13.55 kN/m^2 (top right in Figure F.2) and 34.85 kN/m^2 (bottom right in Figure F.2).

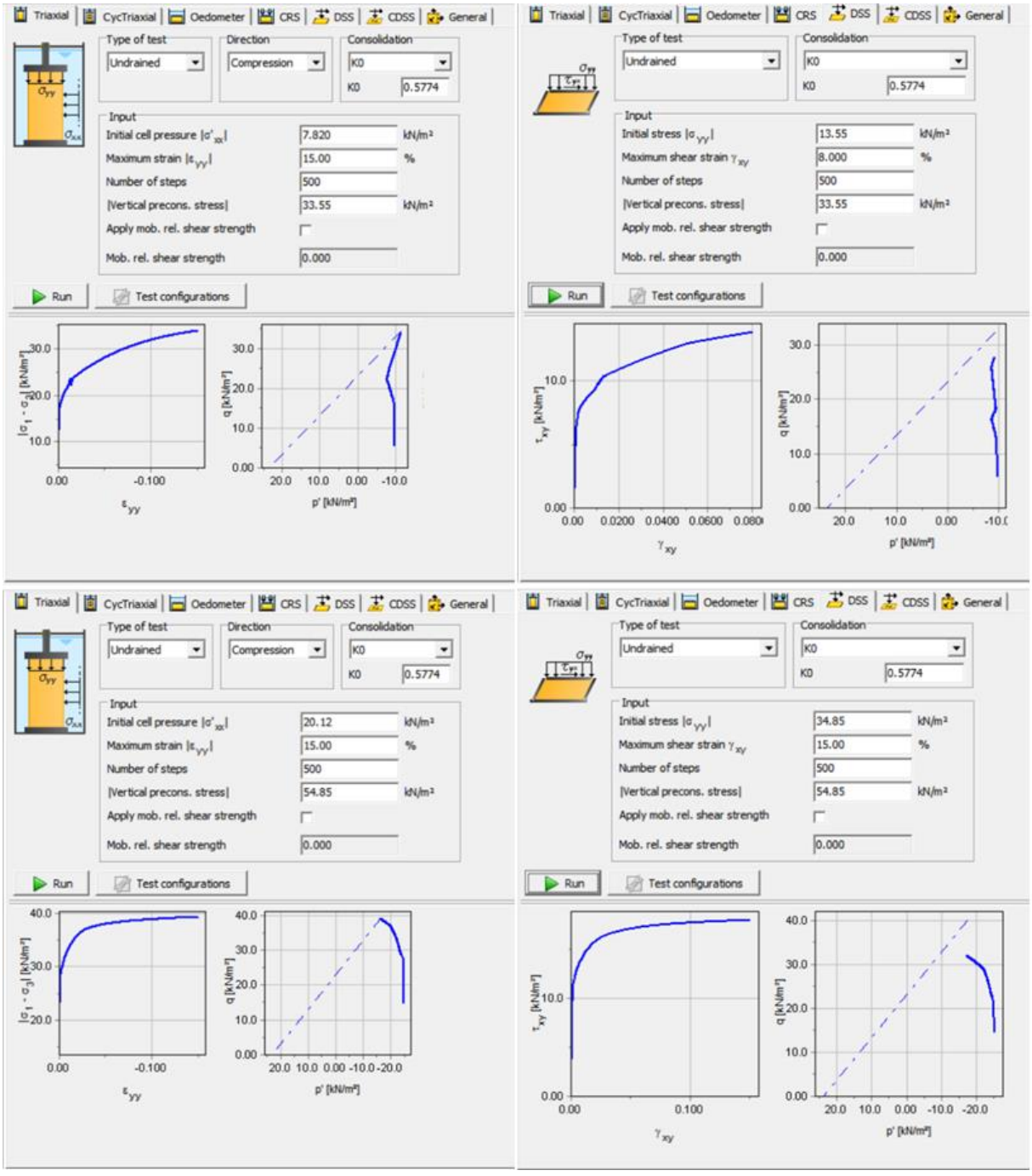

Figure G.2: NA Clay Terp PLAXIS SoilTest results for the upper layer (top) and lower layer (bottom).

Appendix H: Parameter values obtained from empirical formulae

H.1 Angle of internal friction (I)

The reference values for soil friction angle resulting from the application of the empirical formulae of Campanella & Robertson (1983), Mayne (2006), and Robertson & Cabal (2010), presented in subsection 4.3.2, are listed in Table H.2, below.

Table H.1: Friction angle based on Campanella & Robertson (1983), Mayne (2006), and Robertson & Cabal (2010).

Layer:	Layer bottom [m NAP]	φ' [°]
NA Peat	-0.7	28
NA Clay	-2.5	28
NA Sandy Clay	-6.0	38
NA Clayey Sand	-6.4	38
NA Sand	-7.0	40.5
NA Clayey Sand	-7.8	35
NA Clay	-11.0	31
NI Peat	-11.3	N/A
BX Sandy Clay	-12.8	29
BX Clay	-13.7	30.5
BX Clayey Sand	-14.5	38
BX Sandy Clay	-15.0	28
PE Sand	-16.0	43
PE Sandy Clay	-17.0	28
PE Sand	-17.8	38
PE Clay	-18.5	29
PE Sandy Clay	-19.2	29
PE Clayey Sand	-20.8	31
PE Clay	-21.2	29
PE Clayey Sand	-22.4	36
PE Clay	-23.0	28
PE Clayey Sand	-25.0	37
PE Sand	-30	35

H.2 Angle of internal friction (II)

The reference values for soil friction angle resulting from the application of the empirical formulae of Kulhawy & Mayne (1990), Mayne (2006), and Robertson & Cabal (2010), presented in subsection 4.3.2, are listed in Table H.2, below.

Table H.2: Friction angle based on Kulhawy & Mayne (1990), Mayne (2006), and Robertson & Cabal (2010).

Layer:	Layer bottom [m NAP]	φ' [°]
NA Peat	-0.7	N/A
NA Clay	-2.5	28
NA Sandy Clay	-6.0	28
NA Clayey Sand	-6.4	31
NA Sand	-7.0	34
NA Clayey Sand	-7.8	29
NA Clay	-11.0	31
NI Peat	-11.3	N/A
BX Sandy Clay	-12.8	29
BX Clay	-13.7	31
BX Clayey Sand	-14.5	31
BX Sandy Clay	-15.0	28
PE Sand	-16.0	36
PE Sandy Clay	-17.0	28
PE Sand	-17.8	31
PE Clay	-18.5	29
PE Sandy Clay	-19.2	29
PE Clayey Sand	-20.8	26
PE Clay	-21.2	29
PE Clayey Sand	-22.4	30
PE Clay	-23.0	28
PE Clayey Sand	-25.0	31
PE Sand	-30	29

Appendix I: Application of Table 2b (NEN 9997-1)

I.1 Table 2b (NEN 9997-1)

Grondsoort			Karakteristieke waarde [a] van grondeigenschap											
Hoofd-naam	Bijmengsel	Consis-tentie [b]	γ [c] kN/m³	γ_{sat} kN/m³	q_c [d g] MPa	C'_p [g]	C'_s	$C_c/(1+e_0)$ [g] [-]	C_α [f] [-]	$C_{sw}/(1+e_0)$ [g] [-]	E_{100} [g h] MPa	φ' [g] Graden	c' kPa	c_u kPa
Grind	Zwak siltig	Los	17	19	15	500	∞	0,004 6	0	0,001 5	45	32,5	0	N.v.t.
		Matig	18	20	25	1 000	∞	0,002 3	0	0,000 8	75	35,0	0	
		Vast	19 20	21 22	30	1 200 1 400	∞	0,001 9 0,001 6	0	0,000 6 0,000 5	90 105	37,5 40,0	0	
	Sterk siltig	Los	18	20	10	400	∞	0,005 8	0	0,001 9	30	30,0	0	N.v.t.
		Matig	19	21	15	600	∞	0,003 8	0	0,001 3	45	32,5	0	
		Vast	20 21	22 22,5	25	1 000 1 500	∞	0,002 3 0,001 5	0	0,000 8 0,000 5	75 110	35,0 40,0	0	
Zand	Schoon	Los	17	19	5	200	∞	0,011 5	0	0,003 8	15	30,0	0	N.v.t.
		Matig	18	20	15	600	∞	0,003 8	0	0,001 3	45	32,5	0	
		Vast	19 20	21 22	25	1 000 1 500	∞	0,002 3 0,001 5	0	0,000 8 0,000 5	75 110	35,0 40,0	0	
	Zwak siltig, kleiig		18 19	20 21	12	450 650	∞	0,005 1 0,003 5	0	0,001 7 0,001 2	35 50	27,0 32,5	0	N.v.t.
	Sterk siltig, kleiig		18 19	20 21	8	200 400	∞	0,011 5 0,005 8	0	0,003 8 0,001 9	15 30	25,0 30,0	0	N.v.t.
Leem [e]	Zwak zandig	Slap	19	19	1	25	650	0,092 0	0,003 7	0,030 7	2	27,5 30,0	0	50
		Matig	20	20	2	45	1 300	0,051 1	0,002 0	0,017 0	3	27,5 32,5	1	100
		Vast	21 22	21 22	3	70 100	1 900 2 500	0,032 9 0,023 0	0,001 3 0,000 9	0,011 0 0,007 7	5 7	27,5 35,0	2,5 3,8	200 300
	Sterk zandig		19 20	19 20	2	45 70	1 300 2 000	0,051 1 0,032 9	0,002 0 0,001 3	0,017 0 0,011 0	3 5	27,5 35,0	0 1	50 100
Klei	Schoon	Slap	14	14	0,5	7	80	0,328 6	0,013 1	0,109 5	1	17,5	0	25
		Matig	17	17	1,0	15	160	0,153 3	0,006 1	0,051 1	2	17,5	5	50
		Vast	19 20	19 20	2,0	25 30	320 500	0,092 0 0,076 7	0,003 7 0,003 1	0,030 7 0,025 6	4 10	17,5 25,0	13 15	100 200
	Zwak zandig	Slap	15	15	0,7	10	110	0,230 0	0,009 2	0,076 7	1,5	22,5	0	40
		Matig	18	18	1,5	20	240	0,115 0	0,004 6	0,038 3	3	22,5	5	80
		Vast	20 21	20 21	2,5	30 50	400 600	0,076 7 0,046 0	0,003 1 0,001 8	0,025 6 0,015 3	5 10	22,5 27,5	13 15	120 170
	Sterk zandig	-	18 20	18 20	1,0	25 140	320 1 680	0,092 0 0,016 4	0,003 7 0,000 7	0,030 7 0,005 5	2 5	27,5 32,5	0 1	0 10
	Organisch	Slap	13	13	0,2	7,5	30	0,306 7	0,015 3	0,102 2	0,5	15,0	0 1	10
		Matig	15 16	15 16	0,5	10 15	40 60	0,230 0 0,153 3	0,011 5 0,007 7	0,076 7 0,051 1	1,0 2,0	15,0	0 1	25 30
Veen	Niet voorbelast	Slap	10 12	10 12	0,1	5 7,5	20 30	0,460 0 0,306 7	0,023 0 0,015 3	0,153 3 0,102 2	0,2 0,5	15,0	1 2,5	10 20
	Matig voorbelast	Matig	12 13	12 13	0,2	7,5 10	30 40	0,306 7 0,230 0	0,015 3 0,011 5	0,102 2 0,076 7	0,5 1,0	15,0	2,5 5	20 30
Variatiecoëfficiënt v			0,05		–	0,25					0,10		0,20	

[a] De tabel geeft van de desbetreffende grondsoort de lage, respectievelijk de hoge karakteristieke waarde van gemiddelden. Binnen een gebied, vastgesteld door de rij van het bijmengsel en de kolom van de parameter (een cel), geldt:

— als een verhoging van de waarde van een van de grondeigenschappen tot een ongunstiger situatie leidt dan de toepassing van de in de tabel gepresenteerde lagere karakteristieke waarde, moet de rechterwaarde op dezelfde regel zijn gebruikt. Is er rechts geen waarde vermeld, dan moet de waarde er recht onder zijn toegepast;
OPMERKING Dit is bijvoorbeeld het geval bij negatieve kleef op een paal waar een hogere waarde van φ', c' en c_u ook een hogere waarde van de negatieve kleef oplevert.

— voor $C_c/(1+e_0)$, C_α en $C_{sw}/(1+e_0)$ zijn in de tabel de hoge karakteristieke gemiddelde waarden vermeld.

Figure I.1: Table 2b from NEN 9997-1

I.2 Hardening Soil model parameters approximated from Table 2b (NEN 9997-1)

The reference values for soil strength and stiffness parameters resulting from the application of Table 2b from NEN 9997-1, discussed in subsection 4.4, are listed in Table I.1, below.

Table I.1: Strength and stiffness parameter reference values obtained from Table 2b of NEN 9997-1.

Layer:	Layer bottom [m NAP]	φ' [°]	c' [kPa]	E_{100} [MPa]	E_{50}^{ref} [MPa]	E_{oed}^{ref} [MPa]	E_{ur}^{ref} [MPa]
NA Peat	-0.7	15.0	5.0	1.00	1.25	1.0	3.75
NA Clay	-2.5	22.5	0.1	1.52	1.90	1.52	5.69
NA Sandy Clay	-6.0	22.6	3.5	2.60	3.25	2.60	9.74
NA Clayey Sand	-6.4	25.7	0.0	17.63	22.03	17.63	66.10
NA Sand	-7.0	27.0	0.0	35.0	43.75	35.0	131.25
NA Clayey Sand	-7.8	25.3	0.0	16.13	20.16	16.13	60.47
NA Clay	-11.0	22.5	0.0	1.50	1.88	1.50	5.63
NI Peat	-11.3	15.0	5.0	1.00	1.25	1.00	3.75
BX Sandy Clay	-12.8	30.0	0.5	3.50	4.38	3.50	13.13
BX Clay	-13.7	22.6	5.1	3.10	3.88	3.10	11.63
BX Clayey Sand	-14.5	27.7	0.0	23.44	29.30	23.44	87.89
BX Sandy Clay	-15.0	30.0	0.5	3.50	4.38	3.50	13.13
PE Sand	-16.0	29.5	0.0	41.82	52.27	41.82	156.82
PE Sandy Clay	-17.0	30.0	0.5	3.5	4.38	3.50	13.13
PE Sand	-17.8	28.4	0.0	38.75	48.44	38.75	145.31
PE Clay	-18.5	22.5	5.0	3.00	3.75	3.0	11.25
PE Sandy Clay	-19.2	30.0	0.5	3.50	4.38	3.50	13.13
PE Clayey Sand	-20.8	25.8	0.0	17.53	21.91	17.53	65.74
PE Clay	-21.2	23.6	9.0	5.03	6.28	5.03	18.84
PE Clayey Sand	-22.4	26.0	0.0	18.81	23.51	18.81	70.54
PE Clay	-23.0	25.8	12.2	7.80	9.75	7.80	29.25
PE Clayey Sand	-25.0	27.9	0.0	24.65	30.82	24.65	92.45
PE Sand	-30.0	27.4	0.0	36.20	45.25	36.20	135.75

Appendix J: HS parameter calibration based on G_0 profile.

Piunno (2021) suggested a method for calibrating HS model parameters from a CPT-based G_0 vs. depth profile.

The Hs small model predicts the stiffness at small strains (G_0) as a function of the increase in effective stresses and the degree of over-consolidation (OCR), using the following expression:

$$G_0 = G_{0,ref}\left(\frac{c'\cos(\phi')+\sigma_3'\sin(\phi')}{c'\cos(\phi')+p_{ref}\sin(\phi')}\right)^m$$

The stress dependency and the OCR enter both in the term σ_3', which is the minor principal stress (assumed to be the horizontal effective stress in at-rest conditions*). Furthermore, the relationship is hyperbolic, thanks to the exponent m. It is worth remarking that the G_0 predicted by HS small model of a point at a given stress level and characterized by a given OCR is uniquely defined once $G_{0,ref}$, c', ϕ', m, p_{ref} are assigned.

Given the G_0 profile from CPT tests and the HS small model formula for the prediction of G_0, the following procedure can be adopted:

- Draw a first trial stratigraphy using the soil profiling techniques described above.
- Associate a homogeneous material to each identified layer.
- Define $\gamma, G_{0,ref}, c', \phi', m, p_{ref}$ for each material, using the estimate from the CPT empirical formulas where possible, otherwise using first trial values based on literature sources and expert judgment.
- Assign the state of the material in terms of OCR: it is possible to estimate the OCR either using empirical relationships from CPT data or consulting literature references.
- Calculate the effective vertical stress (note that this is a function of the groundwater table level, to be fixed according to available information).
- Calculate the horizontal effective stress as a function of the vertical one and the OCR.
- Calculate the G_0 profile using the HS small model formula.
- Compare the calculated profile with that estimated from the CPT data.
- Iterate the procedure until you find the match between the two profiles, with the desired accuracy.

Once a satisfactory G_0 profile is produced, values for the HS model E-moduli can then be estimated via the following relations:

- $\frac{G_0^{ref}}{G_{ur}^{ref}} \approx 8-10\ (fine\ grained\ soils)$
- $\frac{G_0^{ref}}{G_{ur}^{ref}} \approx 2-4\ (coarse\ grained\ soils)$
- $E_{ur}^{ref} = 2*(1+\nu_{ur})*G_{ur}^{ref}$
- $E_{50}^{ref} \approx \frac{E_{ur}^{ref}}{3}$
- $E_{50}^{ref} \approx 1.25 * E_{oed}^{ref}$

The proposed G_0 calibration method is shown applied to the Fugro DKMP1 CPT in Figure I.1. The blue scatter plot points are the G_0 values obtained from the shear wave velocity, which itself was estimated via the formula presented in section 4.3.3. The black line represents the modelled G_0 profile resulting from the iterative calibration steps listed in this Appendix.

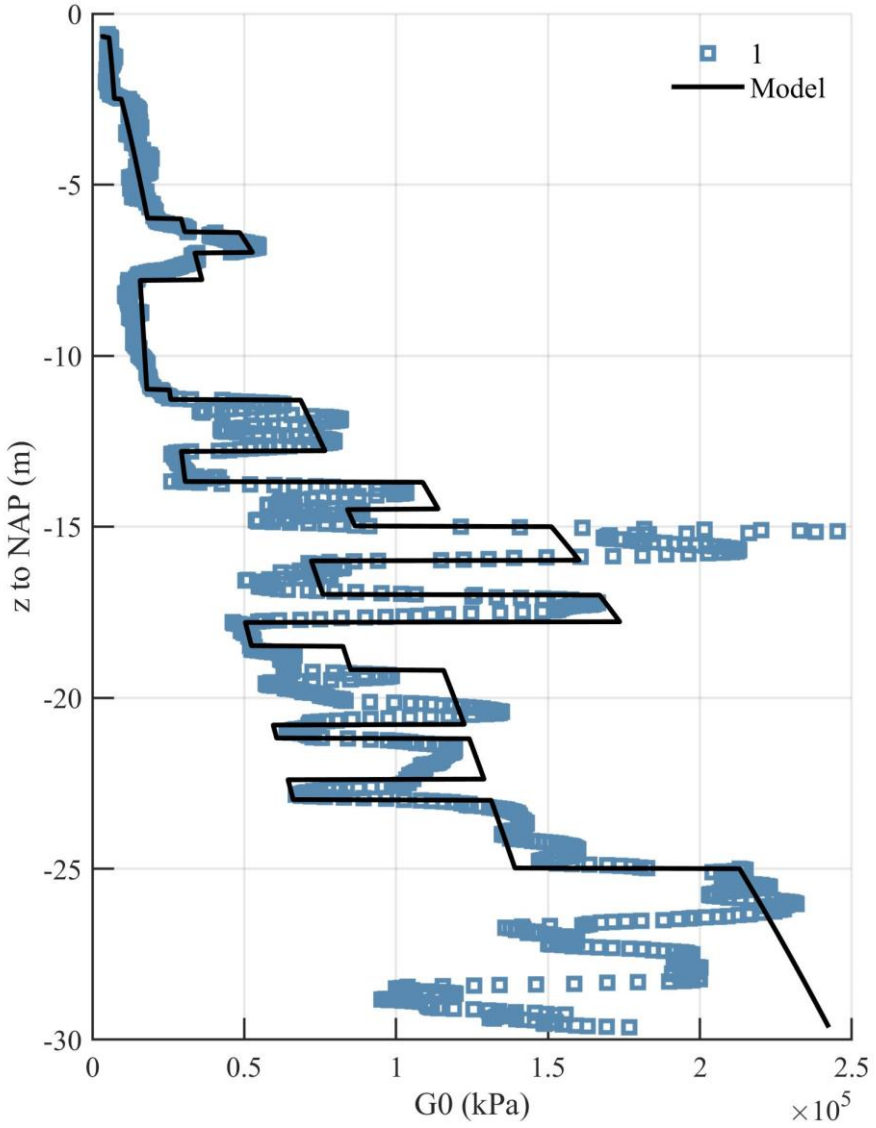

Figure J.1: Calibration of the G_0 profile via the iteration of HSsmall parameters, applied to FUGRO's CPT DKPM1 (Piunno, 2021).

*This assumes that the directions of major and minor principal stresses within the soil are vertical and horizontal, respectively. In reality, this is not the case due to the shear stresses that exist between adjacent blocks of soil, which increase with increasing angles of internal friction. Obtained results can therefore only approximate the real values, and further studies should be performed to assess the degree of accuracy of this method.

Appendix K: Additional 3D models

K.1 Scenarios 1,2,4, & 5 (3D version – 0.5 m extension)

This model was made by extending the 2D model of the Westeremden terp by 0.5 m into the y-direction. The 40 kPa surface loads for scenarios 2 and 5 therefore span the full 0.5 m width.

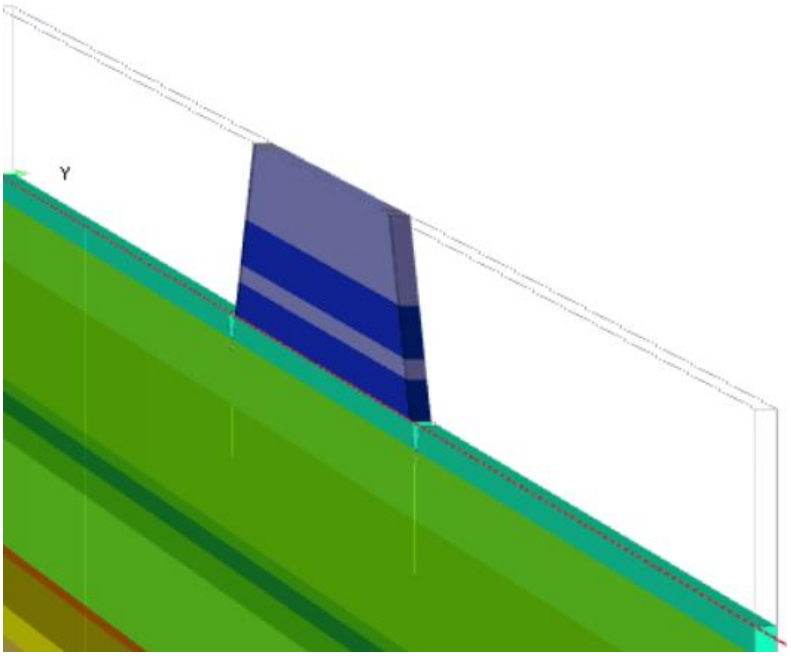

Figure K.1: 3D (0.5 m) model for scenarios 1, 2, 4, and 5.

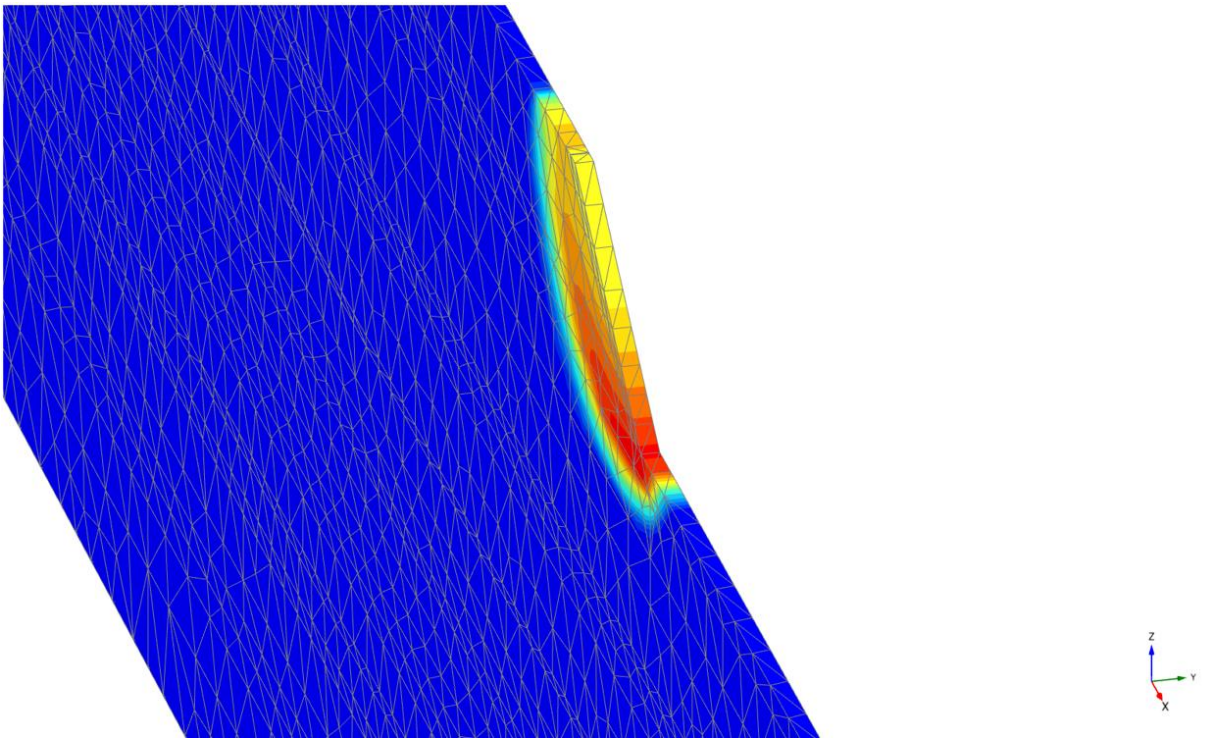

Figure K.2: Element coarseness & failure mechanism of the 3D (0.5 m) model.

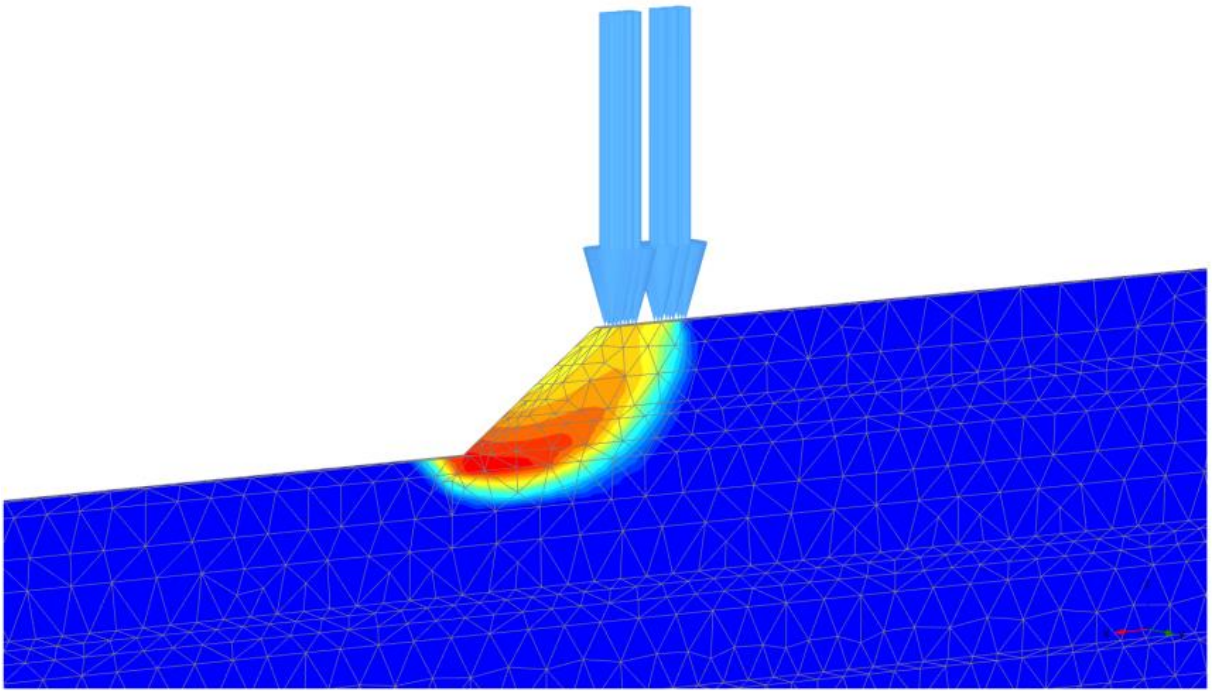

Figure K.3: 3D (0.5 m) model failure mechanism (scenario 4).

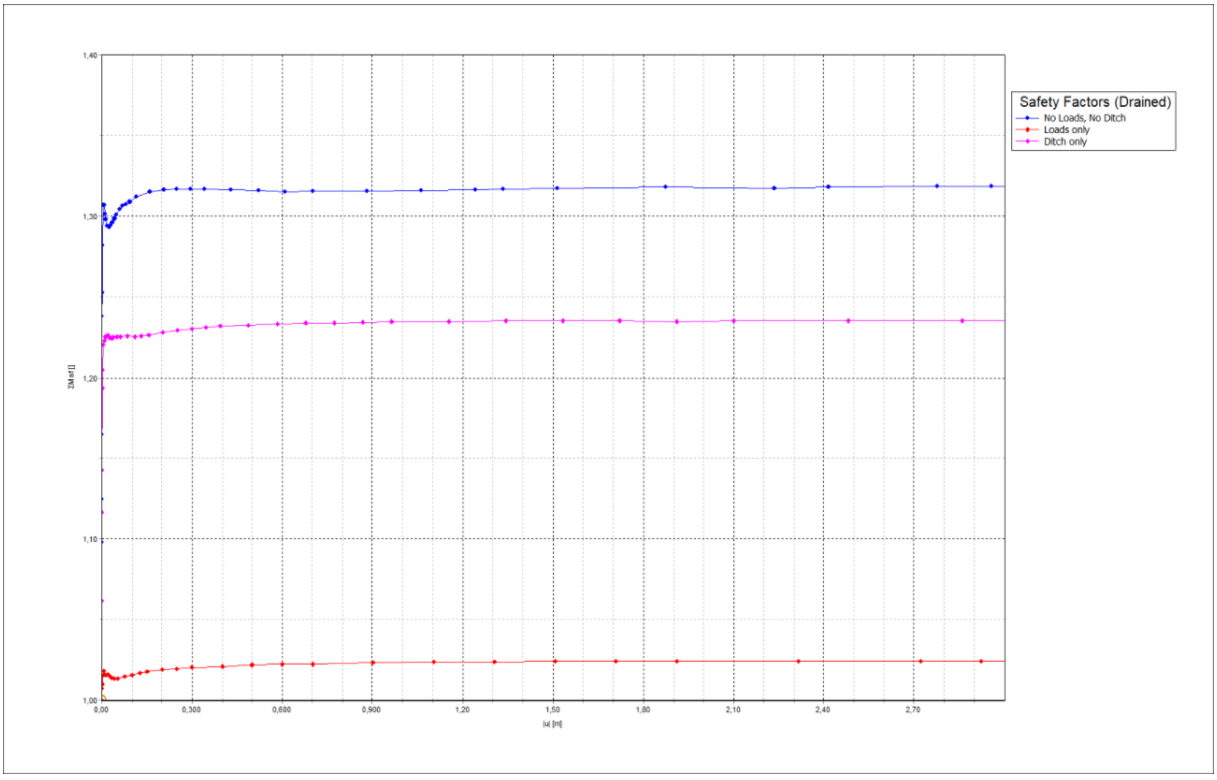

Figure K.4: Safety factors obtained for scenarios 1,2, 4, and 5 from the 3D (0.5 m) model.

K.2 Scenarios 1,2,4, & 5 (3D version – 50 m extension)

In this model, the vehicle loads were characterized as 4 distributed loads, each representing one wheel of the agricultural vehicle. The dimensions and spacing of the wheel loads were defined as in section 5 for the 2D models, but with an added centreline spacing of 3.8 m in the y-direction separating the front and rear wheels, as illustrated in the technical specifications of the combine harvester considered.

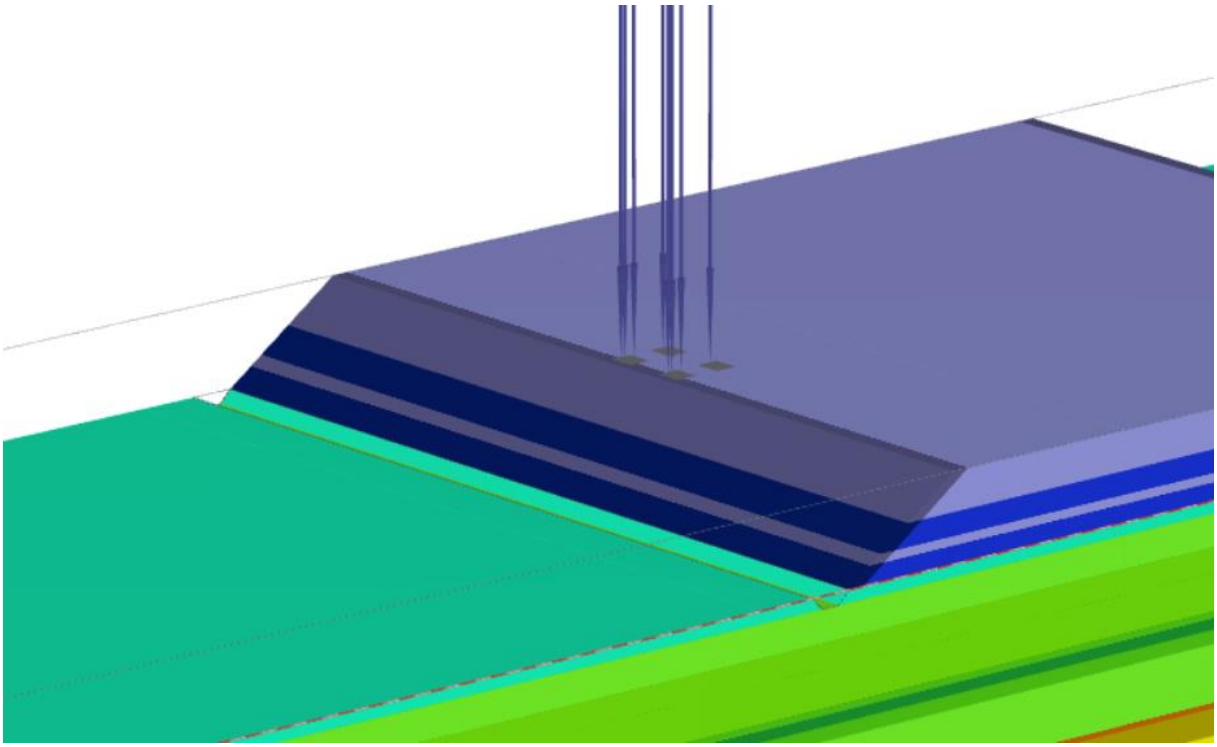

Figure K.5: 3D (50 m) model for scenarios 1, 2, 4, and 5.

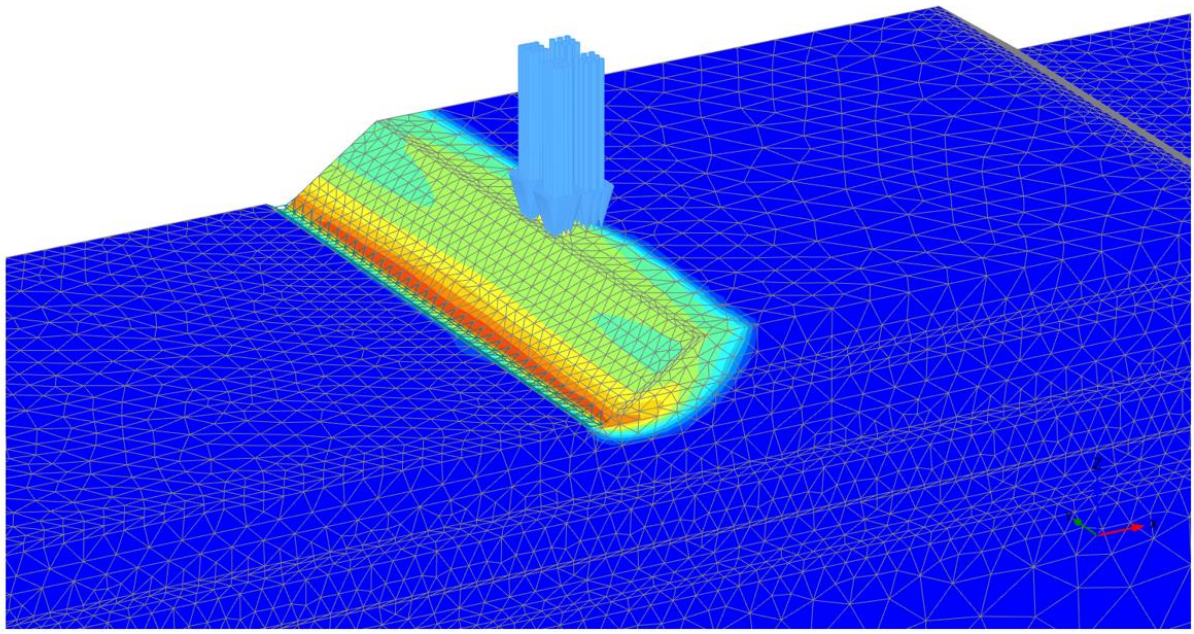

Figure K.6: Failure mechanism of the 3D (50 m) model (scenario 5).

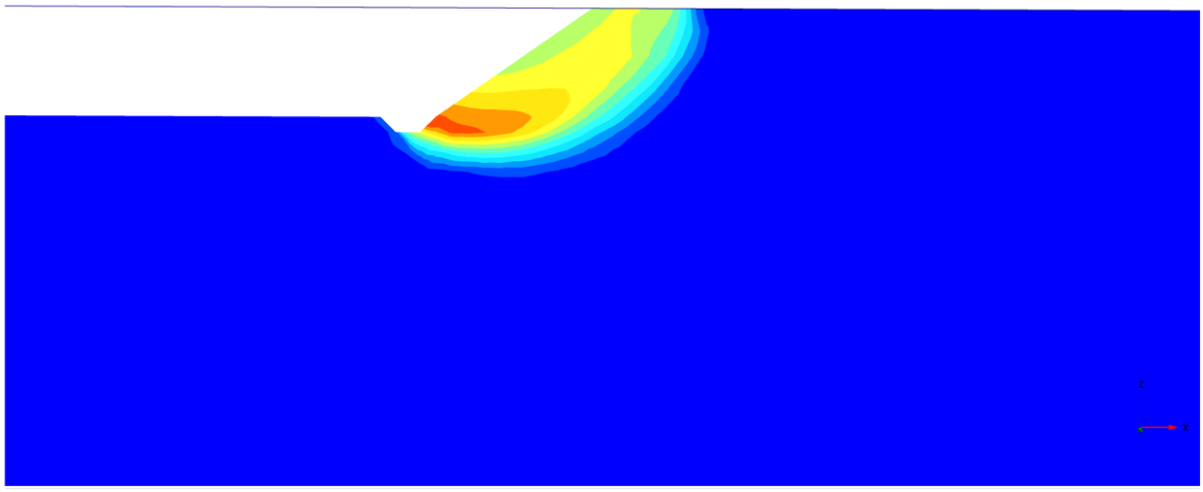

Figure K.7: Central cross-section of the failure mechanism of the 3D (50 m) model (scenario 5).

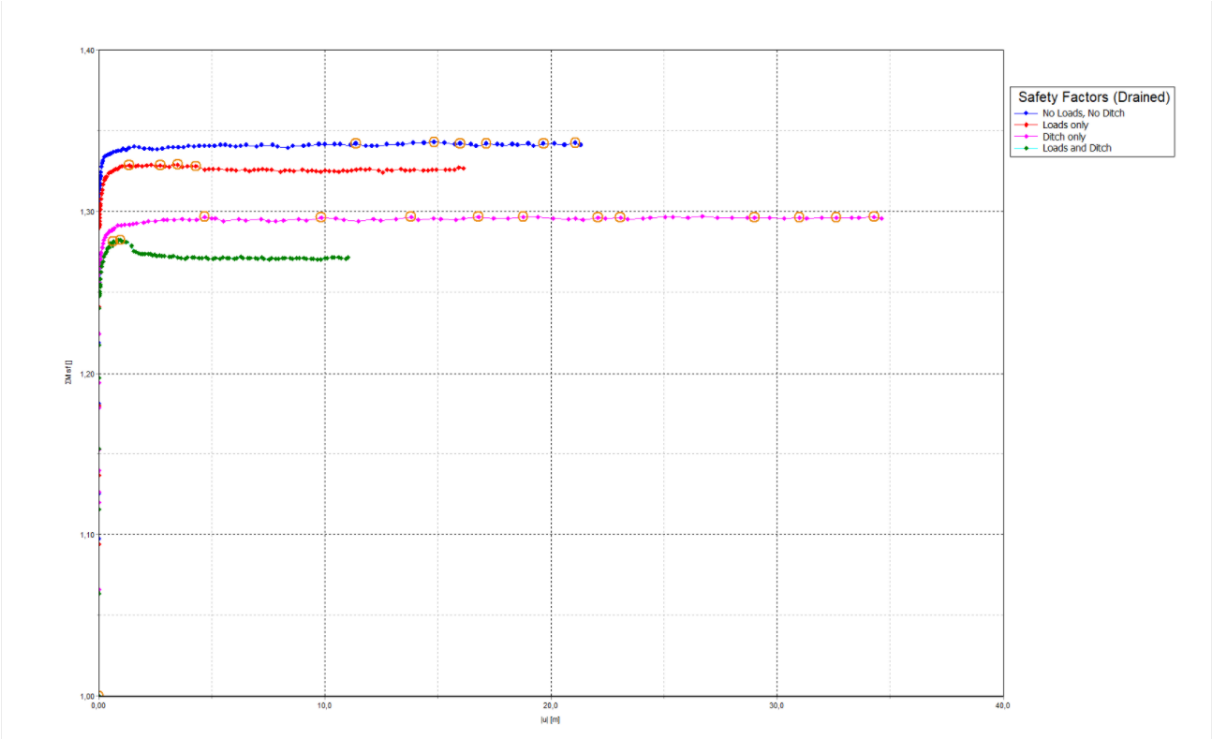

Figure K.8: Safety factors obtained for scenarios 1,2, 4, and 5 from the 3D (50 m) model.

K.3 Scenarios 1,2,4, & 5 (3D version – 50 m extension with plane-strain loading)

This model was made by extending the 2D model of the Westeremden terp by 50 m into the y-direction. The 40 kPa surface loads for scenarios 2 and 5 therefore span the full 50 m width.

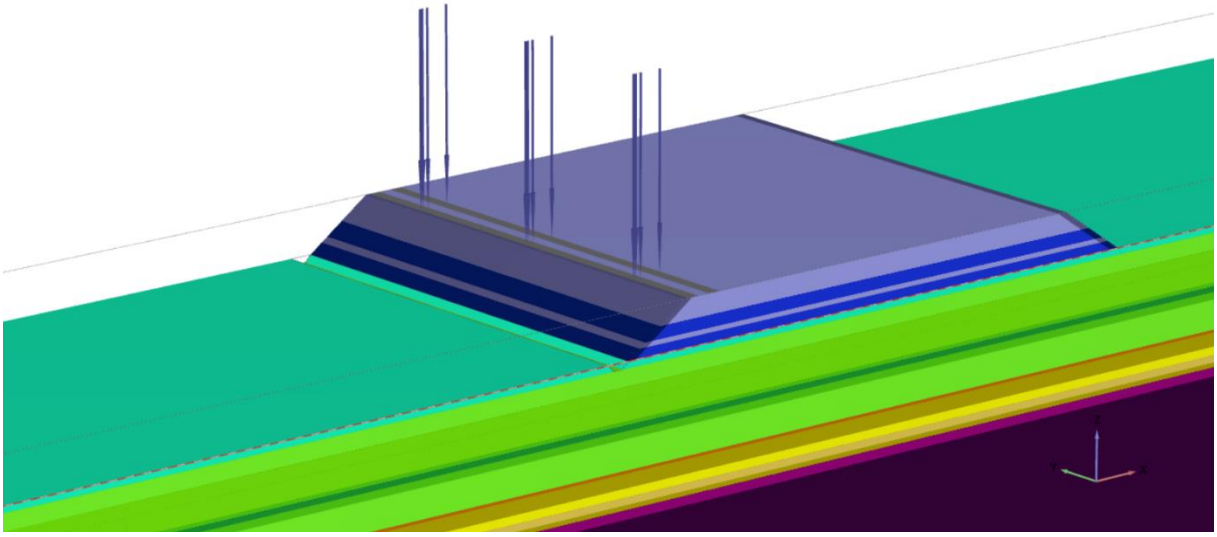

Figure K.9: 3D (50 m) model with plane-strain loading for scenarios 1, 2, 4, and 5.

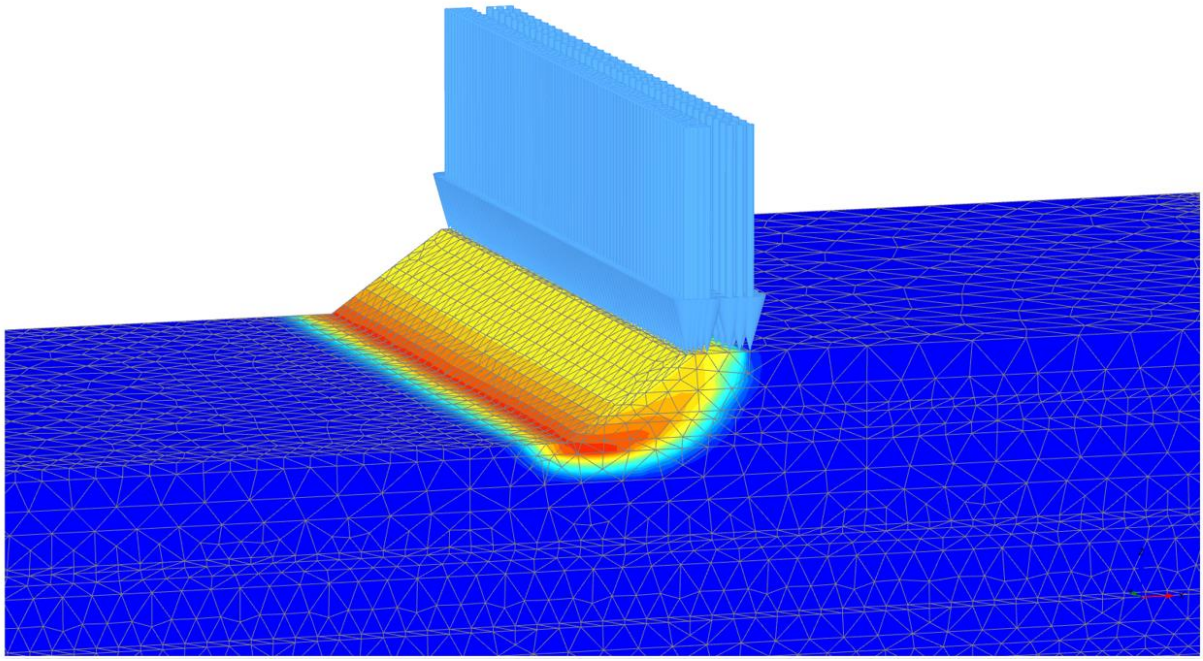

Figure K.10: 3D (50 m) model with plane-strain loading for scenarios 1, 2, 4, and 5 (scenario 4).

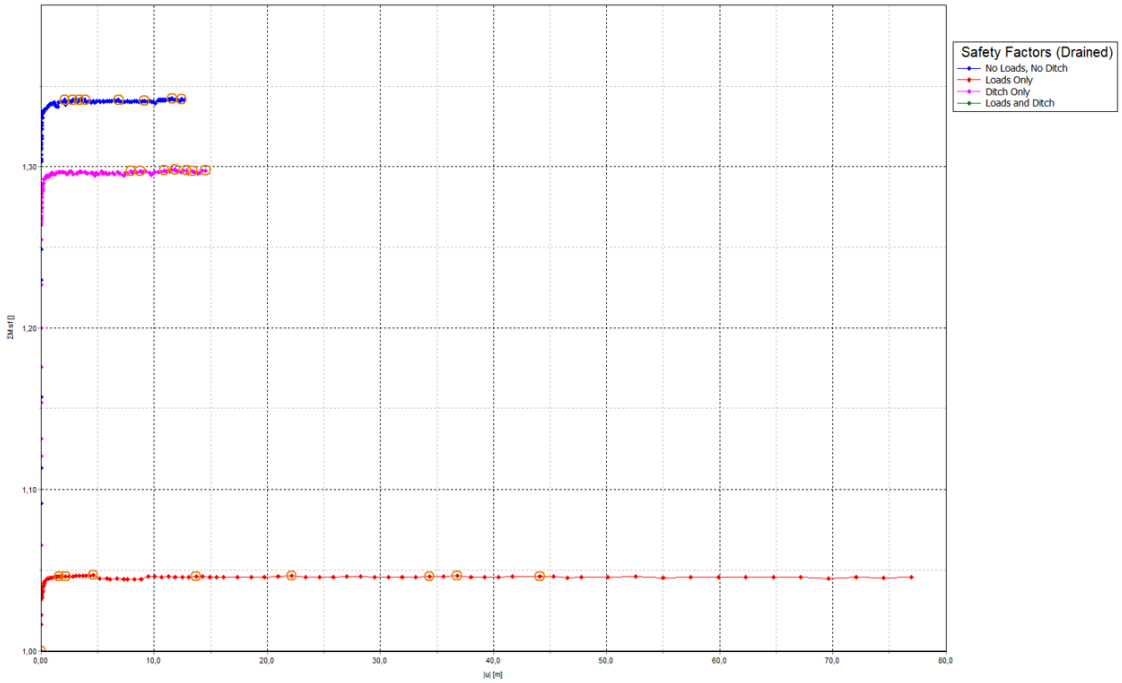

Figure K.11: Safety factors obtained for scenarios 1,2, 4, and 5 from the 3D (50 m) model with plane-strain loading.